CONVECTIVE HEAT TRANSFER UNDER A TURBULENT IMPINGING

SLOT JET AT LARGE TEMPERATURE DIFFERENCES

by

Debmalya Das

A thesis submitted to the Faculty of Graduate Studies and Research

in partial fulfilment of the requirements for the

degree of Master of Engineering

Chemical Engineering Department
McGill University
Montreal, P.Q.
Canada   © August 1982

IMPINGEMENT HEAT TRANSFER AT LARGE

TEMPERATURE DIFFERENCES

Dedicated to the memory

of my grandparents

ABSTRACT

Effect of high temperature differences on local and average heat transfer rates under a confined single slot jet was studied experimentally for nozzle exit Reynolds number from 1000 to 20000, nozzle exit to impingement surface spacing from 5 to 12 nozzle widths, lateral distances from the stagnation line up to 18 nozzle widths and jet-impingement surface temperature differences from 50° to $300^{\circ}C$.

For stagnation Nusselt number, two acceptable forms were obtained for incorporating the effect of temperature difference, the temperature ratio method and the reference temperature method. Use of the former is recommended.

The stagnation Nusselt number, evaluated at nozzle exit temperature, was found to decrease by about 6.5% over the range $0 \leqslant \Delta T \leqslant 300^{\circ}C$ or $1 \leqslant T_j/T_s \leqslant 2.06$. Expressed in terms of effect of temperature difference on stagnation heat transfer coefficients this effect corresponds to an increase in h of about 62% over this same temperature range. Beyond about 7 nozzle widths from stagnation there is no significant effect of temperature difference on Nusselt number but a significant effect on h remains.

A general correlation was developed for average Nusselt number in the form:

$$\overline{Nu}_j = K \, Re_j^{\,a} \, (H/w)^b \, (T_j/T_s)^c \, Pr_j^{\,1/3}$$

where all four correlation parameters are functions of the extent of the impingement surface over which heat transfer is averaged.

Analysis of confined jet impingement heat transfer as a confined flow established that the fraction of available heat which is transferred between the jet and the impingement surface is proportional to $(x/w)^{1/3}$ and to $1/Re_j^{\,0.5}$.

RÉSUMÉ

L'effet de différences de température élevée sur le taux local et moyen de transfert de chaleur sous un jet rectangulaire confiné a été mesuré expérimentalement pour de différence de température, jet à la surface d'impact, de $50^{\circ}C$ à $300^{\circ}C$, pour une gamme de nombre de Reynolds, d'espacement de la surface d'impact et de la longueur de cette surface. Pour l'incorporation de cet effet dans le calcul du nombre de Nusselt au point de stagnation, deux corrélations ont été obtenues, la méthode basée sur le rapport de températures (recommandée), et la méthode basée sur une température de référence.

Au delà de la gamme de température de $0 \leqslant \Delta T \leqslant 300^{\circ}C$ ou $1 \leqslant T_j/T_s \leqslant 2.06$ le nombre de Nusselt au point de stagnation décroît par 6.5% alors que le coefficient h augment de 62%. A une distance supérieure à 7 largeurs de buses du point de stagnation, cet effet devient négligeable sur le nombre local de Nusselt mais demeure significative sur le coefficient local h.

Une corrélation générale pour le nombre de Nusselt moyen est

$$\overline{Nu}_j = K \, Re_j^{\,a} \, (H/w)^b \, (T_j/T_s)^c \, Pr_j^{\,1/3}$$

où les quatres paramètres sont fonctions de la longueur de la surface d'impact.

Une analyse comme système d'écoulement confiné établit que la fraction de chaleur disponible qui est transférée entre le jet et la surface d'impact est proportionnelle à $(x/w)^{1/3}$ et à $1/Re_j^{0.5}$.

ACKNOWLEDGEMENTS

TABLE OF CONTENTS

LIST OF FIGURES

LIST OF TABLES

NOMENCLATURE

a	exponent of Reynolds number
b	exponent of dimensionless spacing
C_p	specific heat, cal/gm °C
c	exponent of temperature ratio
D	nozzle diameter, mm
D_v	volumetric diffusivity, m²/h
d	exponent of Prandtl number
e	exponent of dimensionless distance from stagnation line
H	nozzle-surface spacing, mm
h	heat transfer coefficient, W/m²°C
h_b	local heat transfer coefficient, W/m²°C
K	coefficient of equation 4.16
K', K"	coefficients of equations 4.21 and 4.22
k	thermal conductivity, W/m °C
k_j	mass transfer coefficient, gm-mole/m²-s-unit mole fraction
L	impingement surface length, mm
ℓ	nozzle length, mm
Q_1	heat flux per unit length of impingement surface, W/m
Q_2	heat lost by jet per unit length of impingement surface, W/m
q	heat flux to impingement surface, W/m²
q_c	convective heat flux to impingement surface, W/m²
q_m	heat flux measured by sensor, W/m²
q_r	radiant heat flux to impingement surface, W/m²
T	temperature, °K
T_a	impingement plate bottom temperature, °K

T_b	average temperature, °K
T_e	average temperature at exit port, °K
T_j	jet exit temperature, °K
T_{ref}	reference temperature, °K
T_s	impingement surface temperature, °K
T_s^*	sensor surface temperature, °K
t_j	jet temperature, °C
t_s	surface temperature, °C
ΔT	temperature difference between jet and impingement surface, °K
U_a	arrival velocity, m/s
U_o	velocity at jet exit, m/s
v_j	velocity at jet exit, m/s
w	nozzle width, mm
x	lateral distance from stagnation, mm

Greek Letters

β	coefficient of thermal expansion, /°K
μ	dynamic viscosity N.s/m^2
ρ	density, Kg/m^3
δ	Stefan-Boltzman constant, W/m^{2}K^4

Dimensionless Groups

Gr	Grashof number $\dfrac{g\rho^2 \beta D^3 \Delta T}{\mu^2}$
Nu_o	stagnation Nusselt number, hw/K
$\overline{Nu_b}$	average Nusselt number based on mixing-cup temperature, $\bar{h}_b w/K$
Nu_j	local Nusselt number, hw/K
$\overline{Nu_j}$	average Nusselt number, $\bar{h}w/K$
Pr	Prandtl number, Cpμ/K

Re Reynolds number, $\dfrac{w\, v_j\, \rho}{\mu}$

Sc Schmidt number, $\dfrac{\mu}{D_v\, \rho}$

Sh Sherwood number, $\dfrac{k_j\, D}{D_u\, \rho}$

Subscripts

j jet temperature

s surface temperature

o stagnation line

CHAPTER I

INTRODUCTION

1.0 INTRODUCTION

The high convective heat and mass transfer rates achieved by jets impinging on a surface have led to application of impinging jets in industry. Thus impinging jets are used for the drying of paper, annealing non ferrous metals and plastic sheets, tempering and toughening glass, heating or cooling of leading edges of turbine blades and spot cooling of electronic components. Depending on application, round or slot jets are used individually or in arrary of multiple nozzles.

In the paper industry, high velocity impingement dryers are used extensively on machines where production rates are limited by drying rates. The Yankee dryer for the drying of tissue products, and high velocity dryer on coating machines reflect paper industry use of impingement drying processes. High velocity impingement dryers have also been shown to be very effective for drying newsprint in the Papridryer process which was proposed by Burgess et al. (1972). In this process the impinging drying rates were enhanced by drawing some of the impingement air through the paper.

In many impingement heat transfer applications, very large temperature differences are used. For example, impingement paper dryers are frequently operated with jet temperatures in excess of 400°C (or with temperature differences in excess of 300°C). Yet the majority of impingement heat transfer studies, which are used as a basis for the design of impingement heat transfer equipment, have been made with small temperature differences, typically 20°-70°C. Very little is known about the effects of large temperature differences on impingement heat transfer coefficients and about the validity of using the heat transfer

correlations with low temperature differences to predict heat transfer
rates at high temperature differences.

The objective of this study was therefore to measure the effect
of high temperature differences on impingement heat transfer rates, and
to find ways of accounting for these effects in impingement heat transfer
calculations.

CHAPTER II

LITERATURE REVIEW

2.1 Introduction

Many studies have been published about flow and heat transfer

characteristics of impinging jets. Extensive reviews of these studies

have been made by Gauntner et al. (1970), Mujumdar and Douglas (1972),

Livingwood et al. (1973), Martin (1977) and more recently by Obot (1981).

Hence the review presented here has been made to highlight only those

aspects of the impingement flow and heat transfer work which are rele-

vant to the scope of this thesis. A summary of the references which are

most relevant to this work and which are referred to the subsequent

discussion is presented in Table 2.1.

2.2 Impingement Flow Characteristics

Although the impingement flow characteristics are not the major

issue in this work, they form the basis for the interpretation of

impingement heat transfer characteristics. Hence impingement flow is

presented here.

Poreh and Cermak (1959) made the following characteristics of

the flow field under impinging jet (Figure 2.1):

a)   free jet

b)   stagnation flow

c)   wall jet.

a)   Free jet region.

This is the region of development and expansion of the jet from

the nozzle exit and extending to the position where flow characteristics

of the jet first start to be influenced by the impingement surface. The

profile of axial velocity may undergo considerable change in this region,

especially if the velocity profile at the nozzle exit is far from fully

TABLE 2.1 Experimental Conditions and Heat Transfer Correlations of Impinging Jet Studies

Author and Year	Jet Configuration	Jet Dimension (mm)	Jet Temp (°C)	Surface Temp (°C)	Jet Reynolds Re	Geometric Parameter H/D	r/w	Type of Sensor	Dimension of Sensor (mm)	Experimental Technique	Correlation	Comments
Perry (1954)	Round, single, unconfined	19.51, 21.59	Hot 600	Cold 200	7000–30,000	11,13,16,19	0–19	Calorimetric	16.51	Steady state	$Nu = 0.1010\, Re^{0.7}\, Pr^{0.33}$	The diameter of the calorimeter sensor was used as the characteristic length in calculating Nu and Re. The effect of high temperature was accounted by calculating physical properties at mean film temperature.
Thurlow (1954)	Round, single, unconfined	25.4, 12.7	Hot 93–202	Cold	22,000–57,000	<10	0–10	Heat flux was measured by temperature drop over plate width		Steady state	$Nu_0 = 0.026\, Re^{\frac{2}{3}}\, Gr^{\frac{1}{2}}\, e^{-0.14\,(H/D)}$ $\overline{Nu} = K\, Re^{\frac{2}{3}}\, e^{-0.033\,(H/D)}$	The physical properties were calculated at jet temperature. Grashof number is included to account for the effect of molecular diffusion and natural convection between the hot jet and surrounding still air. The constant K is a function of nozzle diameter.
Dunn and Nan (1961)	Slot, single, unconfined	0.79, 2.38	Cold 24	Hot 38–66	∼1200–15,000	1–38	0–90	Electrically heated graphitic strip		Steady state	$Nu_0 = K_1\, m^{0.70}\, Pr^{\frac{1}{3}}$ $\overline{Nu} = K_2\, m^{0.70}\, Pr^{\frac{1}{3}}$	K_1 is almost constant (~0.038) up to H/w = 8 and decreases thereafter. Nu is computed over r/w = 50. $K_2 = 0.027$ for H/w = 8
Gardon and Cobonpue (1962)	Round, single, unconfined	2.13–9	Cold	Hot	7000–56,000	2–40	0–40	Heat flow transducer	0.5	Steady state	$Nu_0 = 13.0\, Re^{0.5}\ (D/H)$	The correlation is valid for Re > 14,000 and D/H > 20.

4

TABLE 2.1 (cont'd)

Author and Year	Jet Configuration	Jet Diameter (mm)	Jet Temp (°C)	Surface Temp (°C)	Jet Reynolds No.	Geometric Parameter H/w	Geometric Parameter x/w	Type of Sensor	Dimension of Sensor (mm)	Experimental Technique	Correlation	Comments
Huang (1963)	Round, single, unconfined	3.175,2.968, 4.762,5.556 6.35	Hot 150-177	Cold	1000-8,000	1-12	0-20	Fine silver strip, heat flux was measured by temperature rise	25.4 x 25.4 x 6.5 (thickness)	Transient state	$Nu_0 = 0.0233 Re^{0.87} Pr^{0.33}$ $\overline{Nu} = 0.016 Re^{0.87} Pr^{0.33}$	The Reynolds number is calculated on the basis of "arrival velocity" on impingement surface instead of jet exit velocity
Gardon and Akfirat (1966)	Slot, single, unconfined	6.35,3.175, 1.588	Cold	Hot ΔT=20°C	450-22,000	<80	0-20	Heat flow transducer	0.9	Steady state	$Nu_0 \sim 1.2 Re^{0.58} (H/w)^{-0.62}$ $\overline{Nu}_x = 0.36 Re_x^{0.42}$	The correlation is applicable for H/w > 14 and Re > 2000. For 2nd equation the characteristic distance is the averaging distance from stagnation.
Cadek (1974)	Slot, single, unconfined	6.35,12.7, 19.05	Cold	Hot	4650-102,700	2-16	0-30°	Heat flux sensor, name as Gardon and Akfirat	0.914	Steady state	--	
Sparrow and Wong (1975)	Slot, single, unconfined	6.35	Room Temp	--	270-1780	0-20	0-30			Transient state	$Re = (Pr/Sc)^n Sh$	Sherwood number obtained from mass transfer rate of naphthalene was related to Nusselt number by heat-mass transfer analogy n = 1/3 to 0.4
Folayan and Whitelaw (1977)	Slot, single, confined, unconfined	5	Cold	Hot	1750-7100	2-14	0-40	Electrical heating strip of stainless steel	--	Steady state	--	The experiment was carried with a constant heat flux at impingement surface.
Van Heiningen, Mujumdar and Douglas (1977)	Slot, single, confined	6.2 11.1	Hot Cold	Cold Hot	13,700-49,300	6 2.6	0-22.5	Cold film heat flux sensor	1.15	Steady state	--	Both cold and hot jets were studied simultaneously on a rotating impingement surface

TABLE 2.1 (cont'd)

Author and Year	Jet Con-figuration	Jet Diameter (mm)	Jet Temp (°C)	Surface Temp (°C)	Jet Reynolds No.	Geometric Parameter		Type of Sensor	Dimension of Sensor (mm)	Experimental Technique	Correlation	Comments
						H/d	x/w					
Seed, Mujumdar and Douglas (1980)	Slot, multiple, confined	2.5, 3.3, 5.0, 10.0, 13.3	Cold	Hot 55-60	3,000–30,000	4-24	0-16	Heat flux was measured along the width of a porous bronze sensor	2.4	Steady state	$Nu_{o} = 0.5\ Re_{j}^{0.65}\ (H/w)^{-0.56}$	
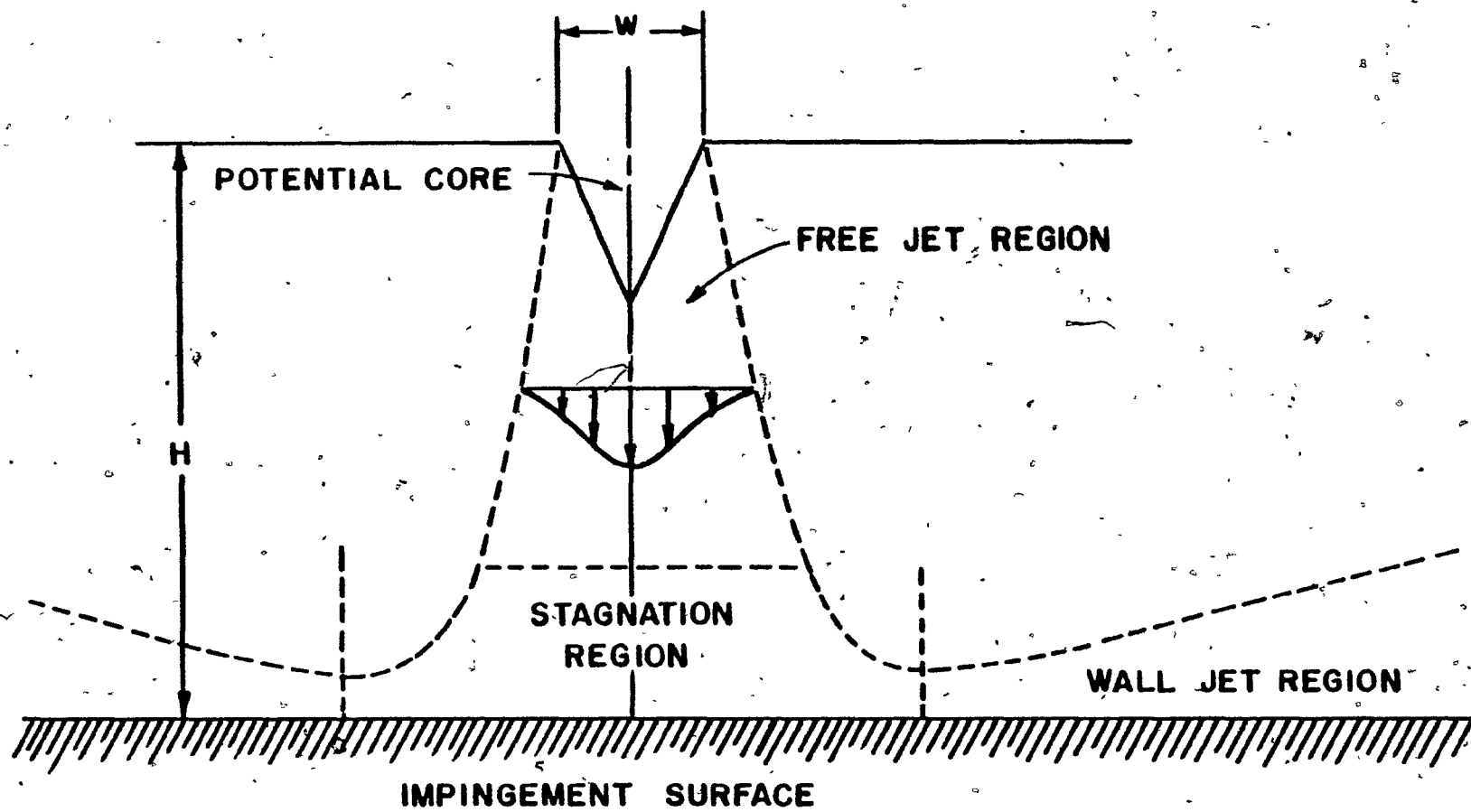
FIGURE 2.1   Flow Field under Impinging Slot Jets

developed profile. Turbulence characteristics change sharply in the free jet region, especially during the initial part of it. The free jet region may be considered to be composed of three sub regions, first the potential core, then the developing jet and finally the developed jet - provided the spacing of the impingement surface from the nozzle exit is sufficient.

The potential core refers to that part of the free jet region over which axial velocity remains unchanged from the values existi the nozzle exit. The length of the potential core is an important parameter for heat transfer applications, since stagnation heat transfe rates tend to reach a maximum when the impingement surface is located at the spacing corresponding to the position of the tip of the potential core. For slot jets potential core length values ranging from 5 to 8 times the nozzle width have been reported. Potential core length is affected by the turbulence characteristics at the nozzle exit, hence is affected by variables which may affect nozzle exit turbulence such as geometry of the nozzle and of the flow channel upstream of the nozzle, and Reynolds number. Some of the diversity in results reported may also be attributed to the velocity measuring techniques used, i.e. pitot tube or hot wire anemometry, as has been discussed in detail by Obot (1981).

The developed flow region, which exists only for sufficiently wide spacing of the impingement surface from nozzle exit, refers to that part of the free jet in which centerline axial velocity decays inversely proportional to $(H/w)^{0.5}$. The region beyond the potential core, i.e. when axial velocity is no longer constant, but before the developed flow region where velocity drops proportional to $(H/w)^{0.5}$, is referred to as the region of developing flow or the transition region.

Both the axial velocity and turbulence characteristics of slot jets have most recently been measured by Saad (1981) who, in integrating

his own new measurements with those of earlier workers, has also provided a general review of this area.

b) Stagnation flow region.

This region begins at the position where the free jet first begins to be affected by the presence of the impingement surface, includes the region where the flow diverges, and extends up to the impingement surface.

In the stagnation region the axial velocity decreases rapidly, axial turbulence intensity increases, and the pressure increases as the axial velocity component is transformed to a lateral velocity. The maximum static pressure occurs at the stagnation line. From this maximum the static pressure along the impingement surface drops sharply. Thus Saad (1981) found that the pressure half width, i.e. where the static pressure was one-half of the stagnation pressure, occurs at $x/H = 0.15 \pm 0.01$. This region of a strongly negative pressure gradient is of particular importance because of its ability to maintain a boundary layer laminar even for a highly turbulent impinging jet.

The approximate dimensions of the stagnation region are of interest. The distance normal from the impingement surface at which the stagnation region begins for a slot jet has been measured by Schauer and Eustis (1963), Beltaos and Rajaratnam (1973) and by Saad (1981), all of whom found that axial velocity begins to feel the effect of an impingement surface at about 0.2H to 0.3H from the surface. However, Saad found that axial turbulence level was not affected by the presence of an impingement surface until less than 0.05 H from the surface. The lateral extent of the stagnation region, defined as the

distance from stagnation where the static pressure gradient becomes negligible, has been reported by Beltaos and Rajaratnam (1974) to be about 0.35 H from the stagnation line for 21 < H/w < 66, while for 4 < H/w < 16 Saad (1981) found his distance to be 0.5H ± 0.1H. It should be noted that H, not w, has been found to be the more relevant characteristic dimension with respect to the stagnation or impingement region.

c) Wall jet region.

In the wall jet region the accelerated stagnation flow transforms to a decelerated wall jet flow with a negligible lateral pressure gradient. The lateral velocity developed in the stagnation region passes through a maximum at the end of the stagnation region. The boundary layer transition from laminar to turbulent also occurs in the wall jet region. An extensive characterization of both the mean velocity and turbulence characteristics in the stagnation and wall jet regions of an impinging jet has recently been given by Obot (1981) for the similar case of a round turbulent jet.

2.3 Effects of Geometric and Flow Parameters on Slot Jet Impingement Heat Transfer

The major geometric and flow parameters affecting heat transfer under a single stationary slot jet are the nozzle to impingement surface spacing, the lateral distance along the impingement surface from the stagnation line and the jet exit Reynolds number.

The effect of nozzle impingement surface spacing on stagnation line Nusselt number at two Reynolds numbers for a turbulent slot jet is

illustrated on Figure 2.2 with data from Gardon and Akfirat (1966),
Cadek (1974) and Saad (1981). The results from these three references
show the same trend; the stagnation line Nusselt number passes through
a maximum at a nozzle to surface spacing of about 7w to 8w. As heat
transfer increases with both mean velocity and turbulence the occurrence
of this maximum in Nu_o reflects the fact that for H/w spacings less than
that for the maximum, Nu_o is dominated by the increasing turbulence
while for larger values of H/w, Nu_o is dominated by the decreasing mean
velocity.

The variation of local Nusselt number with lateral distance from
the stagnation line is illustrated for a single slot jet with the data
of Gardon and Akfirat (1966), Cadek (1974) and Saad (1981) on Figure
2.3 (a) for H/w = 2 and on Figure 2.3 (b) for H/w = 8. The striking
difference between these two figures is the presence of an off-stagnation
minimum and maximum in the profiles at the lower spacing. The off-
stagnation peaks at low spacing are associated with the onset of and the
completion of transition from a laminar to a turbulent boundary layer.
The combination of a high jet Reynolds number and a low spacing produces
a negative pressure gradient in the stagnation region which is suffi-
ciently strong as to maintain the boundary layer as laminar even for a
highly turbulent jet. Beyond the region of steep negative pressure
gradient the onset of boundary layer transition is marked by the off
stagnation minimum in the profile, while completion of this transition
is marked by the secondary maximum.

The effects of Reynolds number on stagnation Nusselt and average
Nusselt numbers are illustrated on Figures 2.4 and 2.5 using the results
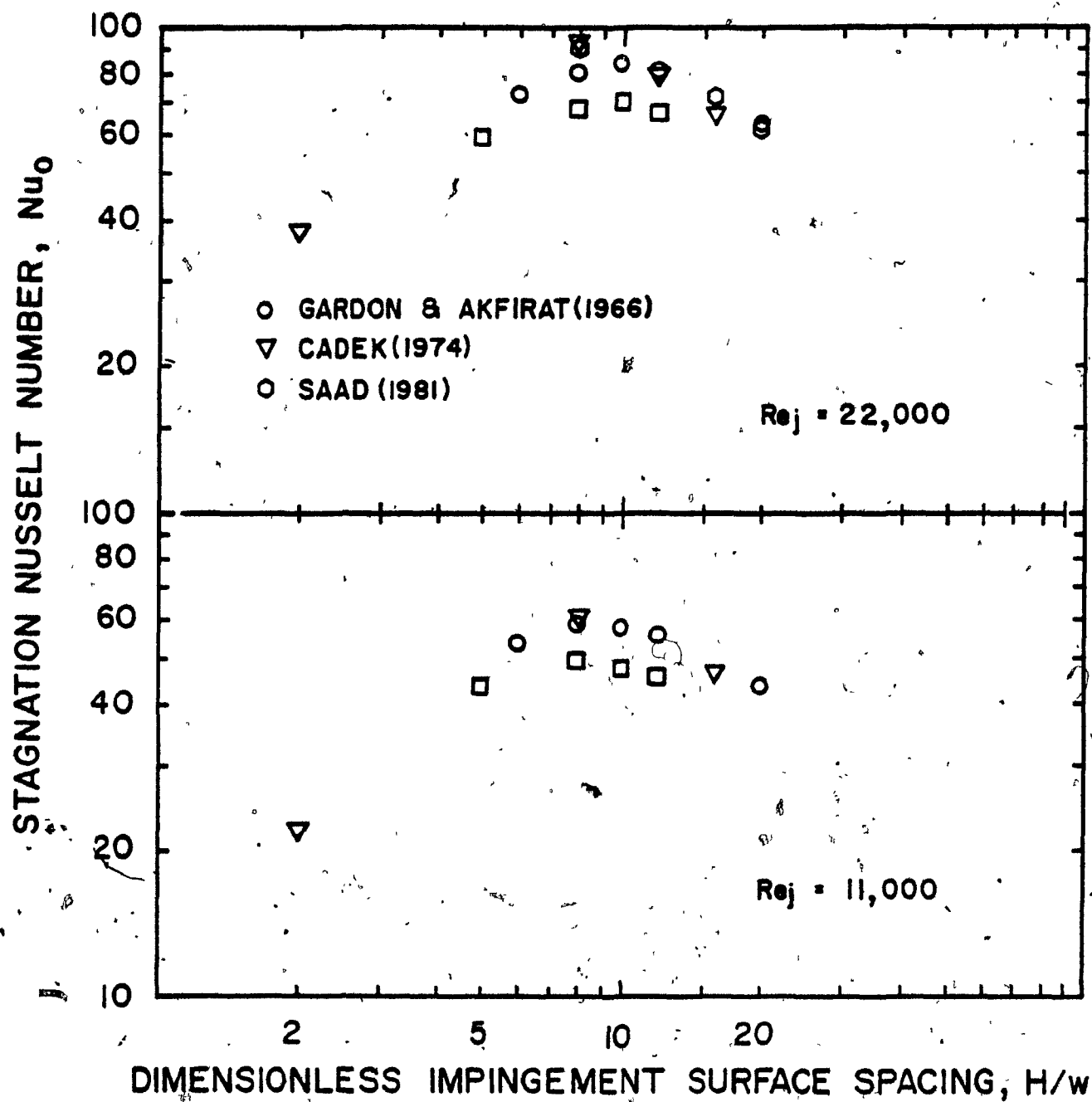
FIGURE 2.2   Comparison of Nu_o for Slot Jets
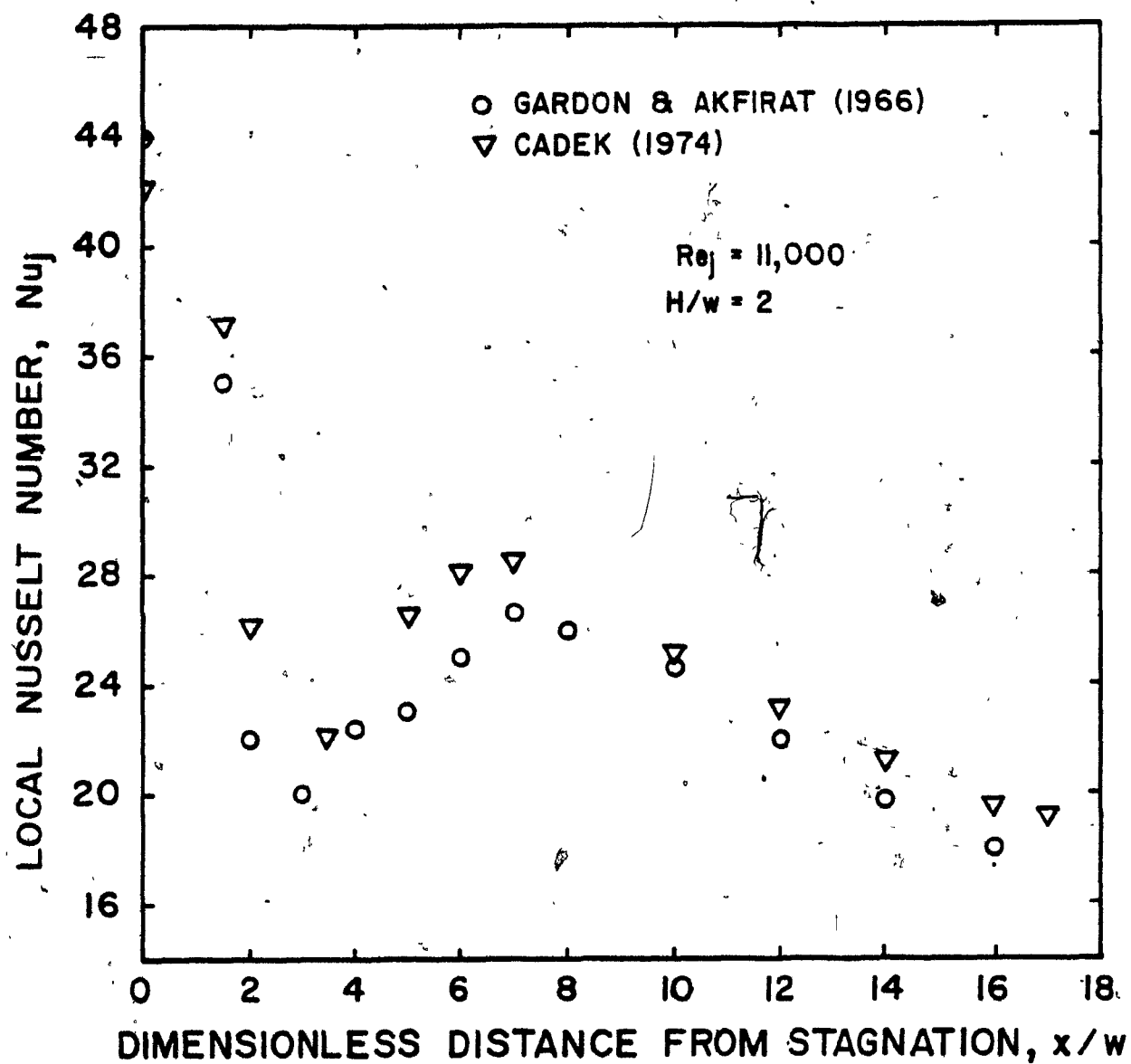
FIGURE 2.3a   Comparison of Local Nu Profile at H/w = 2
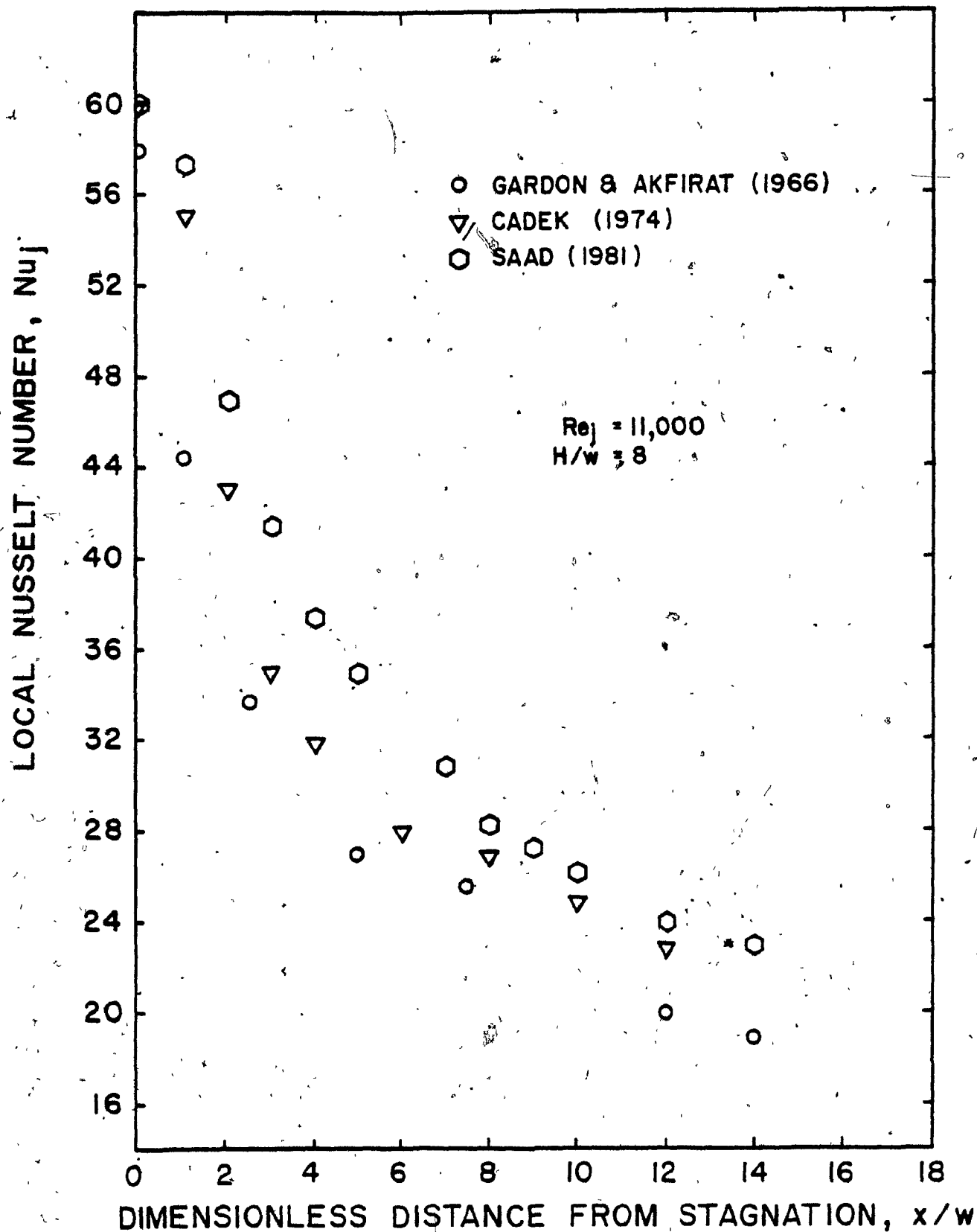
FIGURE 2.3b   Comparison of Local Nu Profile at H/w =8

H/w = 8

GARDON & AKFIRAT (1966)
CADEK (1974)
FOLAYAN (1977)
DAANE & HAN (1961)
SAAD (1981)

STAGNATION NUSSELT NUMBER, Nu_{oj}

REYNOLDS NUMBER, Re_j
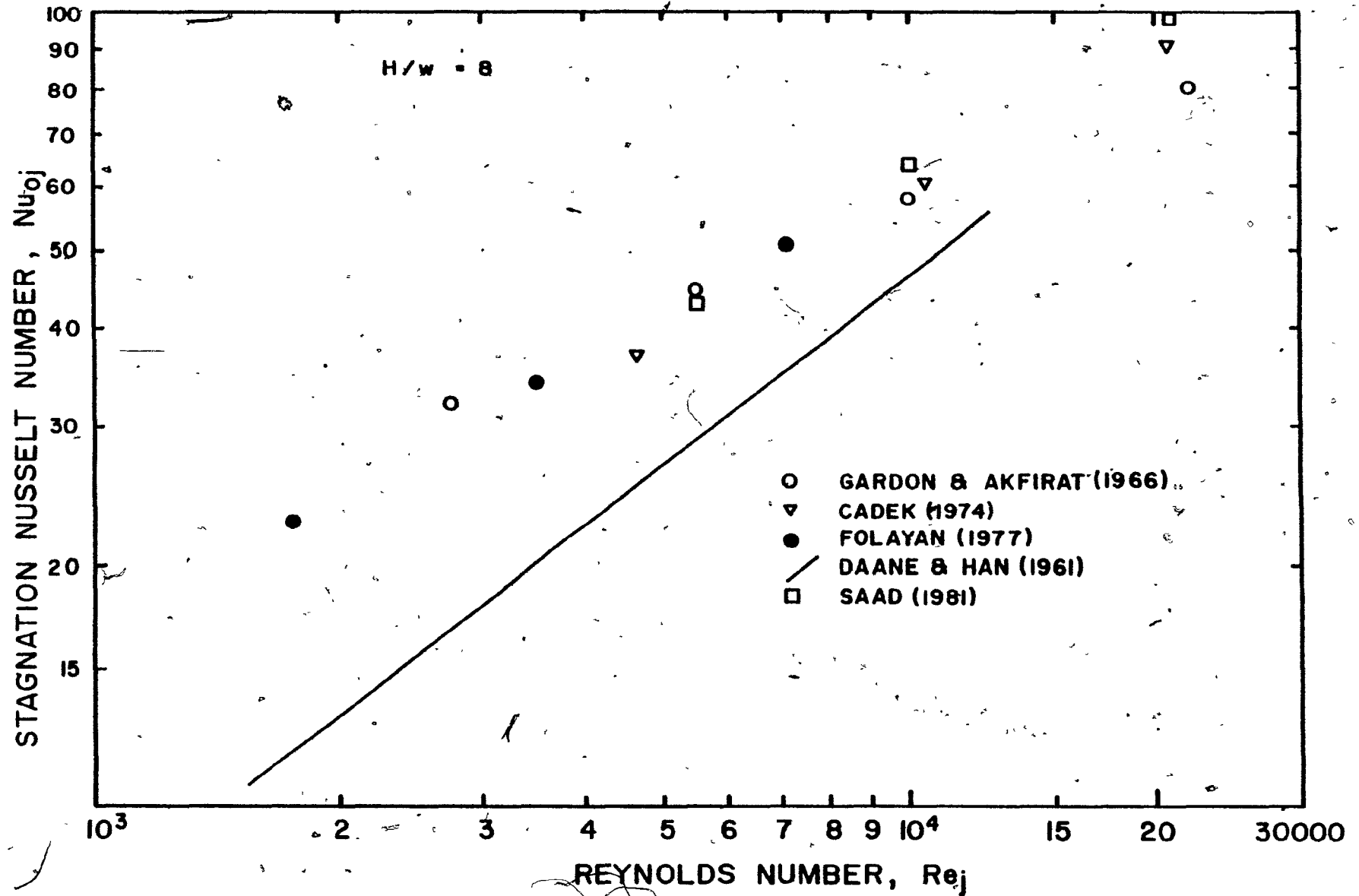
FIGURE 2.4   Comparison of Nu_o for Slot Jets

15
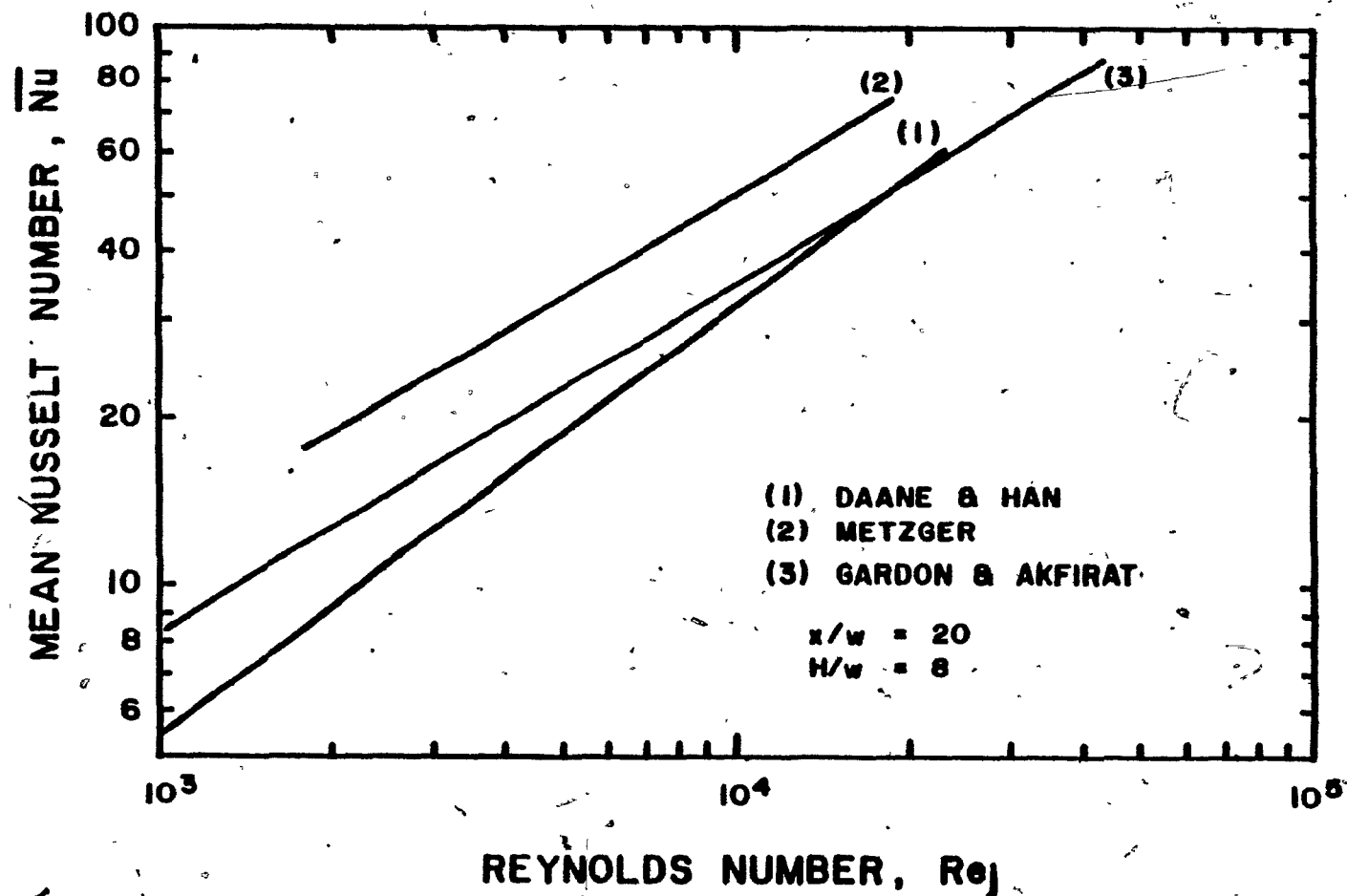
FIGURE 2.5   Comparison of $\overline{Nu}$ for Slot Jets

of various workers. The slopes of 0.5 to 0.6 on Figure 2.4 are an indication of the laminar character of the boundary layer in the stagnation region, even for turbulent jets. The higher slopes of 0.6 to 0.8 for the relationships between $\overline{Nu}$ and Re_j on Figure 2.5 reflect the fact that beyond some distances from stagnation the boundary layer is turbulent, hence in that region the effect of jet Reynolds number on Nusselt number is that normally found for turbulent flow.

Another important parameter, one which has not received appropriate attention until recently, is the effect of confinement of the impingement system with a surface or hood parallel to the impingement surface. Most industrial process applications involved confined jet systems whereas most experimental work has been carried out with unconfined jets. Folayan (1977), who used a shroud at the plane of a slot nozzle exit, observed both stagnation and wall jet region heat transfer were 10%-20% less than for unconfined jets. van Heiningen et al. (1977) also observed reduced Nusselt number in the wall jet region from a slot nozzle. The same trend was also observed by Obot (1981) for a round nozzle, with largest effect of confinement occurring at the smallest spacing.

Reduction in Nusselt number is attributed to the effect of the confinement surface in reducing or eliminating entrainment of fluid from the environment by the jet. Such entrainment affects both the flow field and the temperature field in the impingement system, and hence affects the heat transfer.

It is evident that in an experimental facility of an unconfined jet the results would become a function of whether a heating or a cooling jet were used because fluid entrainment from the environment would have

the opposit effect on the temperature field in the impingement system for those two cases. Earlier workers had largely ignored this effect which can be quite significant.

2.4 Effect of Temperature Difference

The listing in Table 2.1 of previous studies documents the lack of attention to the measurement of impingement heat transfer for large temperature differences between the jet and impingement surface. This deficiency, understandable because of the experimental difficulty involved is none the less unfortunate because important industrial applications such as paper drying and turbine blade cooling involve high temperature differences. Only three experimental studies with high temperature differences have been reported, all for impinging round jets, Perry (1954), Thurlow (1954) and Huang (1963). Unfortunately none of them made any systematic study to induce the temperature difference effect in a way useful in others.

In the earlier study, Perry (1954) for his unconfined round jet used up to 600°C jet temperature and a temperature difference varied from 100° to 400°C. A relationship, independent of temperature, was developed with properties evaluated at the mean film temperature. The usefulness of Perry's results is limited by uncertainties concerning his impingement surface spacing from the nozzle exit and his basis for determining the temperature difference used for converting from the heat flux measured to the Nusselt number reported. It appears that Perry did not base his temperature difference, ΔT, on jet temperature, T_j, but instead, on an estimate of temperature of a free

jet at some unspecified distance greater than 8 nozzle diameters from the nozzle exit.

Thurlow (1954) in a communication to previous author, reported his results for a unconfined hot (53°-202°C) round impinging jet. Thurlow confirmed a definite effect of temperature dependent fluid properties, even at T_j = 53°C, but did not include this aspect in his correlation.

Huang (1963) used an unconfined hot (150°-177°C) air jet impinging on a cold surface. He used arrival velocity, U_a, as the characteristic velocity in his Reynolds number, thus making it diffi-cult to interpret results. However, using the empirical relation U_a = 6.63 U_o (D/H) proposed by Gardon and Cobonpue (1963), Huang's Reynolds number is transformed to jet exit Reynolds number to facilitate comparison.

The high temperature difference results of Perry, Thurlow and Huang are compared with the reliable low temperature data of Gardon and Cobonpue (1963) on Figure 2.6. The results of Perry and Gardon and Cobonpue are in excellent agreement with each other but an order of magnitude higher than those of Huang and Thurlow. However this agreement between Perry, who used an ambiguous temperature difference term to convert heat flux to heat transfer coefficient and Gardon and Cobonpue, using the temperature difference between jet and surface, is apparently somewhat fortuitous. The lower values for Huang's Nusselt numbers as compared to Gardon and Cobonpue and Perry may be attributed at least in part to the use of incorrect equations for, U_a, the arrival velocity for a jet issuing from short sharp-edged inlet nozzles which unfortunately have not been specified in Huang's paper.
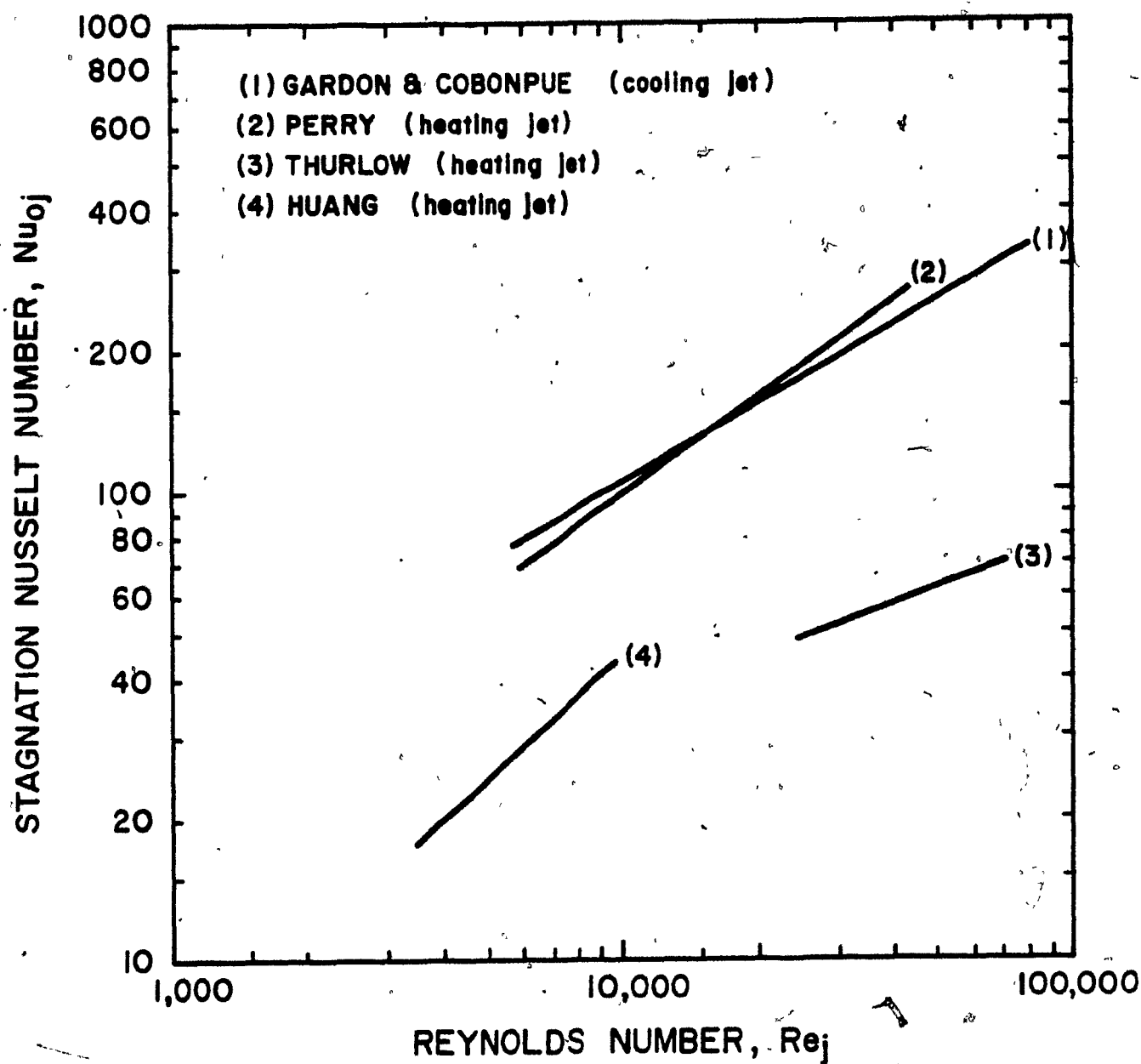
FIGURE 2.6   Comparison of Nu_o for High Temperature Round Jets

Due to incomplete information available from the publication of these early works with high temperature differences it is not possible to determine the source of the large discrepancies nor to use any of the results with confidence.

Very recently van Heiningen (1982) examined the effect of temperature difference but over quite a small range 10°C to 50°C of ΔT. After testing several alternate forms of incorporating the effect of temperature dependent physical properties van Heiningen adopted the procedure of evaluating all properties at the nozzle exit temperature, T_j, and including a dimensionless temperature ratio, T_j/T_s.

A number of studies are available on the effect of high temperature difference on heat transfer for confined and unconfined flows. Extensive reviews have been made by Kays (1966), Petukhov (1970), Shah and London (1978).

In engineering applications, one of two methods, the temperature ratio method and reference temperature method, are conventionally used to account for the large variation in physical properties which affects the value of all nondimensional parameters. In the first method the ratio of Nusselt number at bulk temperature (for a confined flow) and that at the constant property condition is related to the ratio of bulk temperature to a reference temperature, i.e.

$$\frac{Nu_b}{Nu_{Cp}} = \left(\frac{T_b}{T_o}\right)^n$$

where subscripts b, Cp and o refer to evaluation at the bulk, constant property and reference temperature condition. Usually surface temperature is used as reference temperature. By contrast, in the reference

temperature method all the properties are evaluated at some reference temperature so that no temperature ratio term is required in the correlation. The "film" temperature, the mean temperature between that of the surface and either the bulk temperature (for a confined flow) or a boundary condition temperature (for an unconfined flow) is a frequent choice of this reference temperature. Each method finds its own proponents in the literature. For design purposes the temperature ratio method can have some advantage in simplicity of use.

For the case of impinging jets, the temperature ratio equation can be written as

$$\frac{Nu_j}{Nu_s} = \left(\frac{T_j}{T_s}\right)^n$$

where subscripts j and s refers to measurements at the nozzle exit and impingement surface. Kays (1966) solved numerically for the case of a laminar two dimensional flow and obtained n = -0.1 for heating and -0.07 for cooling at the stagnation line. The experimental study on flow past cylinder for a cooling air by Kays and Nicoll (1963) showed n = 0.02 at stagnation. Over a small range of temperature difference, as noted before, van Heiningen did not observe any effect of temperature for heating and cooling impinging slot jet. However using n = -0.1 as suggested by Kays for hot jets, the maximum value of $(T_j/T_s)^n$ correction term for his data was less than 2% which was within the range of his experimental error. The author recommended the exponent values proposed by Kays for temperature ratio, T_j/T_s, in impinging jet correlations.

2.5 Objectives of Present Work

From literature review it is evident that no reliable data
exist on impingement heat transfer at variable and large temperature
differences between the jet and the impingement surface. A study was
therefore designed to investigate the effect of high temperature
differences on impingement heat transfer, with the following specific
objectives:

i) To obtain an extensive set of data on both local and
average heat transfer under a confined high temperature impinging slot
jet.

ii) To derive correlations for heat transfer in this system
which would adequately allow for the large variation in physical
properties associated with high temperature differences in such a way
as the correlations would embrace impingement heat transfer rates at
both high and low temperature differences.

CHAPTER III

EXPERIMENTAL EQUIPMENT AND PROCEDURE

3.1 Introduction

The experimental apparatus was designed for the study of impinging jet heat transfer at high temperature differences. Choice of the flow configuration and major parameters was influenced by those used in other studies in the program of investigation by the McGill impinging jet drying group. Thus for the present study equipment was built for measurement of profiles of local heat transfer under a confined, turbulent impinging slot jet. As high temperature differences between the jet and the impingement surface was the prime objective, a facility, with a hot jet impinging on a cool surface, was built which made it possible to use temperature differences up to 300°C. The effect of temperature difference up to this high level was determined for jet Reynolds numbers, over a range of 1000 to 20,000 and at impingement surface spacing from the nozzle exit in the range of 5 to 12 nozzle widths. This equipment and the experimental procedures used for obtaining profiles of local heat transfer are reported in this chapter.

3.2 Description of the Equipment

A schematic flow diagram for the experimental facility is shown in Figure 3.1. The hot air supply system, the blower, heater and accessories will be described following consideration of the impingement apparatus.

3.2.1 Impingement Apparatus

The impingement apparatus consists essentially of five sections:

i) Entrance section

ii) Plenum chamber
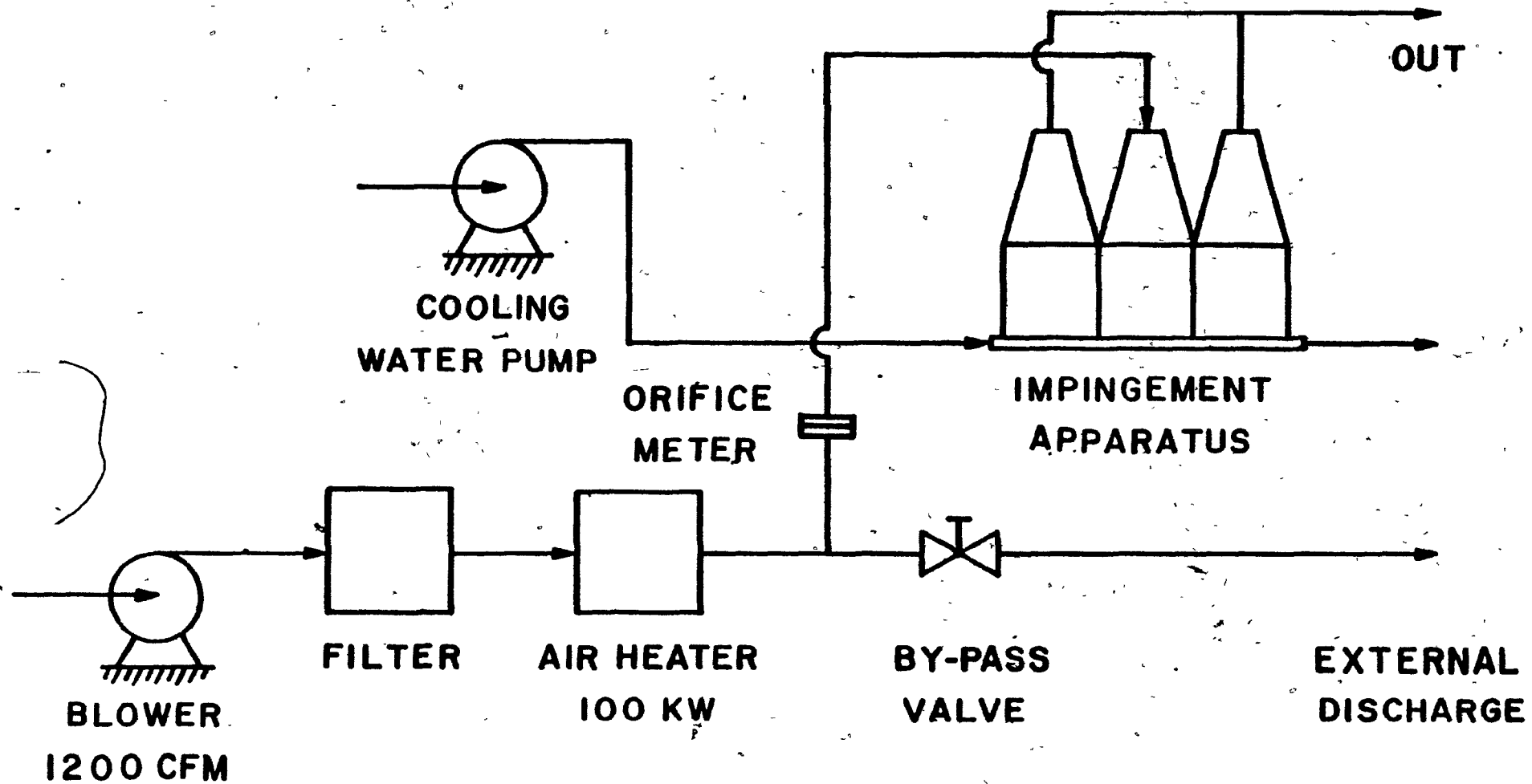
FIGURE 3.1   Flow Diagram of the Experimental Apparatus for High Temperature Impingement Heat Transfer

OUT

COOLING
WATER PUMP

ORIFICE
METER

IMPINGEMENT
APPARATUS

FILTER

AIR HEATER
100 KW

BY-PASS
VALVE

EXTERNAL
DISCHARGE

BLOWER
1200 CFM

iii) Nozzle, confinement surface, exit ports

iv) Side wall assembly

v) Impingement surface.

A general view of the impingement apparatus is provided by the photograph of Figure 3.2 while the close up photograph of Figure 3.3 shows the main elements with the front cover removed. The entire assembly, exclusive only of the impingement surface, was fabricated from 12.7 mm thick Marinite I (Johns-Manville Canada Ltd.), a material formed of calcium silicate with inert fillers and reinforcing agents. The usual application of Marinite I is as fireproof structural insulation. The substance was chosen as the construction material for the high temperature jet apparatus not only for its good insulating property but for its excellent structural strength, good machinability, high temperature resistance, low thermal expansion and non-corroding qualities. A detailed specification of Marinite I is presented in Appendix D. Two 1.2 m x 2.4 m sheets of Marinite I were sufficient for construction of the impingement assembly.

i) Entrance section:

As shown in Figure 3.3 this part of the apparatus has three compartments, i.e. the flow entrance central section between two exhaust flow duct at the sides. The central section connected the circular 76 mm ID inlet pipe to the 190 mm square plenum chamber. Thus the inside dimensions of this square cross section duct tapered from 76 mm to 190 mm over a length of 0.64 m, dimensions chosen to keep the angle of divergence to 5°. The two tapered side compartments of rectangular

FIGURE 3.2   Impingement Apparatus
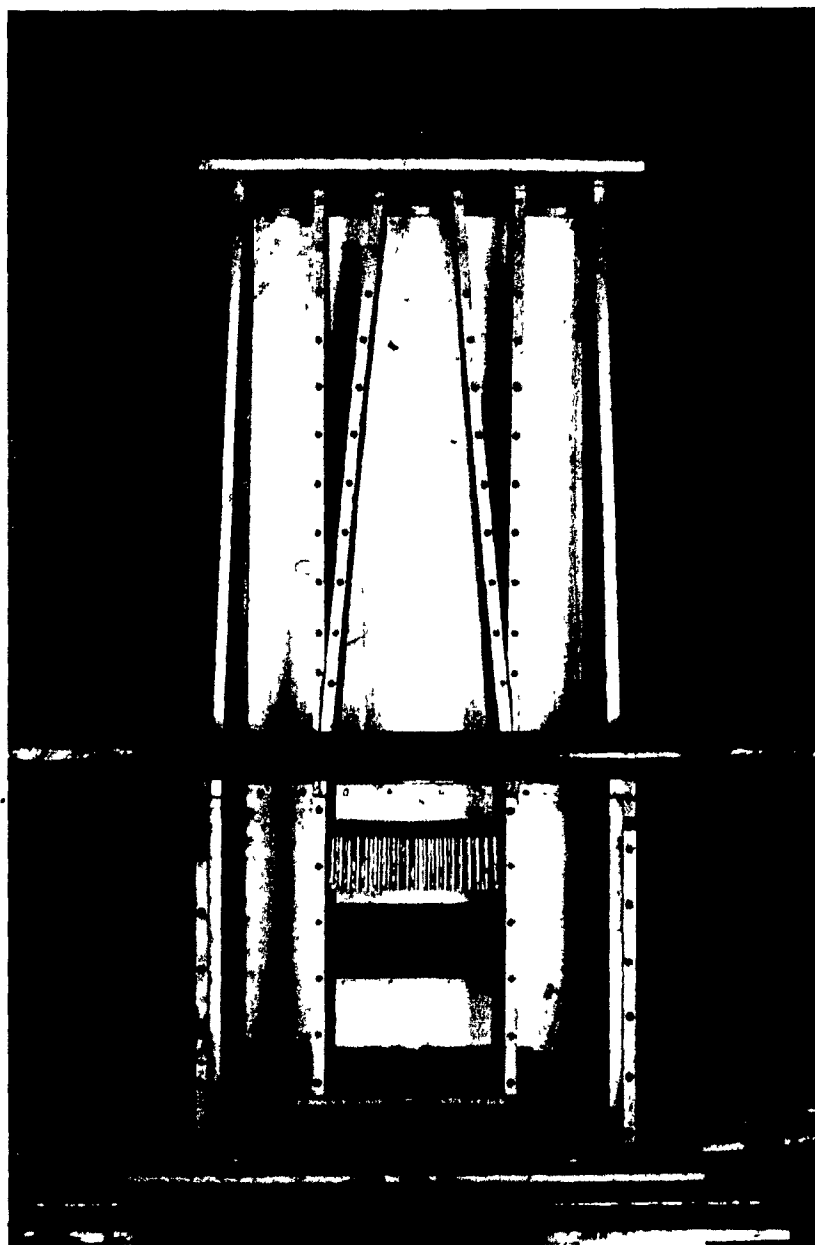
FIGURE 3.3   Inside View of Impingement Apparatus

cross section connected the rectangular exhaust chambers (190 x 92.5 mm inside dimension) to the upper flange where these sections terminated with a 76 mm square cross-section to match the two 76 mm ID exhaust pipes. As may be seen from both photographs a pair of large flanges provided the connection between the three square ducts of Marinite I and the corresponding three circular pipes for entrance and exhaust flows.

ii) Plenum chamber:

The objective of using a plenum chamber before the nozzle is to produce a uniform velocity over the length of the slot nozzle and to provide a controlled low turbulence level in the flow to the nozzle so that the flow characteristics of the jet at the nozzle exit would match those of previous studies, thus facilitating comparison of results. The plenum chamber, 190 mm square inside cross-section, was 305 mm in the flow direction. The 50 mm length of aluminium honeycomb (5 mm cell dimension) and two 100-mesh screens, all spaced about 40 mm apart can be seen on Figure 3.3.

iii) Nozzle, confinement surface, exit ports:

The present high temperature difference impingement heat transfer study was carried out with a confined single slot jet 6 mm wide, with the spent flow exiting through two exhaust ports each 61 mm wide. The nozzle was fabricated with an elliptic inlet and a square exit according to the ASME standard, in order to provide a jet of flow characteristics comparable to studies at low temperature difference. Although there are more numerous studies of unconfined jets, the present investigation with a confinement surface continues the orientation of the program of studies from this laboratory which are motivated by industrial applications such

as the drying of paper for which a confinement hood must be used. The dimensions were selected to provide the same ratio of jet width to centreline spacing between inlet nozzle and exhaust ports as existed in pilot plant Papridryer, i.e. a ratio of 0.035, conventionally termed as 3.5% open area.

A pair of Marinite plates, 9.6 mm thick, machined at one end with an elliptic profile for the inlet jet and at the other end with a square edge for the exhaust port, were fixed to the bottom of the plenum chamber, thus providing three elements of the impingement apparatus, i.e. a 6 mm wide nozzle, 136 mm wide confinement surfaces and 61 mm wide exhaust ports.

This pair of plates is seen clearly in Figure 3.3. As the nozzle plates were fixed to the inside of the retaining side walls of the apparatus, the transverse length (ℓ) of the nozzle was the same as this dimension of the nozzle plate confinement surface, i.e. 190 mm. The corresponding high aspect ratio ($\ell/w = 31.67$) assured two dimensional flow over most of the width of the impingement surface, as has been documented in a recent study by Saad (1981) in this laboratory.

The nozzle plates were fabricated of Marinite I because of the low coefficient of thermal expansion of this material (Appendix D). Thus from ambient temperature to the maximum jet temperature used, about 300°C, a 136 mm wide sheet of Marinite would expand only by 0.14 mm, 2.3%, a very small value relative to 6 mm nozzle width. A schematic diagram of nozzle is shown in Figure 3.4.

(iv) Side wall assembly:

The flow retaining hood of the impingement apparatus comprised

$w = 6\,mm$
$r_1 = w = 6\,mm$
$r_2 = 2/3\,w = 4\,mm$
$L_f = 0.6\,w = 3.6\,mm$
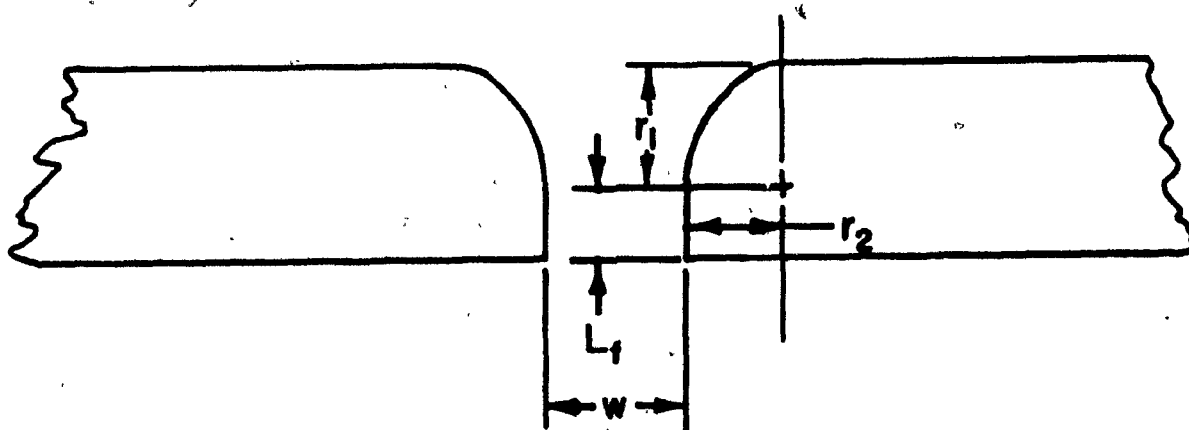
FIGURE 3.4   Schematic of Nozzle

the assembly of four side walls and the confinement surface 136 mm wide
from nozzle inlet to exhaust port. As the side walls made a closely
fitting, sliding contact on the plenum-exhaust chamber assembly, 425 x
215 mm, inside dimension of the former was also the outside dimension of
the latter. This sliding arrangement derived from the objective of
varying the impingement surface spacing from the nozzle exit, while
maintaining a totally enclosed, two dimensional flow impingement system
from which the spent flow exited only through the two exhaust ports.
Slotted grooves two on the ends and three on the sides, and retaining
screws provided a convenient vertical adjustment of the side wall assem-
bly. The impingement surface could thereby be spaced from 30 to 72 mm
(i.e. from 5 to 12 nozzle widths) from the nozzle exit.

v) Impingement Surface:

The impingement surface was a copper plate, 305 x 165 x 6.4 mm
thick. Copper was selected for its good thermal conductivity which
facilitated obtaining a nearly uniform surface temperature as this, not
the constant heat flux, boundary condition was chosen for the present
study. The impingement surface was kept nearly isothermal by a high
throughput channel flow of cold water in direct contact with the lower
surface of the copper impingement plate. For the extreme case of a
300°C jet the variation of surface temperature was only by 2°C from
stagnation to a position 20 nozzle widths from the nozzle centreline.
This cooling water passed through a rectangular channel of galvanised
steel soldered to the copper impingement plate. The channel was 7 mm
deep, 165 mm wide (i.e. the same as the impingement plate width) and
was somewhat longer (350 mm) than the impingement plate length (305 mm).

High melting (221°C) silver solder was used because of the necessity to
cure the heat flux sensor adhesive at 150°C, as described subsequently.
Two tapered galvanised steel sections 0.7 m long provided adaptation
from the 165 x 7 mm rectangular cooling channel to the 51 mm diameter
cooling water pipe. To allow for lateral and vertical traversing of
the impingement surface, the final connections to inlet and outlet water
lines were made through flexible rubber hoses. As may be seen in
Figure 3.3, the impingement assembly comprising the copper plate and
steel cooling channel was supported in a 600 x 300 x 40 mm thick Marinite I
base so that the 305 x 165 mm copper impingement surface was flush with
the surrounding Marinite I surface. The two tapered steel cooling
channels extending on either side of the plate were likewise made flush
with the Marinite surface using Kyanex cement (Canadian Refractories
Ltd.).

The research objectives required that the impingement surface
position be adjustable both vertically and horizontally, the vertical
positioning to provide variable spacing from the nozzle exit, the hori-
zontal traversing to enable lateral profiles of local heat transfer to
be made. The horizontal traversing was provided by mounting the 40 mm
Marinite base on a horizontal aluminium platform (760 x 380 x 10 mm)
which could be moved horizontally along the longer axis by a screw
mechanism connected to the traversing control wheel visible in the
central part of Figure 3.2. This horizontal platform was in turn
supported on a sturdy, inverted L-shaped platform, the vertical leg of
which could be moved up and down by a second screw mechanism, the verti-
cal positioning control wheel which appears near the left bottom of
Figure 3.2. This system for control of vertical and horizontal position

of the impingement surface exceeded the requirements of the present study, i.e. vertical positioning of impingement surface spacing from 30 to 72 mm (5 to 12 nozzle widths) from the nozzle exit, and horizontal traversing up to 72 mm (12 nozzle widths) on either side of the nozzle centreline.

Temperature of the impingement surface was measured by Teflon insulated, Chromel-Constantan thermocouples supplied by Omega. Twelve thermocouples were placed from the centre along the longer axis at a spacing of 10 mm. Thermocouples were located in holes drilled from the bottom to within 0.5 mm of the surface, the leads being carried out through 1 mm ID copper tubes soldered to the bottom of the impingement plate and to the cooling duct before passing through the Marinite I base. The thermocouple beads were epoxied to prevent electrical contact with copper plate. The thermocouple leads were connected to the 40 point selection switch (Omega) which was in turn connected to a digital readout meter (Model 410A, Omega) through a cold junction compensator (Model CJ-E, Omega).

3.2.2 Heat Flux Sensor

Local heat flux at the impingement surface was measured with extremely thin (0.18 mm), "micro-foil" heat flux sensors (Model 20450-1) manufactured by RDF Corporation, Hudson, New Hampshire. The working principle and specifications of the sensors are given in Appendix E. The overall size of the rectangular sensor used was 11 mm x 7 mm, but the heat sensing area was much smaller, 4.78 mm x 1.9 mm. The sensors were flush mounted in the plate with longer sensor dimension parallel to the longer axis of the nozzle. Thus the small ratio of sensor width to

nozzle width (0.32) provided excellent resolution of local Nusselt number. The overall thickness of this sensor was 0.18 mm, including its protective polymide film.

A sensor was mounted in a groove (11.25 x 7.25 x 0.31 mm deep) in the impingement surface. The sensor was fixed in place by a highly conductive (k = 22.5 W/m°K) silver suspended, epoxy adhesive (Uniset) supplied by American Polymer Products Ltd. The surface of the sensor was flush with the impingement surface. The sensor leads were taken out through a 1.5 mm ID copper tube placed in a small groove along the copper surface and surrounding Marinite base. The space between the copper tube and the copper impingement surface was filled with Uniset which required one hour curing at 150°C. The surface was then flush ground.

After completing a set of runs at the lowest jet temperature, 50°C, two more sensors were mounted in the same way at a distance of 36 mm on each side of the central one in order to reduce experimental time. Unfortunately, after completion of the experiments at 100°C jet temperature one of the additional sensors was accidentally rendered inoperative, so the remainder of the experiments were completed with two sensors, still a considerable advantage over the single sensor initially installed.

The leads from the heat flux sensors were connected to a digital nanovoltmeter (Model 180, Keithley Instruments) through a low resistance (0.004 m ohm), 40-point selection switch (Model OSW5-40), Omega Engineering Inc., Connecticut.

3.2.3 Air and Cooling Water Supply System

A blower of capacity at 1200 cfm at 30 psi (Canadian Sirocco Co. Ltd.), directly driven by a two speed (3470/1730 rpm), 30 HP, 550 Volts, three-phase synchronous motor (Bepco Canada Ltd.) drew air from the laboratory at a flow rate controlled by a gate valve at the blower inlet. The air was passed through a fire resistant filter (American Air Filter of Canada Ltd.) to remove dust which could damage the heater. The air was heated by a single-stage 100 KW, 550 Volts duct heater (E.W. Playford Co., Montreal) of square cross-section 0.6 m x 0.6 m. Adapting sections, 0.7 m in length, connected the 0.6 m square heater to 0.2 m diameter aluminium pipe on either side. As the air heater could not be operated at full power at a flow rate of less than 400 cfm, a flow considerably greater than that required for the maximum jet Reynolds number was used. This restriction required installation of a by-pass for discharge of excess hot air outside the building. The air flow rate to the jet apparatus was controlled by a butterfly valve in the 0.2 m diameter by-pass line. All lines were joined with aluminium flanges with high temperature resistant (650°C) asbestos used for gaskets. All pipes were insulated by 25 mm or 50 mm thick fibreglass.

The exit air temperature from the heater was designed to be controlled by a 150 A SCR proportional controller (Honeywell Model R7308E1259) with a 135 ohm potentiometer and a mercury filled temperature sensing element in the discharge air line. To protect the heating elements there was also an over-temperature cut-out (Canadian Chromalox Co. Ltd. Model ARC254). As in practice this instrumentation did not provide a sufficiently steady temperature, this control system was replaced by a

simpler arrangement. Thus in all experimental work for jet temperatures at and above 150°C the power to the heater was controlled simply by a 135 ohm potentiometer set manually by reference to the temperature of the jet nozzle.

For runs at jet temperatures up to 300°C (heater exit temperature corresponding to about 350°C), the heater was insulated on all sides to a thickness of 12.5 mm with ceramic blanket. When that temperature level was reached it was necessary to strip the insulation from the heater in order to prevent overheating and thus structural weakening of the walls of the heater which, unfortunately, had not been insulated on the inside by the heater manufacturer. With the air flow rate to the heater reduced by the valve at the blower inlet to about 400 cfm, the maximum heater exit temperature which could be obtained with the heater uninsulated was just slightly above 350°C, thus limiting the present study to a maximum jet temperature of about 300°C.

The air flow rate in the 76 mm diameter aluminium line to the impingement apparatus was measured by a square edged, 38.1 mm diameter, stainless steel orifice plate using flange taps. The orifice plate was located at 1.2 m (i.e. 16 pipe diameters) downstream of flow straightening vanes, a 120 mm length of honeycomb with 5 mm wide cells installed in this pipe. The pressure difference across the orifice was measured by a U-tube manometer with Merium fluid or, for lower flow rates, by an inclined manometer.

Temperature of hot air at the orifice and at the nozzle exit was measured by 2.4 mm diameter, high temperature resistance (540°C) glass braid insulated, Chromel-Constantan thermocouples. These temperatures were also read from the digital readout meter.

The large flow of cooling water required to maintain an essen-
tially uniform impingement surface temperature was provided by a Fair-
bank-Morse pump of capacity 0.57 m^3/min at 150 kPa pressure, driven by a
550 V, 5 H.P. motor. The cooling water was recirculated through a 1 m^3
tank with a bleed to the drain and a make-up connection.

3.3 Experimental Procedure

A straight forward steady state technique was used in this
experiment. At a particular nozzle to impingement surface spacing, jet
Reynolds number and jet temperature, the system was allowed to reach
steady state, which took about an hour. The flow rate, temperature at
the orifice and at nozzle exit were measured. The local heat transfer
profile was obtained by lateral traversing of the impingement surface
with its heat flux sensors. About 5 minutes were required at each lateral
position in order to reach steady state. —As mentioned earlier, nozzle
width, w, was 6 mm and spacing between the two sensors was 36 mm, i.e.
6w. The output from the sensors read from nanometer in microvolts was
converted to heat flux in Watt/m^2 by the calibration factor and surface
temperature correction factor supplied by the manufacturer. The pro-
cedure used with three sensors is illustrated on Figure 3.5. Horizontal
traversing of the impingement surface was carried out in increments of
6 mm (1w). Although five increments would provide a complete set of
measurements, six increments were used in order to provide a check
between different sensors at the same position. The heat flux was
thereby measured at 19 positions, out to 18 w from the stagnation line,
including heat flux measurements by different sensors at the same

SENSORS

6w, 12w, 18w, etc.
are distances from
stagnation point O.

A B C

B

C

O   A   6w   12w   18w

INITIAL POSITION
OF IMPINGEMENT SURFACE

A   B   C

A   B   C

DIRECTION OF
TRAVERSING OF SURFACE

FINAL POSITION OF
IMPINGEMENT SURFACE
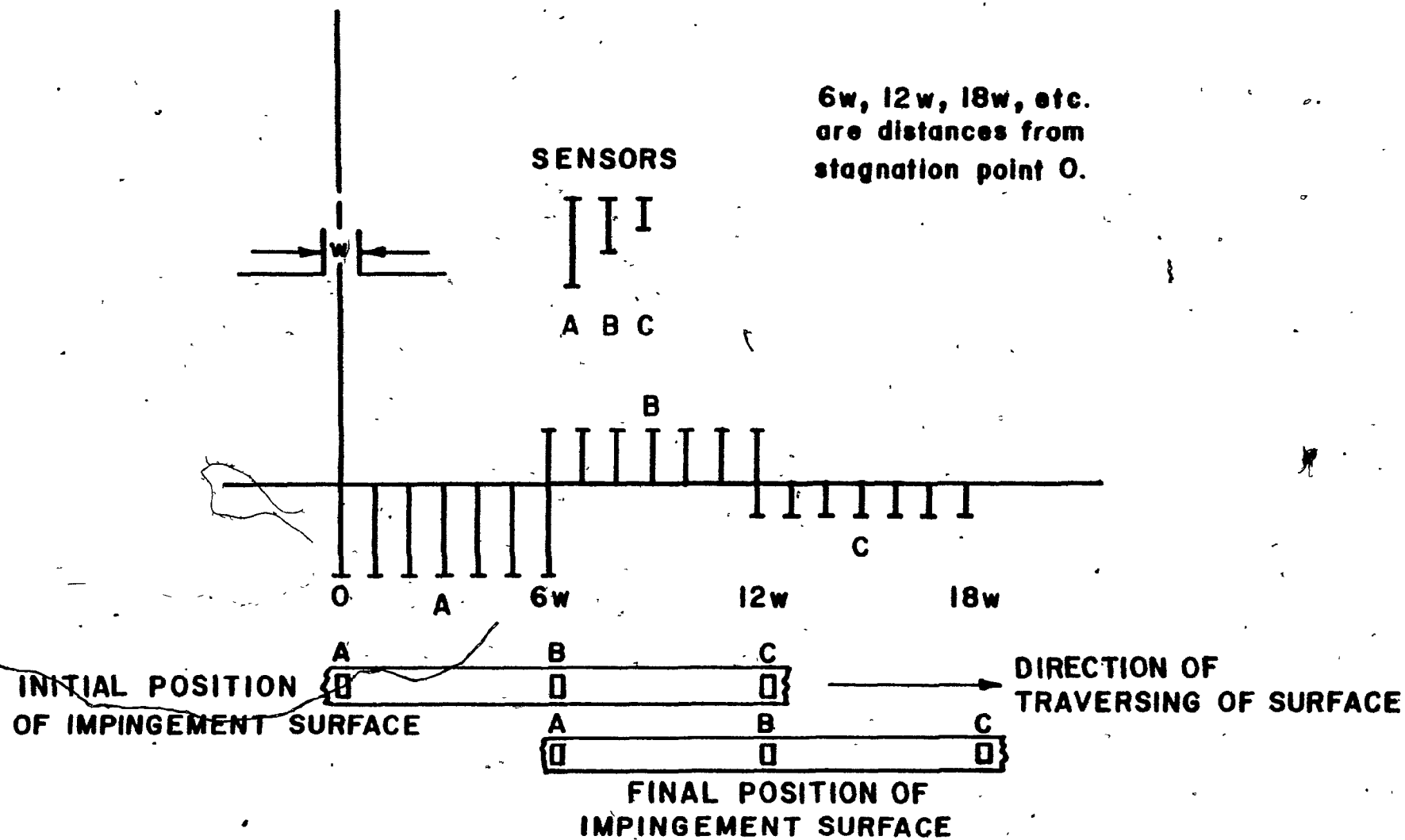
FIGURE 3.5   Traversing for Lateral Profile of Local Heat Flux

39

position. Symmetry of the heat flux distribution was also checked for each run.

For each position of the impingement surface, the temperature at nozzle exit and temperature of the surface near the sensor were measured. As the thermal conductivity of the protective polymide layer on the sensor was less than that of the copper impingement plate, the temperature of the sensor surface was slightly higher than the impingement surface. Also there was some radiative heat transfer from the hot air jet to the cold impingement surface. Corrections for radiative heat transfer and differences in sensor and surface temperature are shown in Appendices F and G.

CHAPTER IV

RESULTS AND DISCUSSION

4.1 Results

4.1.1 Range of Experimental Conditions

The range of experimental conditions used in this study of con-
fined impinging-slot jet heat transfer is given in Table 4.1. Three
independent parameters were varied: the temperature difference, nozzle
exit to impingement surface, $\Delta T = T_j - T_s$; the dimensionless impingement
surface spacing from the nozzle H/w; and the nozzle exit Reynolds number,
Re_j. Local heat flux was measured at 19 poistions along impingement
surface, from x/w = 0 to x/w = 18, for all combinations of values of ΔT,
H/w and Re_j shown in Table 4.1, with the sole exception that runs at
Re_j = 20,000 were carried out only for values of ΔT of 50° and 100°C.
A total of 104 runs were made.

Table 4.1 shows the nominal or target conditions for the experi-
ments. The actual operating conditions, which varied somewhat from
these nominal values, are shown in Appendix A.

The range of dimensionless nozzle to surface spacing, H/w, from
5 to 12, was chosen to bracket the value, H/w = 8, which has been
reported to give maximum heat transfer rates at the stagnation line.

The dimensionless flow and heat transfer parameters, Reynolds
and Nusselt numbers, and the Prandtl-number require physical properties
viscosity, μ, density, ρ, thermal conductivity, k, specific heat, Cp,
which vary significantly with temperature. For the present case which
focusses on high differences in temperature between nozzle exit, T_j, and
impingement surfaces, T_s, the reference temperature used for evaluation
of all such physical properties was the nozzle exit temperature, T_j, for
reasons discussed in detail later. These properties are then designated
as μ_j, ρ_j, k_j, Cp_j.

Table 4.1 Nominal Values of Independent Variables

Variable	Nominal Values of Variables
Re_j	1000, 5000, 10000, 15000, 20000*
H/w	5, 8, 10, 12
$T_j - T_s$, °C	50, 100, 150, 200, 250, 300
T_j/T_s	1.18, 1.35, 1.53, 1.71, 1.88, 2.06
x/w	0, 1, 2, 3, 4, ... 18

* $Re_j = 20000$ was used only at $\Delta T = 50°$ and $100°C$.

The basic flow parameter, jet exit Reynolds number, taken then as

$$Re_j = \frac{wv_j \rho_j}{\mu_j} \tag{4.1}$$

was varied from 1000 to 15000 (and 20,000 for values of ΔT of 50°C and 100°C). This range included that of the mill trial Papridryer at the low end (Re_j of 1000 to 3000), while the higher values provide comparison with the low ΔT results of previous studies by Gardon and Akfirat (1966), Cadek (1974) and Saad (1981).

The independent variable of prime interest in the present work is the ΔT between the hot jet, T_j, and impingement surface, T_s. The surface temperature was kept low and essentially uniform over the surface, at levles in the range 3° to 11°C (Appendix A). During a run temperature variation over the impingement surface was less than 2°C along the entire length of the surface. The nominal ΔT was varied from 50°C to 300°C in increments of 50°C. This range bridges the gap between the low ΔT results of previous investigations and the high ΔT of interest in industrial application of impingement heat transfer for drying.

4.1.2 Basis of Local and Average Nusselt Number

The dependent variable measured in this study was local heat flux (q_c) from the heating jet to the impingement surface. From this heat flux the convective heat transfer coefficient is first obtained in the way conventional for impingement heat transfer, by normalizing the flux to the temperature difference $T_j - T_s$, i.e.

$$h = \frac{q_c}{T_j - T_s} \tag{4.2}$$

In this conventional representation the heat flux, q_c, is a function of lateral position along the heat transfer surface while the ΔT used, $T_j - T_s$, is not a function of lateral profile. Thus the heat transfer coefficient profile, as defined by equation 4.2 is essentially the heat flux profile, not heat transfer profile. An alternative to this conventional treatment is developed in Section 4.5 using temperature difference as a function of lateral position.

For the dimensionless heat transfer coefficient, Nusselt number, the characteristic dimension, nozzle width, w, was used, i.e.

$$Nu_j = \frac{hw}{k_j} \qquad (4.3)$$

Average Nusselt number was calculated by numerical integration as

$$\overline{Nu_j} = \frac{1}{x/w} \int_0^{x/w} Nu_j \, d(x/w) \qquad (4.4)$$

The results for local and average heat transfer rates for all 104 runs are listed in Appendices B and C respectively.

4.2 Stagnation Heat Transfer

Although heat transfer rates at the stagnation line have only limited practical significance they have been studied by numerous investigators because stagnation heat transfer constitutes a sensitive standard characteristic of an impinging jet.

4.2.1 Effect of Reynolds Number and Spacing

The effect of Re_j on Nu_{oj} at all values of H/w is shown by

Figure 4.1. The data shown cover the full experimental range of ΔT and may be represented logarithmically by straight lines of slope 0.5. Detailed discussion of the quantitative relationships derived from these data follows in Section 4.2.3.

The effect of impingement surface spacing, H/w, appears explicitly on Figure 4.2 for all five levels of Re_j used. The data at $\Delta T = 50°C$ shown are typical of the trends at all values of ΔT. Stagnation Nusselt number passes through a maximum at a spacing of approximately 8w except for the laminar jet case, $Re_j = 1000$. This maximum for turbulent jets is well known from previous studies by Gardon et al. (1966), Cadek (1974), Daane and Han (1961) and most recently by Saad (1981). This maximum derives from the combined effect of centreline velocity and turbulence intensity, as convective heat transfer increases with both these variables. In the potential core of a slot jet, which extends to about 8w from the nozzle exit, the centreline velocity remains essentially constant while the turbulence intensity increases rapidly with distance from the nozzle exit. Beyond the potential core the turbulence intensity increases more slowly but the centreline velocity drops sharply. Thus the maximum in Nu_{oj} at about H/w = 8 reflects the fact that Nu_{oj} is dominated for lower spacings by the increase of turbulence with distance from the nozzle exit, and for larger spacings by the decay of mean velocity. Saad (1981) has presented a quantitative analysis of the combined effect.

For the case of the jet which is laminar at the nozzle exit, i.e. for $Re_j = 1000$, it is necessary also to consider whether the jet is still laminar on arrival at the impingement surface. In this regard
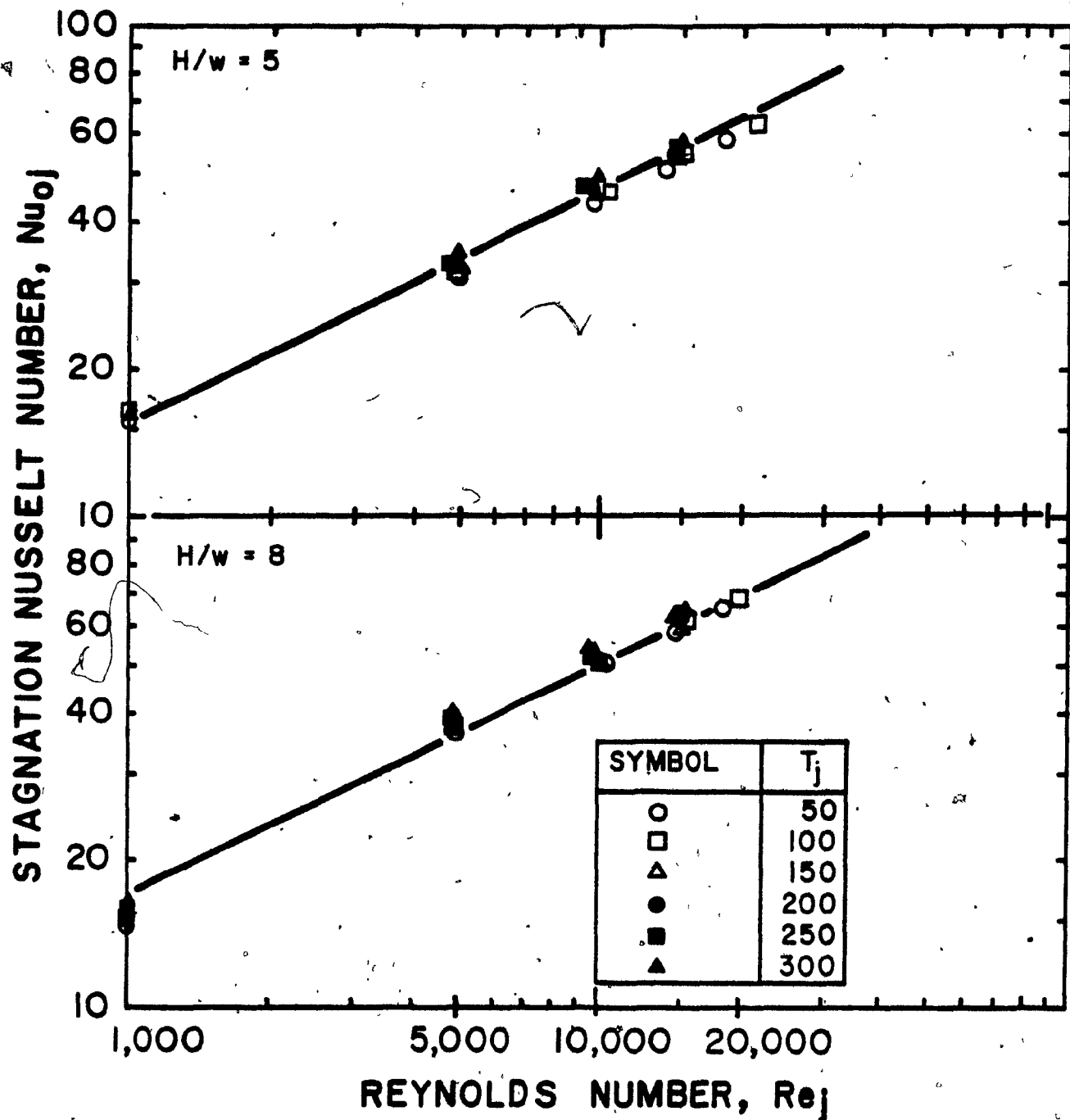
FIGURE 4.1a Effect of Re_j on Nu_o with ΔT as Parameter at Spacing 5 and 8
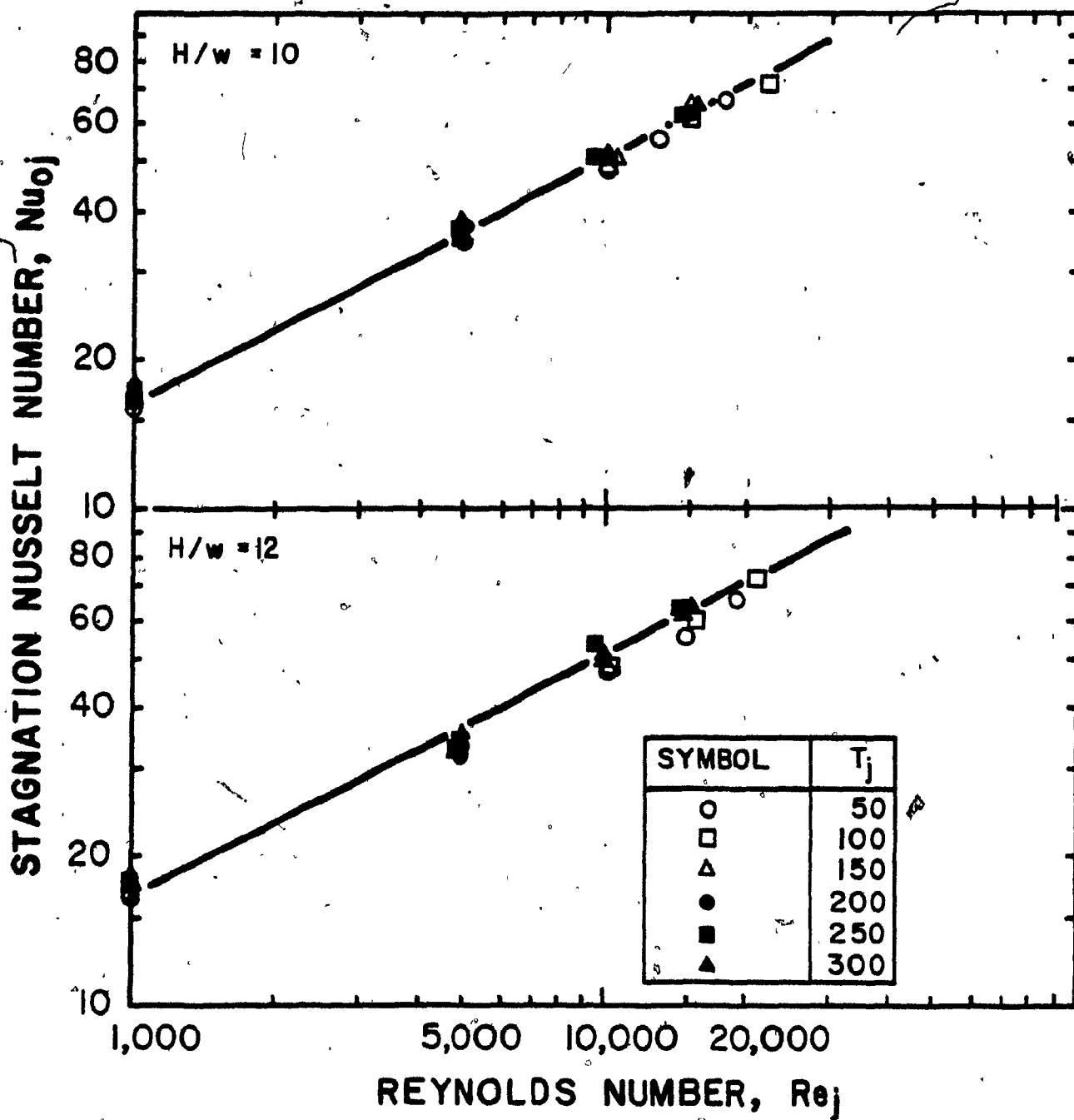
FIGURE 4.1b . Effect of Re_j on Nu_o with ΔT as Parameter at Spacing 10 and 12
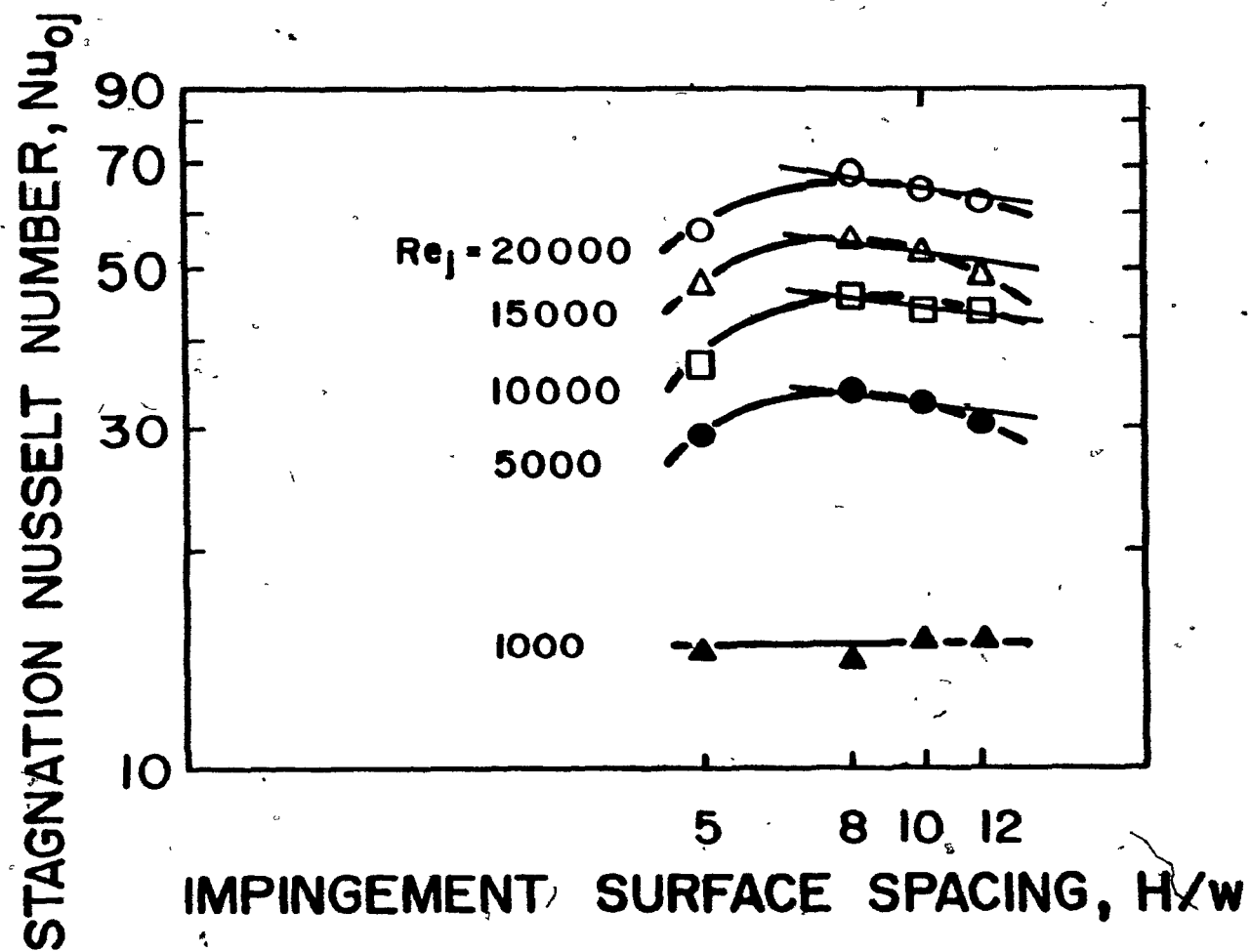
FIGURE 4.2   Effect of H/w on Nu_o with Re_j as Parameter

the data of Sparrow and Wong (1975) indicate that, for $Re_j = 950$, a jet will still be laminar for an impingement surface spacing $H/w < 10$. Thus it appears that, for the present case of $Re_j = 1000$, the jet remains laminar except for the largest spacing, $H/w = 12$, for which transition to a turbulent jet may be starting as the jet arrives at the impingement surface. The numerical predictions by van Heiningen (1976) show that heat transfer under a laminar impinging slot jet, $Re_j = 950$, is quite insensitive to spacing, a prediction that is confirmed by the experimental findings of the present study.

4.2.2 Effect of Temperature Difference

As the present study is particularly oriented towards the influence of large differences in temperature between jet and impingement surface, this effect on stagnation heat transfer when the latter is represented as Nu_{oj} is illustrated on Figure 4.3. The data presented in this figure, i.e. for $H/w = 8$, at two values of Re_j, 5000 and 10000, are representative of all levels of H/w and Re_j tested. With heat transfer expressed as Nu_{oj} it is seen that Nu_{oj} is only a slight function of the temperature variable T_j/T_s. The slope displayed on Figure 4.3 corresponds to Nu_{oj} proportional to $(T_j/T_s)^{-0.11}$, a relationship to be discussed in detail subsequently.

4.2.3 Quantitative Analysis

With all physical properties evaluated at T_j, stagnation Nusselt number may be conveniently expressed as a power function of the independent variables in the form

$$Nu_{oj} = K \, Re_j^a \, (H/w)^b \, Pr_j^c \qquad (4.5)$$
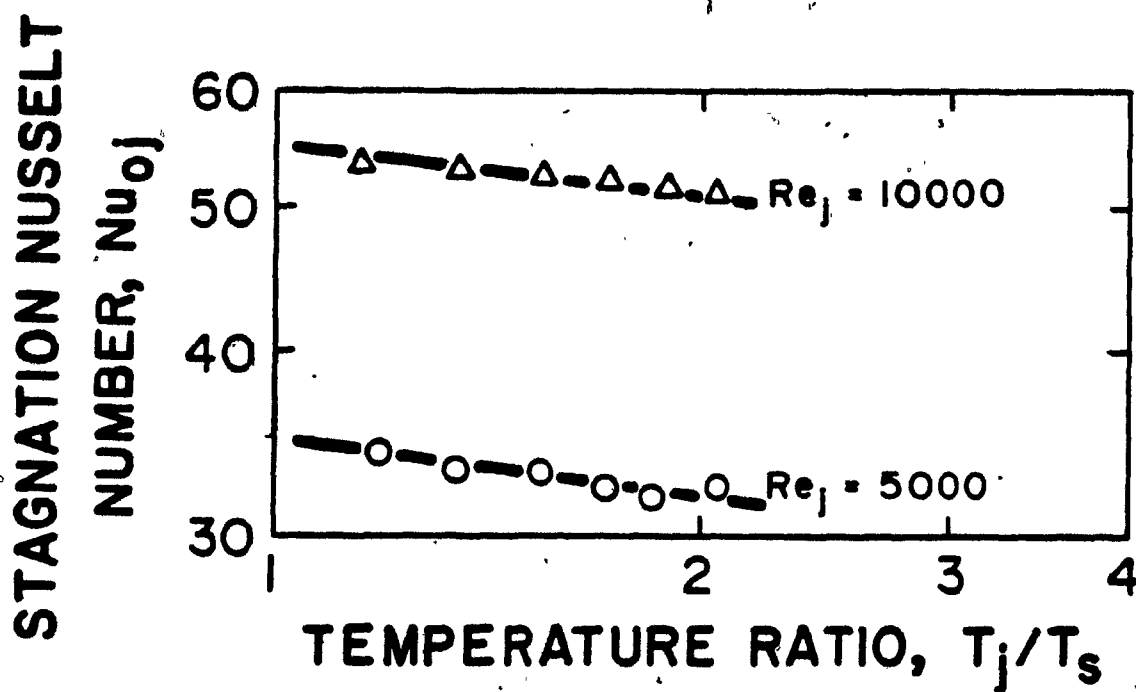
FIGURE 4.3   Effect of T_j/T_s on Nu_o with Re_j as Parameter

The correlations developed by various workers are summarized in Table 2.1.

The temperature dependency of physical properties was not a major effect for earlier studies made at low temperature differences between the jet and the impingement surface. However, as the basic focus of the present investigation is impingement heat transfer for values of ΔT up to 300°C, treatment of the very large variation of physical properties between the limits of T_j and T_s becomes a central concern.

As discussed in Section 2.4, the effects on heat transfer of variable physical properties at high temperature differences can be accounted for by either the temperature ratio method or the reference temperature method. The critical analysis of these alternate methods is carried out using the experimental measurements of heat transfer rate at the stagnation line.

In the temperature ratio method the Nusselt number is taken as proportional to some exponent of the ratio of relevant temperatures, expressed as absolute temperature. For impinging jet heat transfer the relevant temperatures are the nozzle exit and the impingement surface temperatures, T_j and T_s. Thus the temperature ratio approach may be expressed for stagnation line heat transfer in the form

$$Nu_o = K \, Re_j^{\ a} \, (H/w)^b \, (T_j/T_s)^c \, Pr_j^{\ d} \qquad (4.6)$$

thereby indicating that Re and Pr are evaluated at T_j while leaving open the choice of temperature basis for evaluating Nu_o. In the evaluation of Reynolds number the use of T_j is the logical physical property reference temperature as this is the temperature at the position of the characteristic dimension, w, used in Re, i.e. at the nozzle exit. However,

as heat transfer occurs throughout the entire extent of the fluid there is no such clear choice for the temperature to be used for the physical property appearing in Nusselt number.

The concept of the reference temperature method is to choose the temperature basis for the Nusselt number so that without a temperature ratio term the correlation accounts adequately for the effect of temperature dependent physical properties. For the stagnation Nusselt number, this equation may be expressed as

$$Nu_o = K \, Re_j{}^a \, (H/w)^b \, Pr_j{}^d \qquad (4.7)$$

indicating that Re and Pr are evaluated at T_j while Nu_o is evaluated at a reference temperature, T_{ref}, which eliminates the need for a temperature ratio term.

The temperature ratio approach was applied for three alternate bases of expressing Nu_o, i.e. evaluation of Nu_o at T_j, T_s and at T_f, the flux temperature conventionally defined as, $T_f = 0.5(T_j + T_s)$. As the variation of Pr_j was not great, the exponent, d, in equation 4.6 is chosen as 1/3 from literature. The best values of the four constants K, a, b, c were determined by a linearized logarithmic fit of these equations to the data using the standard multiple linear regression "STATPAK" program of the McGill Computing Centre for each of the three alternatives noted, i.e.

$$Nu_{oj} = K_1 \, Re_j{}^{a_1} \, (H/w)^{b_1} \, (T_j/T_s)^{c_1} \, Pr_j{}^{1/3} \qquad (4.8)$$

$$Nu_{of} = K_2 \, Re_j{}^{a_2} \, (H/w)^{b_2} \, (T_j/T_s)^{c_2} \, Pr_j{}^{1/3} \qquad (4.9)$$

$$Nu_{os} = K_3 \, Re_j{}^{a_3} \, (H/w)^{b_3} \, (T_j/T_s)^{c_3} \, Pr_j{}^{1/3} \qquad (4.10)$$

With respect to the effect of H/w the well known fact of a maximum in Nu_o around H/w = 8 was noted in Section 4.2.1 and displayed in Figure 4.2. Thus all data for H/w = 5 was excluded from the correlation which thereby represents a linearization of the data over the range of spacing, H/w, from 8 to 12. The constants of equation 4.8, 4.9 and 4.10 are listed in Table 4.2 for two Reynolds number ranges (1000-20000 and 5000-20000). The numbers in parentheses below the exponents are the "t" values for each exponent.

For the wider Reynolds number range (1000-20000), the exponents for H/w are not significantly different from zero at the 95% confidence level. Figure 4.2 clearly indicates that Nu_o does not vary significantly with H/w for the laminar jet case. Thus inclusion of the results for Re_j = 1000 is not valid and moreover obscures the effect of H/w for turbulent jets. When the Re_j = 1000 data are excluded, the exponents for H/w also become significant. The exponents of Re_j and T_j/T_s did not change significantly with exclusion of the laminar jet results.

The exponents for Re_j and H/w are seen from Table 4.2 to be quite insensitive to the temperature basis used to calculate Nu_o. The exponent for T_j/T_s, on the other hand is quite sensitive to the choice of reference temperatures. But for all these equations this temperature exponent was highly significant. As all three reference temperatures yield equally good correlations, the most convenient choice was made; equation 4.8 in which all fluid properties are evaluated at T_j. Should this equation be applied to iterative calculations to determine T_s as is frequently the case in drying rate calculations, the physical properties based on T_j remain unchanged throughout all of the iterations.

TABLE 4.2. List of Coefficients and Exponents of Equation 4.8, 4.9, 4.10

Equation No.	Coefficient K	Range of Re_j	Exponent a, for Re_j	Range of H/w	Exponent b, for H/w	Range of T_j/T_s	Exponent e, for T_j/T_s	Nu_o evaluated at
4.8	0.648	1,000–20,000	0.485 (113.2)	8–12	−0.045 (1.7)	1.18–2.06	−0.111 (4.9)	T_j
4.9	0.664	1,000–20,000	0.484 (114.2)	8–12	−0.048 (1.8)	1.18–2.06	+0.188 (8.4)	$T_f = (T_j + T_s)/2$
4.10	0.644	1,000–20,000	0.484 (111.6)	8–12	−0.041 (1.5)	1.18–2.06	+0.650 (28.5)	T_s
4.8	0.791	5,000–20,000	0.485 (58.3)	8–12	−0.134 (5.5)	1.18–2.06	−0.115 (5.6)	T_j
4.9	0.800	5,000–20,000	0.486 (59.7)	8–12	−0.138 (5.8)	1.18–2.06	+0.185 (9.2)	$T_f = (T_j + T_s)/2$
4.10	0.750	5,000–20,000	0.490 (56.7)	8–12	−0.129 (5.1)	1.18–2.06	+0.645 (30.4)	T_s

The exponent of T_j/T_s in equation 4.8 is -0.115. The only other value in the literature for this exponent of the temperature ratio is the value -0.10 , evaluated numerically by Kays (1966) for a laminar stagnation Nusselt number. The exponents for equation 4.8, 0.485 for Re_j and -0.134 for H/w were used in the regression lines on Figures 4.1 and 4.2 respectively. Figure 4.3 illustrates the use of T_j/T_s as a correlating parameter for Nu_{oj} over the wide range of ΔT covered by the present experimental study. The recommended form of the temperature ratio correlation for a turbulent jet is then

$$Nu_{oj} = 0.79 \, Re_j^{0.485} \, (H/w)^{-0.134} \, (T_j/T_s)^{-0.115} \, Pr_j^{1/3} \qquad (4.11)$$

As Table 4.2 shows the considerable dependency of the temperature ratio exponent on the temperature basis for calculating Nu_o (i.e. T_j, T_f or T_s), these results provide an effective way of determining the value of T_{ref} which would eliminate the need for a temperature ratio term, as is illustrated on Figure 4.4. It is evident from this figure that the temperature which makes the exponent, c, vanish is $T_{ref} = T_j - 0.2(T_j - T_s)$. Evaluation of Nu_o at this temperature in fact gave the following regression equation:

$$Nu_{oT_{ref}} = 0.648 \, Re_j^{0.485} \, (H/w)^{-0.138} \, (T_j/T_s)^{-0.002} \, Pr_j^{1/3} \qquad (4.12)$$

The maximum effect of the temperature term, $(T_j/T_s)^{-0.002}$, is totally insignificant, corresponding to only a 0.15% correction for the most wide temperature range investigated. Hence for a turbulent slot jet over the range of spacing, H/w, from 8 to 12, the correlation for Nu_o using the reference temperature method is:
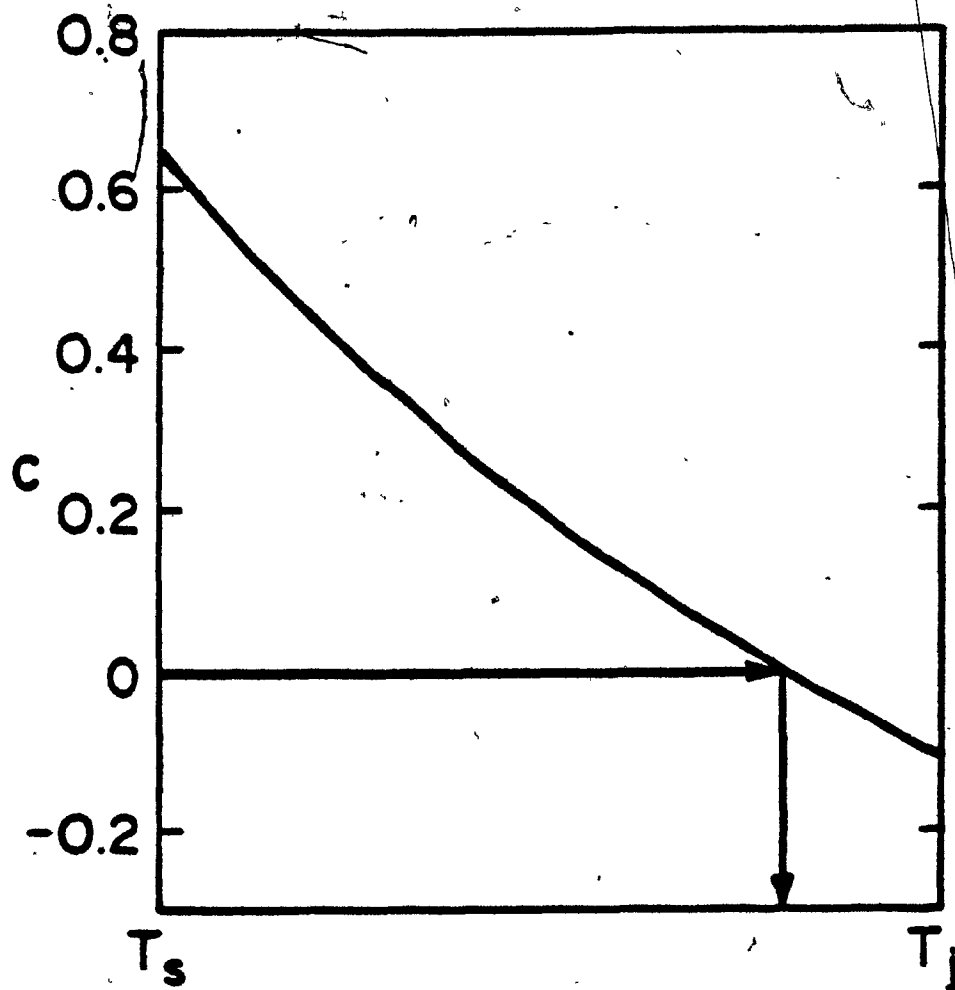
BASE TEMPERATURE FOR
PROPERTY EVALUATION,
T_{REF}

FIGURE 4.4   Effect of Temperature of Property Evaluation
on Temperature Ratio Exponent

$$Nu_{oT_{ref}} = 0.648 \, Re_j^{0.485} (H/w)^{-0.138} Pr_j^{1/3} \qquad (4.13)$$

with $T_{ref} = T_j - 0.2 (T_j - T_s)$.

Both the temperature ratio method (equation 4.11) and reference temperature method (equation 4.13) yield correlations for Nu_o which adequately allow for the wide variation in physical properties associated with large values of ΔT. The temperature ratio method is the more straightforward method to use, in that less complex iterations are involved in a typical application in design than would be the case for Nu_o evaluated at T_{ref}. Thus the preferred correlation is that based on the temperature ratio method, i.e. equation 4.11.

On Figure 4.5 are displayed the regression equation 4.11, experimental data at $Re_j = 10000$, $\Delta T = 50°C$ from the present study and the published data of Gardon et al. (1966), Cadek (1974), and Saad (1981). The three reference studies, all used cooling jets impinging on a heated surface, the opposite of the present work. Also, the first two works cited used unconfined jets. Saad used a confined jet system of geometry similar to that used in the present investigation. The fact that the results for the two studies involving unconfined jets are higher than the present results may reflect the fact that confinement reduces entrainment of ambient air. Folayan (1977) has observed that, for a slot jet, confinement can cause a reduction in Nu_o by 20%. A similar observation was also made by Obot (1980) for round jets. However, as Saad's measurements were also for a confined impingement system, the reason for this 20% difference between his results and those from the present investigation is not apparent. As turbulence is an important parameter but turbulence measurements were not part of the scope of the
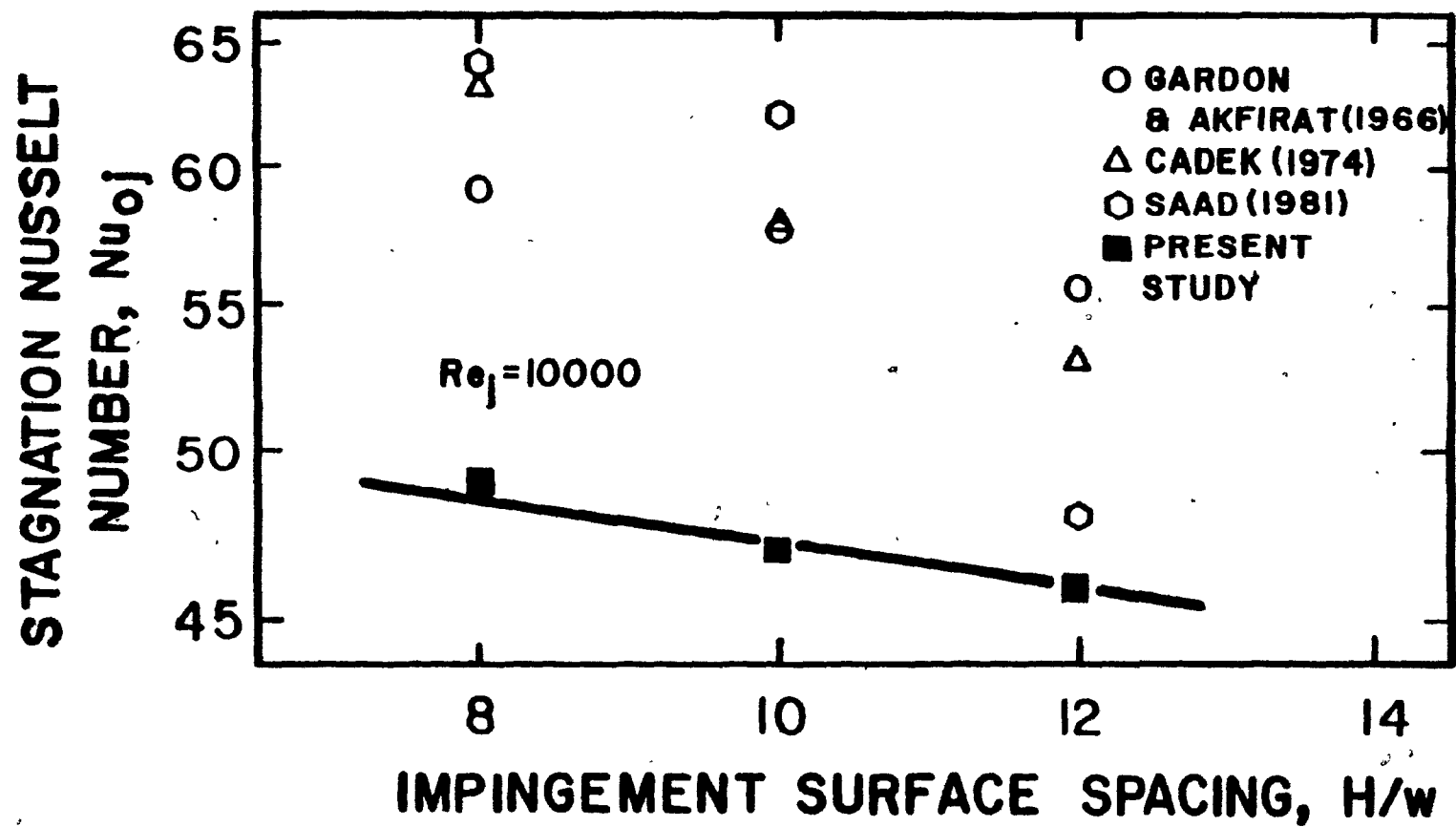
FIGURE 4.5   Comparison of Nu_o with Previous Results

present study, a difference in turbulence level could be the source of this difference in results. Saad in fact documented the high sensitivity of stagnation heat transfer to variables which may affect turbulence at the nozzle exit. Thus in his case Nu_o could be changed by up to 20% through changes in turbulence associated with changing nozzle width, w, while maintaining all dimensionless variables fixed. His documentation in this regard supports the possibility that differences in turbulence of the jet may be the source of this observed difference in results.

Comparison of Tables 2.1 and 4.2 show that the exponents found in the present work both for Re_j and H/w differ substantially from those reported previously. Reynolds number exponents in the range from 0.566 to 0.87 have been reported, significantly larger than the value of 0.485 of the present work. However the most recent work reported, that of van Heiningen (1982) has established that heat transfer from a turbulent slot jet for Re_j from 5200 to 31800 at spacings, H/w, of 2.6 and 6, may be represented adequately with Reynolds number exponent of 0.5. The use of the value of 0.5 as the Re_j exponent derives from considerations of laminar flow and is justified for application to a turbulent jet on the basis that the boundary layer in the near vicinity of the stagnation line is laminar even for the case of a highly turbulent jet.

For the range of dimensionless impingement surface spacing, H/w, above 8, the value at which Nu_o typically exhibits a maximum, the values of the exponents on H/w for dependence of Nu_o that have been reported in the literature vary from -0.37 to -0.68. The value determined from the present measurement is -0.134. This lower sensitivity to H/w in the present results is a direct consequence of the non-

linearity of the relationship between log Nu_o and log H/w, and of the narrow range of H/w, 8 to 12, over which the results are linearized. As the exponent is in fact zero at H/w = 8, due to the maximum in Nu_o at that spacing, depicted on Fig. 4.2, it is evident that linearization of the effect over the limited range to H/w near this maximum must yield a smaller exponent than linearization over a wider range of H/w (up to H/w = 25), as was used by previous workers.

The differences in values of the exponents between the present and previous work cannot be attributed to excessive scatter in the present data, because these data show quite acceptable precision. This fact is illustrated in Figure 4.6, where the experimental data are compared with predictions made using equation 4.11. The 24 experimental results picked at random from the entire range of parameters over which the equation 4.11 is applicaable are well within ±5% of the predicted values.

4.3 Local Nusselt Number Profile

As the analysis of stagnation Nusselt number showed that the effect of temperature dependent physical properties, large for high values of ΔT, could be well accounted for in terms of temperature ratio T_j/T_s, with all dimensionless variables evaluated at T_j, all subsequent analysis is made on this basis.

4.3.1 Effect of Reynolds Number and Spacing

For the lowest nozzle to impingement surface spacing, H/w = 5, the profile of local Nusselt number for $\Delta T = 150°C$, shown on Figure 4.7 are typical of results at this spacing measured at all 6 levels of ΔT. Nozzle exit Reynolds number is shown as the parameter.
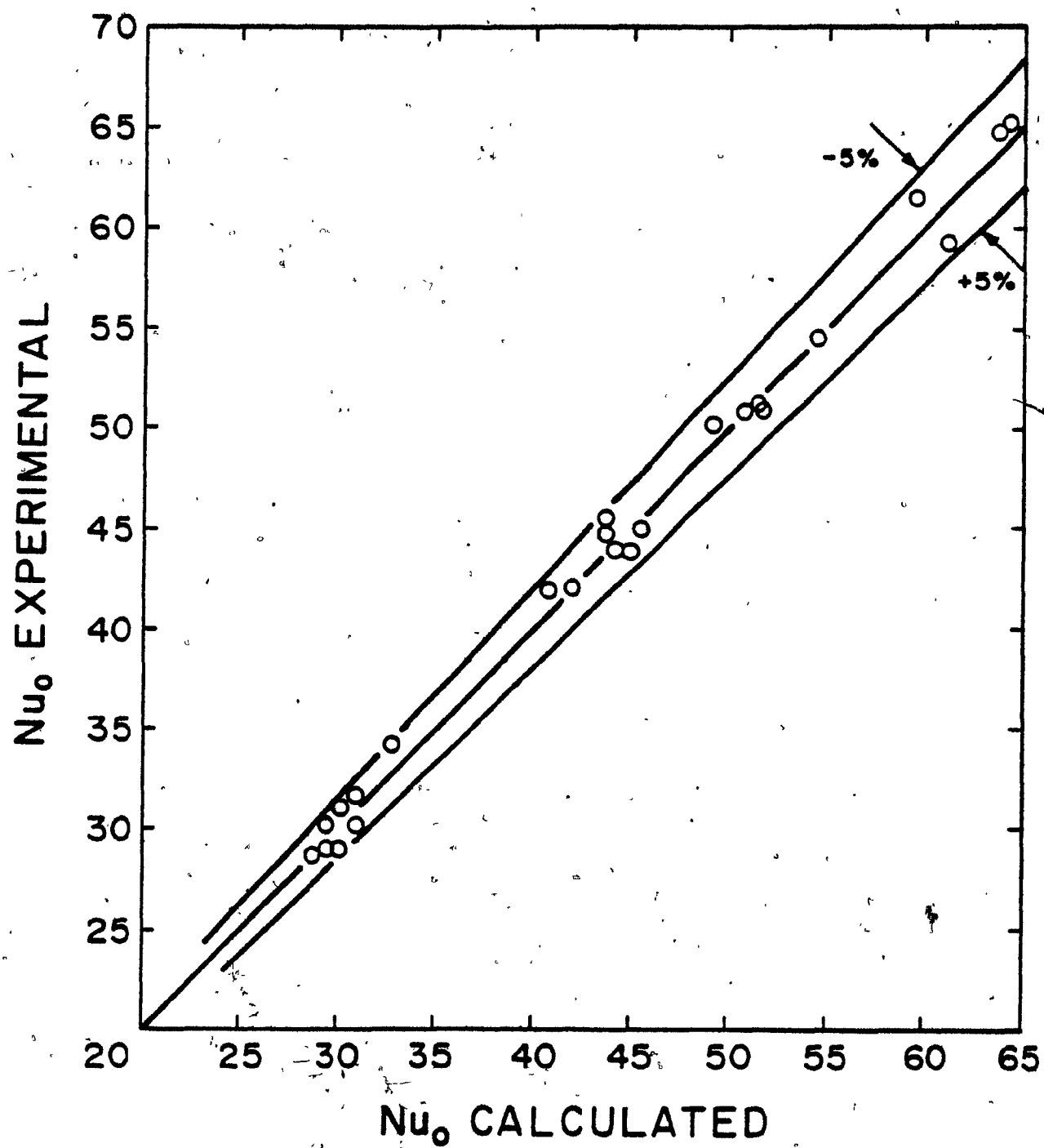
FIGURE 4.6 Comparison of Calculated Nu_o with Experimental Nu_o
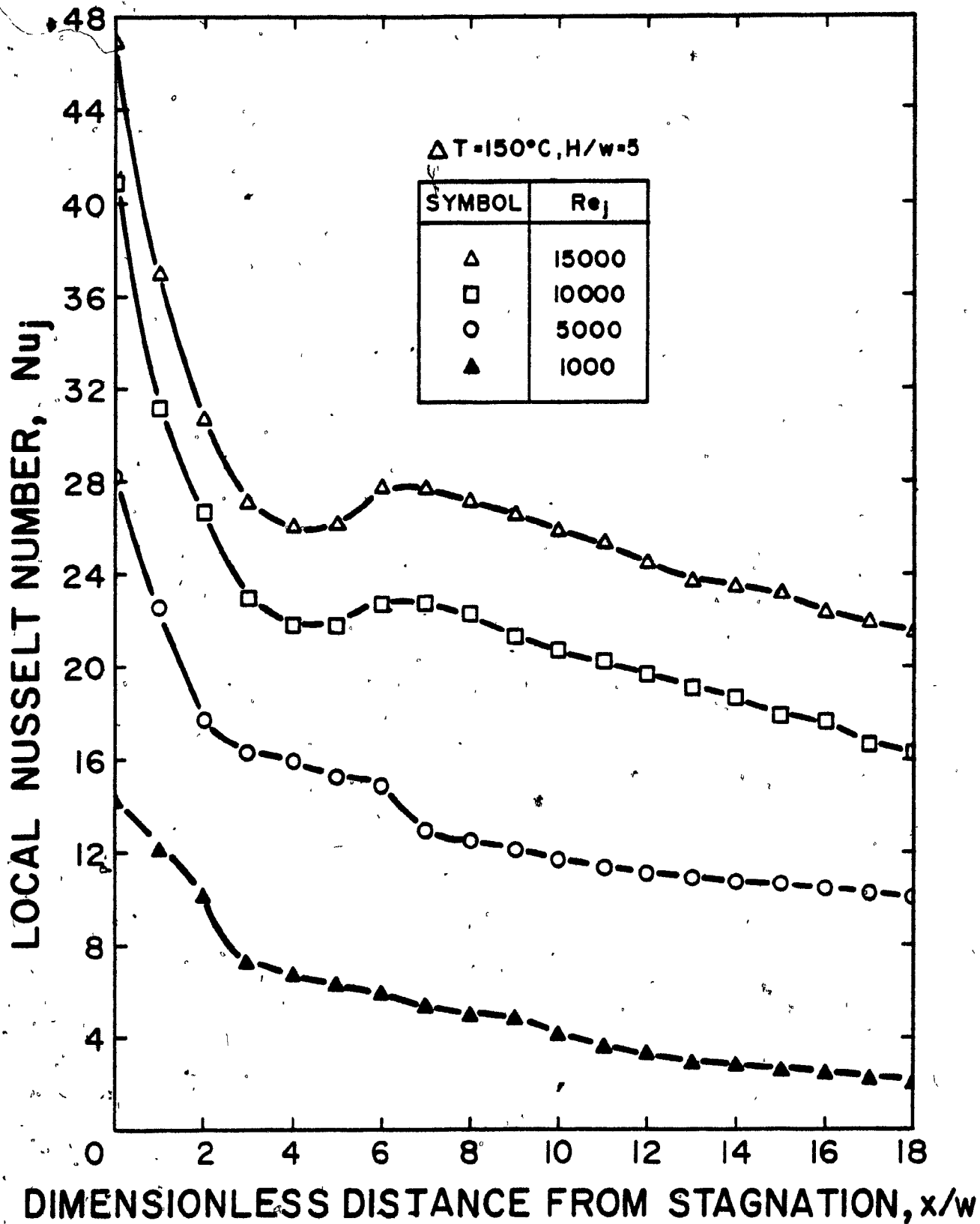
FIGURE 4.7   Local Nu Profile at H/w = 5

The data points on Figure 4.7 and some subsequent figures have been joined by straight lines simply to aid visual interpretation. The characteristic feature of the data for all values of ΔT at a spacing as close as $H/w = 5$ and at a sufficiently high Re_j, is the presence of a minimum and a secondary maximum in the impingement region. For a turbulent single slot jet the existence of such a minimum and secondary maximum was reported by Gardon and Akfirat (1966), Cadek (1968) and most recently by Saad (1981) and van Heiningen (1982). Analogous observations have been made by Gardon et al. (1968) and Obot (1980) for single round turbulent jets.

The source of the minimum and off-stagnation maximum at combinations of sufficiently low spacing and sufficiently high Reynolds number is that these conditions produce such a steep, negative gradient in impingement surface pressure near the stagnation line that the boundary layer is initially laminar even for a highly turbulent jet. Once beyond the region of steep, negative pressure gradient, boundary layer transition from laminar, to turbulent begins. This transition is accompanied by a large increase in transport rate at the impingement surface. For the low H/w - high Re_j combination of conditions this transition occurs with such strength and over such a narrow lateral distance as to be the source of this minimum-maximum in the heat transfer profile.

Along the impingement surface, lateral distance from stagnation, x, is usually represented nondimensionally by reference to the nozzle width, w, as x/w. However for the lateral region out to the onset of boundary layer transition, i.e. out to the minimum in such heat transfer profiles, Saad (1981), using his results for a wide range of values of w, H and H/w, established that H, not w, is the preferred characteristic

length for the nondimensional lateral distance, i.e. x/H. Specifically,
Saad showed that for his wide range of w, H and H/w, the transition
point minimum in heat transfer profiles regularly occurs at a lateral
position equal to or slightly under x/H = 1, whereas measured as x/w,
this position varies widely. Thus the occurrence of the transition
point minimum on Figure 4.7 at x/w = 4, which corresponds to x/H = 0.8,
is consistent with Saad's analysis. Further, the recent findings by van
Heiningen that the transition point minimum occurred near x/H = 0.6 at
a spacing H/w = 6, and near x/H = 1 for H/w = 2.6 is consistent with
the location of the minimum at x/H = 0.8 found in the present study.
The section of the heat transfer profile over which Nu increases with
lateral distance ends at the secondary maximum, the point of completion
of transition to a turbulent boundary layer. The observation in the
present study that this peak occurs about 2.5w beyond the minimum in the
profile at the onset of transition, is consistent with the observations
of previous investigators. The decrease in heat transfer rate beyond
the secondary maximum results from the growing thickness of the now
turbulent boundary layer.

Typical results for higher impingement surface spacings are
shown on Figure 4.8 for H/w = 10 and ΔT = 300°C. These bell shaped
profiles without the secondary peaks have been observed by Gardon et al.
(1966), Cadek (1974) and Saad (1981) for single slot jets, but of course,
never at the high levels of ΔT of the present investigation.

4.3.2 Effect of Temperature Difference

The effect of temperature difference on local Nu distributions
is illustrated on Figures 4.9 and 4.10 for H/w = 5. Both figures show
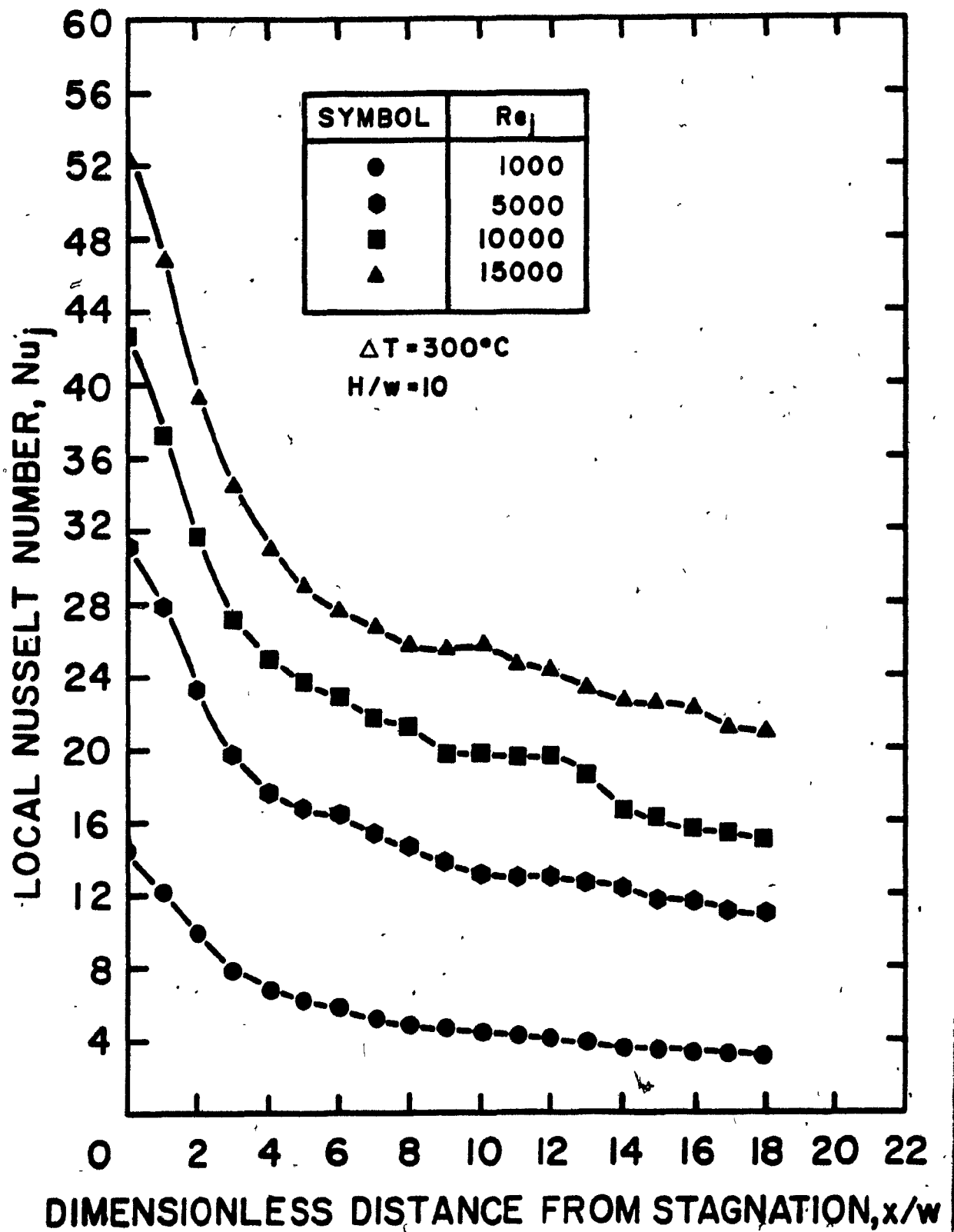
FIGURE 4.8   Local Nu Profile at H/w = 8
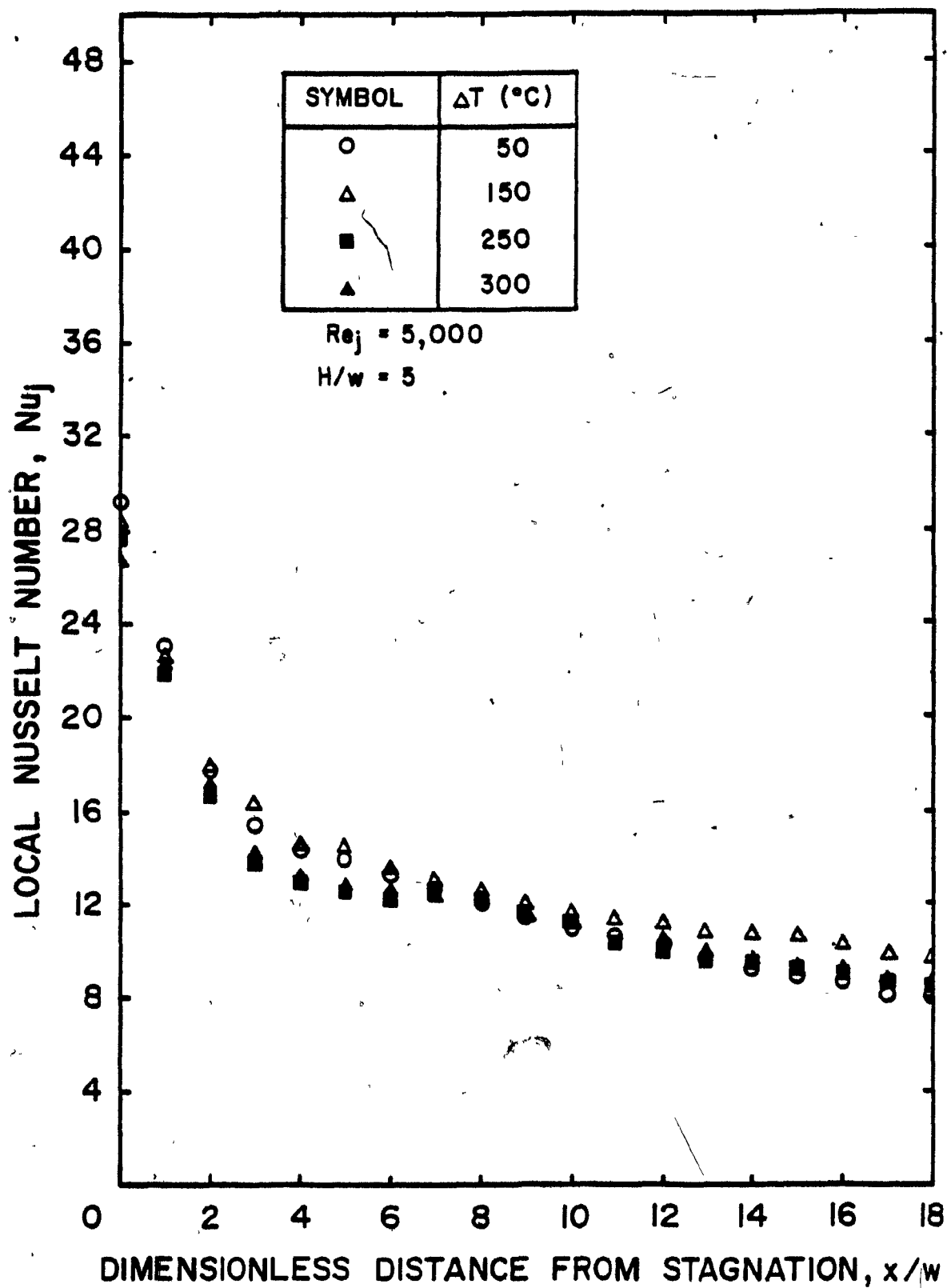
FIGURE 4.9   Effect of ΔT on Local Nu Profile at H/w = 5,
$Re_j = 5000$
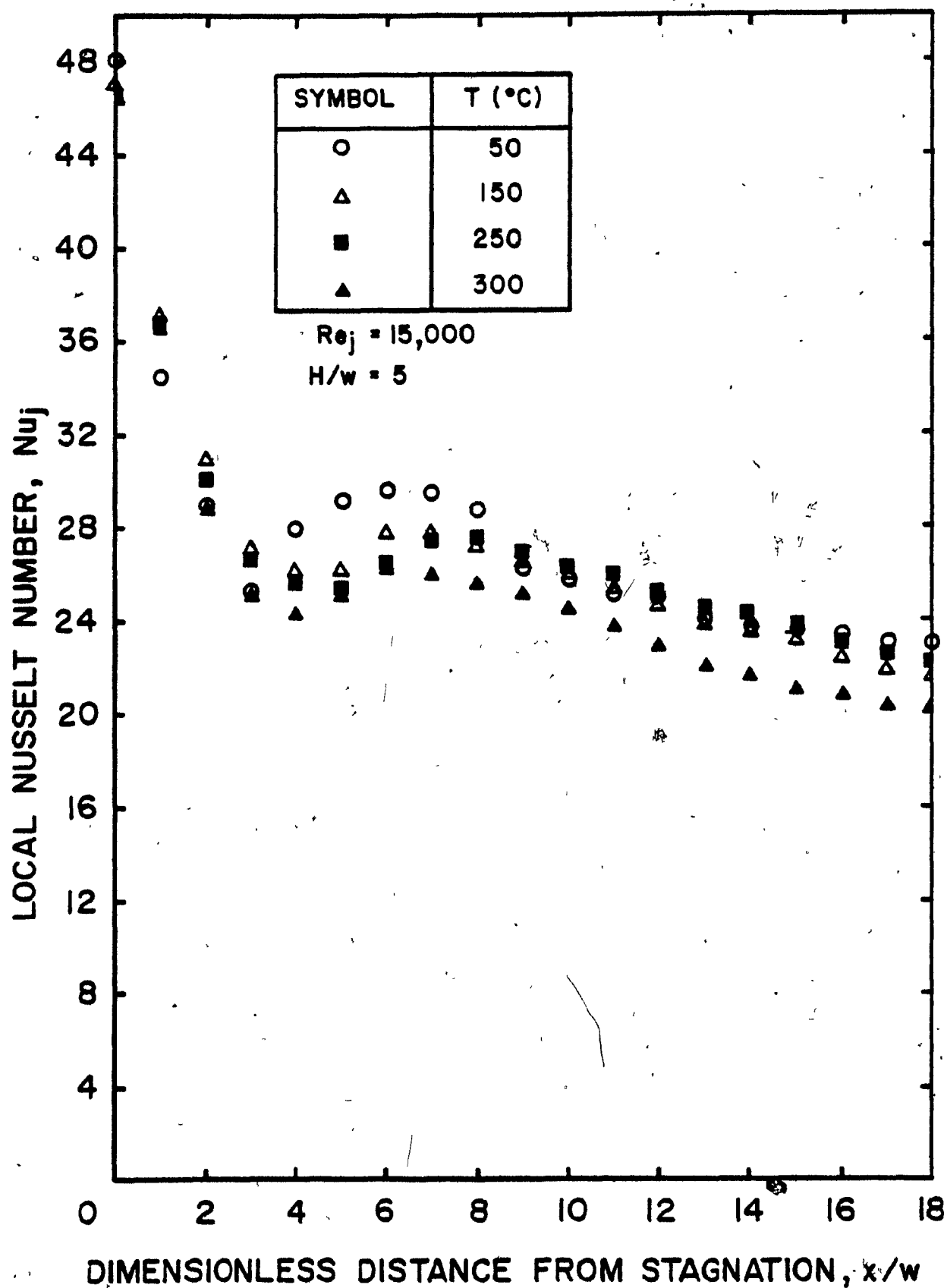
FIGURE 4.10   Effect of ΔT on Local Nu Profile at H/w = 5,
Re$_j$ = 15000

the decrease of stagnation Nusselt number with increasing temperature difference, as was shown even more clearly on Figure 4.3. However, beyond the stagnation region the profiles frequently cross, thus indicating. that outside the impingement region, ΔT is no longer a predominant variable when heat transfer is expressed as Nusselt number evaluated at T_j.

The effect of ΔT on local heat transfer rate at higher impingement surface spacing of $H/w = 8$ is shown on Figures 4.11 and 4.12. These profiles are typical for all results at the higher spacings, H/w, of 8 and 12. In both figures, the effect of temperature difference is quite pronounced and consistent out as far as 6w to 8w from the stagnation line. Throughout this region, local Nusselt number decreases with increasing ΔT, as was indicated at the stagnation line on Figure 4.3. In the wall jet region, beyond $x/w = 8$, the local Nu_j profiles cross and ΔT ceases to be a significant variable.

On Figure 4.13, results from the present study are compared with those of Gardon and Akfirat (1966), Cadek (1974) and Saad (1981). The geometry used by the first two workers differs somewhat from that used in the present work whereas Saad used a similar configuration. Both Gardon et al. and Cadek used unconfined cooling jets on heated impingement surfaces. Gardon et al. used a nozzle width of 3.175 mm, about half of that of the present work, while Cadek's nozzle width was 6.35 mm. The present data agree well with these works for $x/w > 3$ but are lower by as much as 20% at and in the immediate vicinity of the stagnation line. Saad used 5 mm width-confined cooling jets on a heated·surface. The present data is lower by as much as 18% at $x/w = 0$ to 11% at $x/w = 18$.
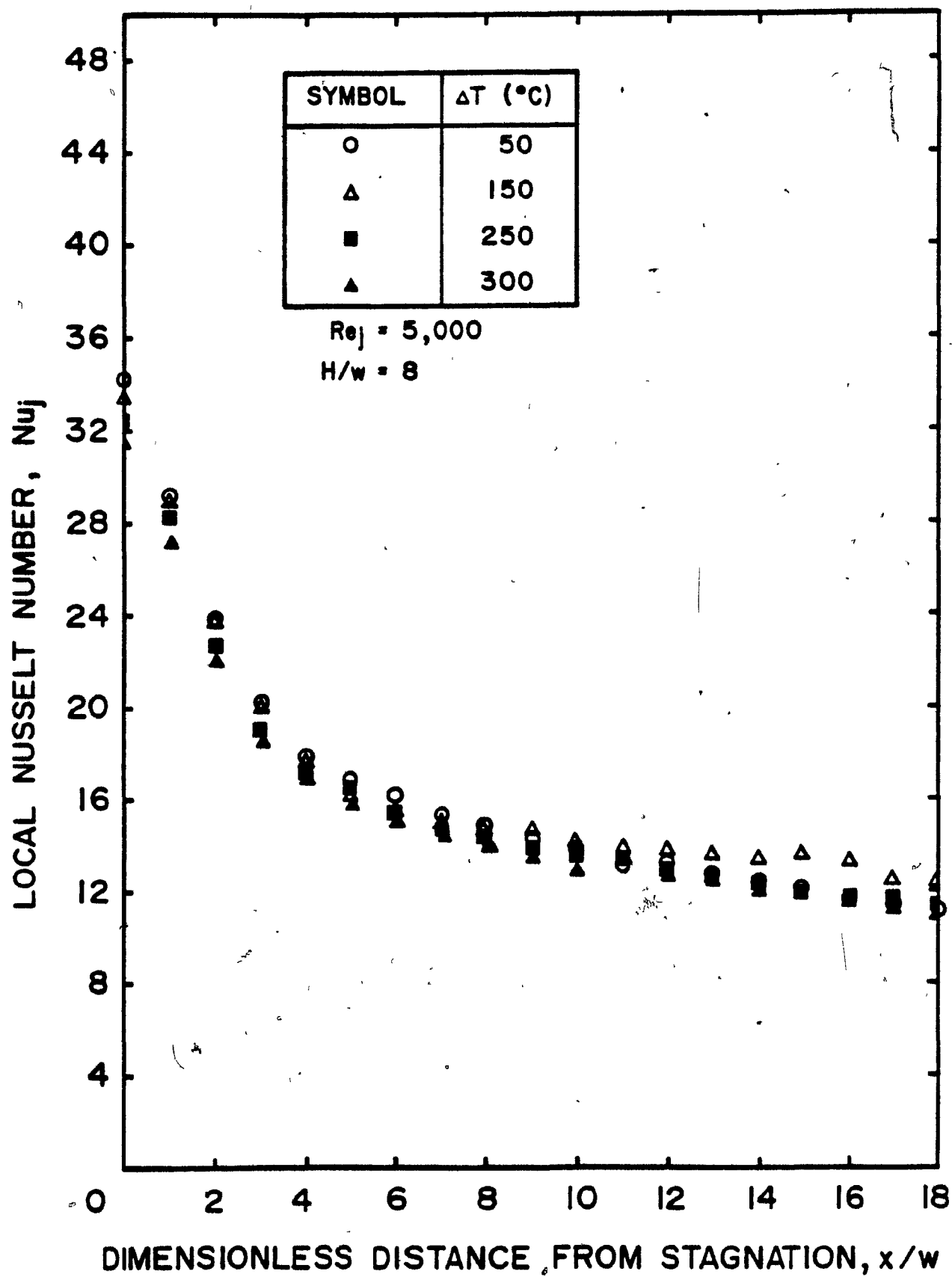
FIGURE 4.11   Effect of ΔT on Local Nu Profile at H/w = 8 and Re_j = 5000
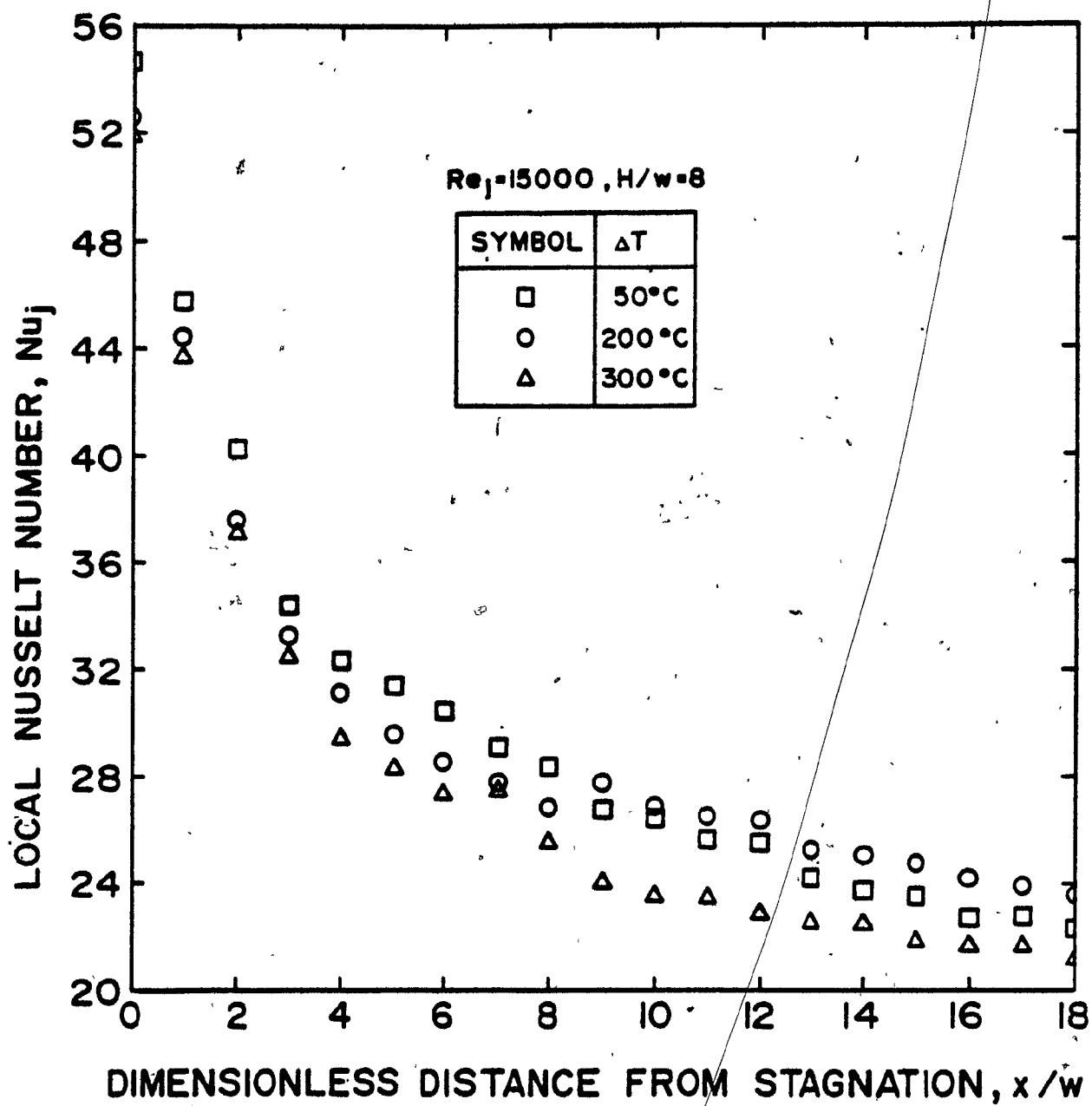
FIGURE 4.12   Effect of ΔT on Local Nu Profile at H/w = 8 and Re_j = 15000
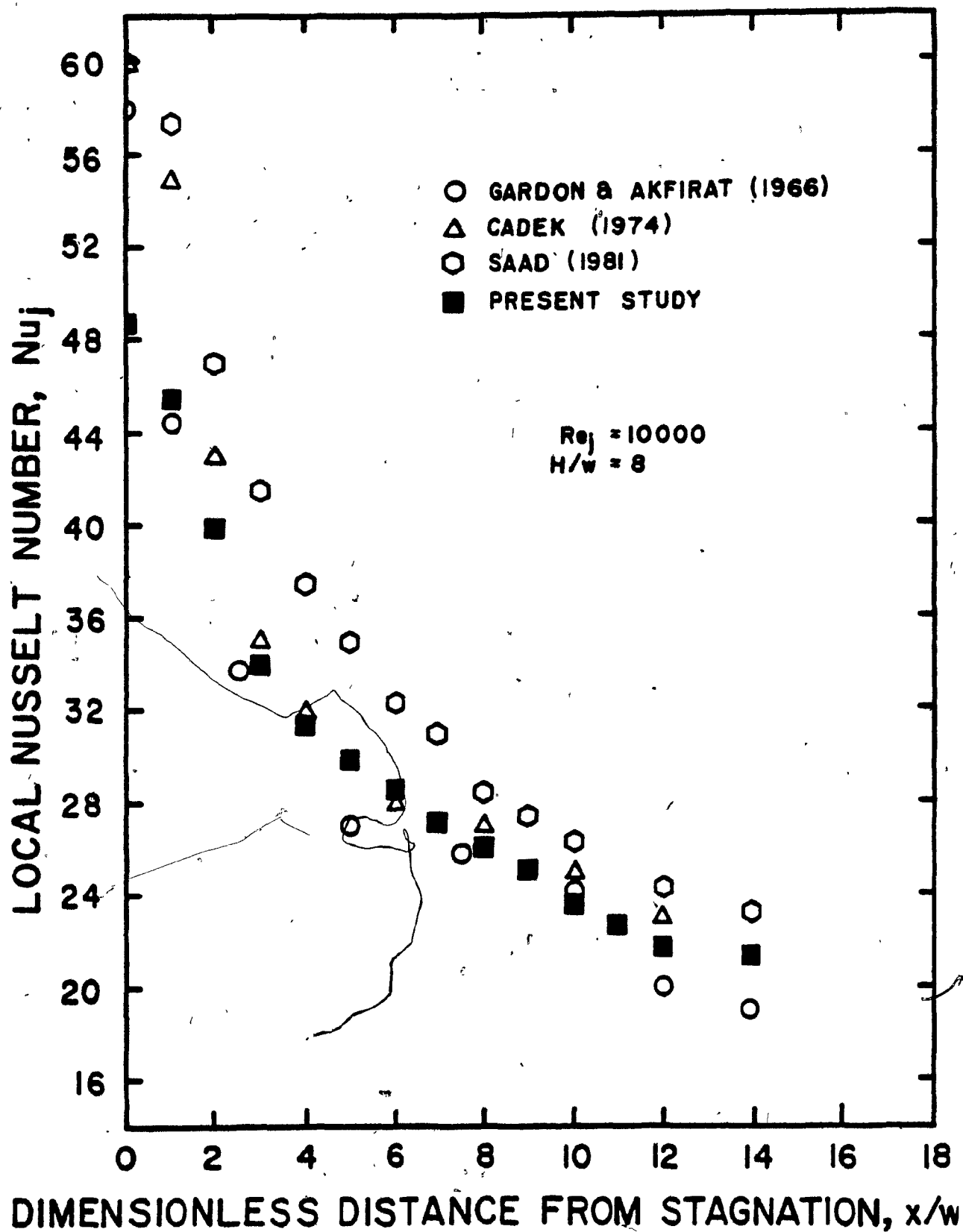
FIGURE 4.13   Comparison of Local Nu Profile with Previous Results

The possible sources for these differences were discussed in Section 4.2.3 in connection with the analysis of stagnation heat transfer. However the discrepancy of the present data with Saad's results beyond the stagnation region could not be justified in light of the turbulence effect.

4.4 Average Nusselt Number

In the use of experimental impinging jet heat transfer results for process design in industrial applications such as the drying of paper and other wet webs, it is average rather than local values of the heat transfer coefficient which is needed. Hence an average Nusselt number was obtained from the local Nu_j by integration, using equation 4.4. Thus the average Nusselt number obtained is based on fluid properties at the nozzle exit temperature, T_j, as for Nu_j. The complete set of values of $\overline{Nu}_j$ is listed in Appendix C. A typical local Nusselt number distribution, Nu_j, and average Nusselt number distribution, $\overline{Nu}_j$, for Re_j = 5000, H/w = 8, and ΔT = 300°C are shown together on Figure 4.14. The difference between Nu_j and $\overline{Nu}_j$ naturally increases with lateral distance from stagnation.

The search for a correlation for $\overline{Nu}_j$ was approached in the same manner as outlined in Section 4.2 for the case of Nu_{oj} except of course with inclusion of the additional variable, dimensionless distance from stagnation, x/w. Use of the power law function

$$\overline{Nu}_j = K \, Re_j^{\,a} \, (H/w)^b \, (T_j/T_s)^e \, Pr_j^{\,d} \, (x/w)^e \qquad (4.14)$$

does not fit to a satisfactory correlation because the coefficient K and the exponents a, b and c are functions of x/w. The sensitivity of these
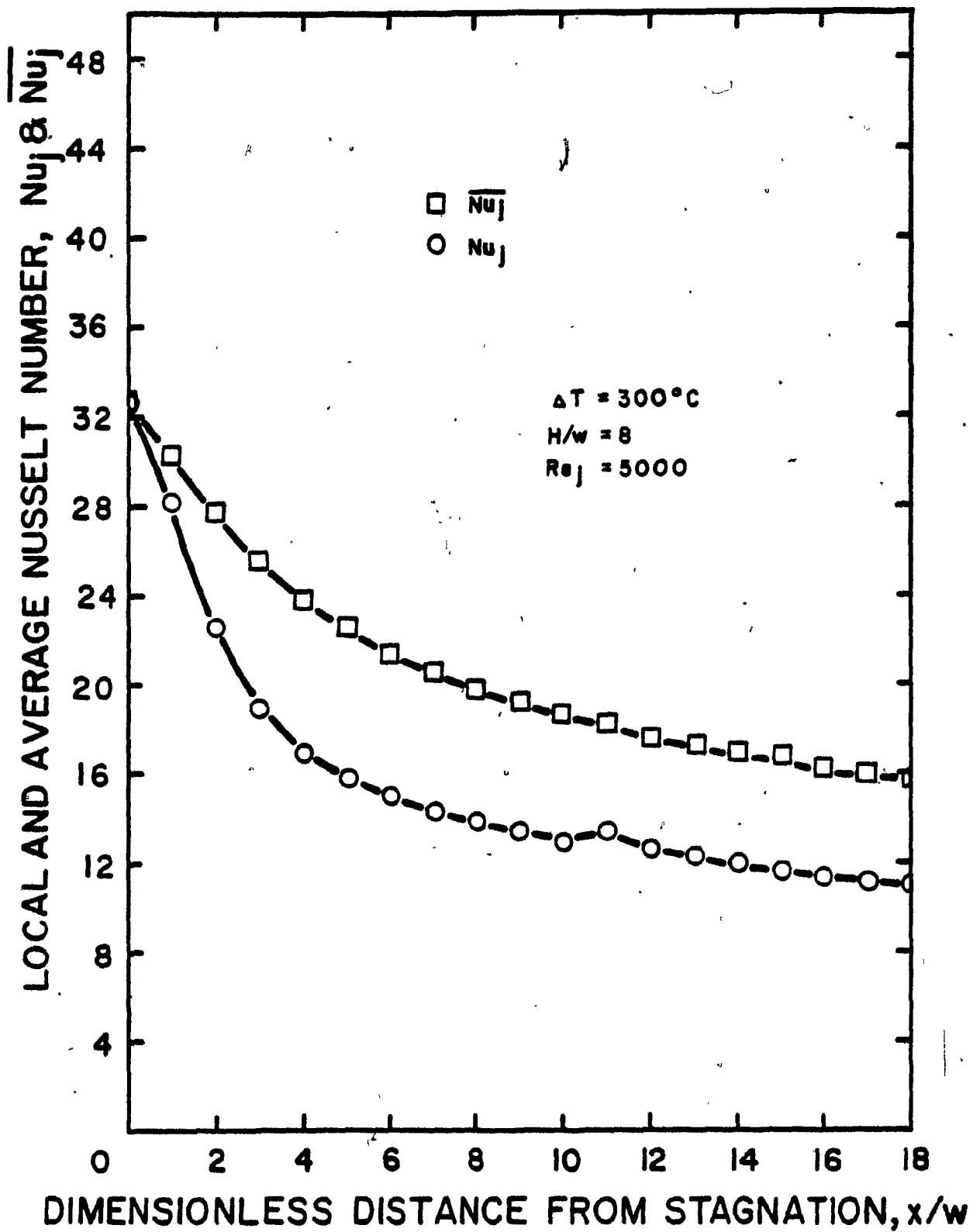
FIGURE 4.14 Local and Average Nu Profile

exponents to x/w is illustrated on Figures 4.15(a, b and c). An increase
in slope of the logarithmic linear relationship between $\overline{Nu}_j$ and Re_j
with increasing x/w is clearly evident on 4.15 (a). On Figure 4.15 (b),
the slope of the logarithmic $\overline{Nu}_j$ - H/w relationship changes from negative
to zero as x/w increases. Likewise, Figure 4.15 (c) shows that the
logarithmic $\overline{Nu}_j$ - T_j/T_s slope is negative at x/w = 0 but approaches
zero as x/w increases.

Because of the dependency of these exponents on x/w the following
regression equation

$$\overline{Nu}_j = K \, Re_j^{\,a} \, (H/w)^b \, (T_j/T_s)^c \, Pr_j^{\,d} \qquad (4.15)$$

was fitted at each value of x/w. For each regression only 60 data
points were used, because the data at Re_j = 1000 and H/w = 5 were
excluded for reasons discussed previously in Section 4.2.3.

The coefficient K and the exponents a, b and c are listed in
Table 4.3 and plotted on Figure 4.16. The ordinate scale used in each
of the four figures was chosen to correspond approximately to the magni-
tude of the effect of the parameters on $\overline{Nu}_j$, over the range of parameters
used in the experiment.

For lateral positions farther than 2w from stagnation, the
coefficient K varies exponentially with x/w, as is suggested by Figure
4.16 and confirmed by Figure 4.17. From the latter figure the slope, or
exponent for x/w, was determined to be approximately -2/3. It must be
remembered that this form for the dependence of K on x/w is not valid
for x/w < 2. This finding is used subsequently in Section 4.5, in the
treatment of impingement heat transfer as a confined heat exchanger
system.
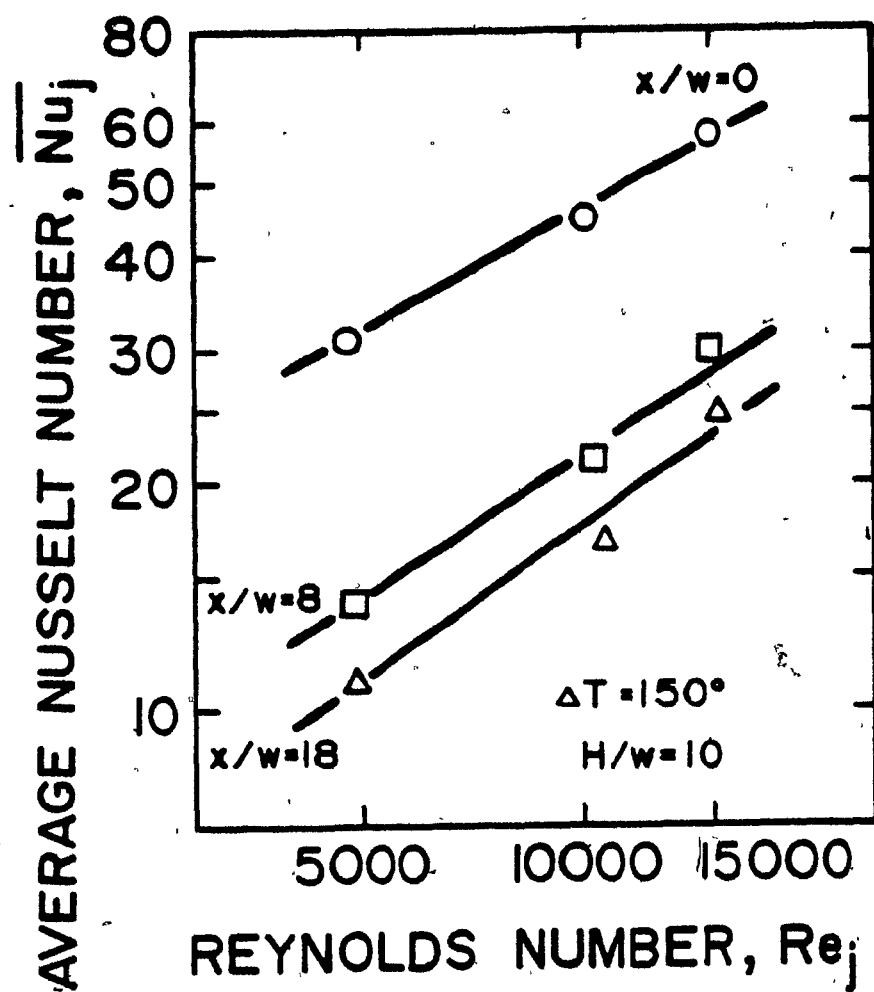
FIGURE 4.15a Effect of Re_j on $\overline{Nu}_j$ with x/w as Parameter
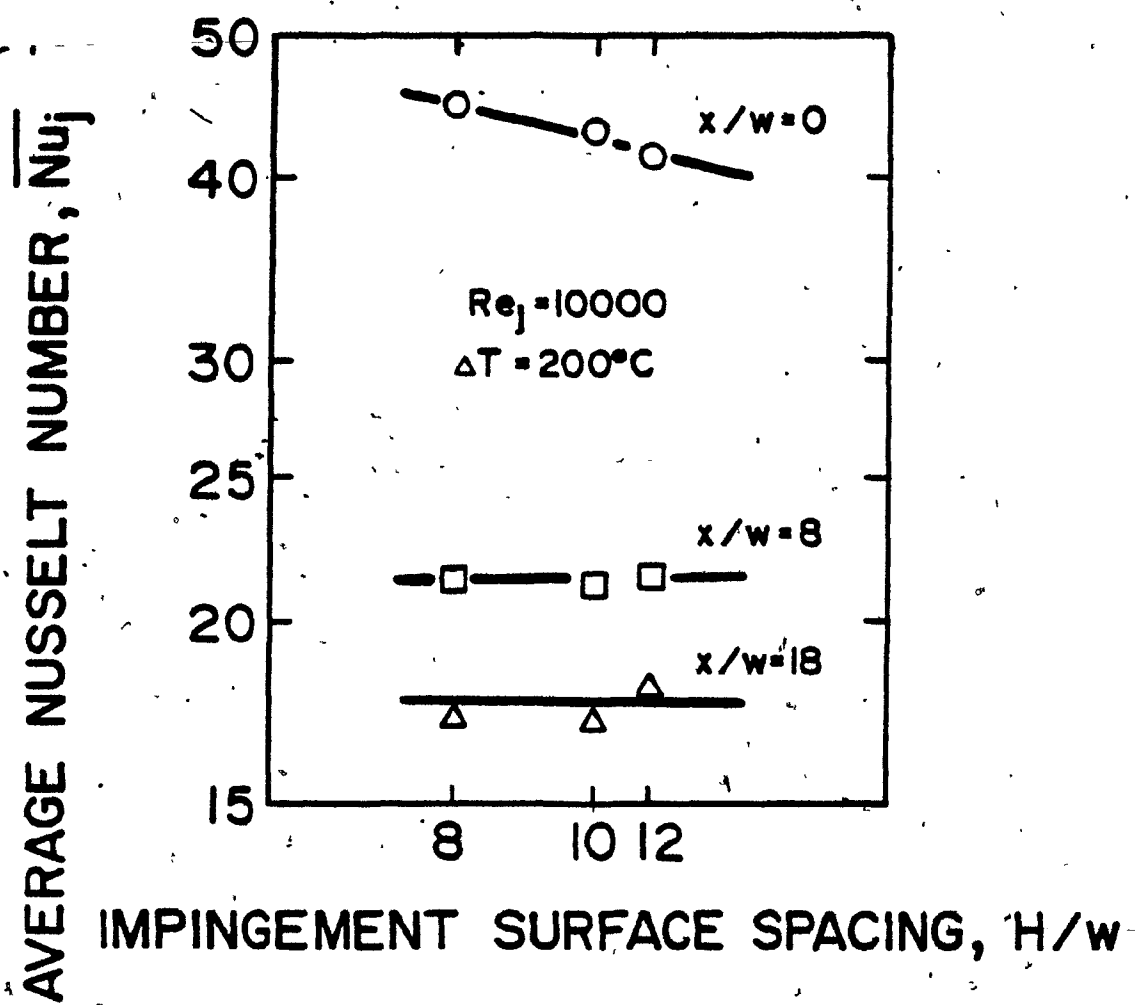
FIGURE 4.15b   Effect of H/w on $\overline{Nu}_j$ with x/w as Parameter
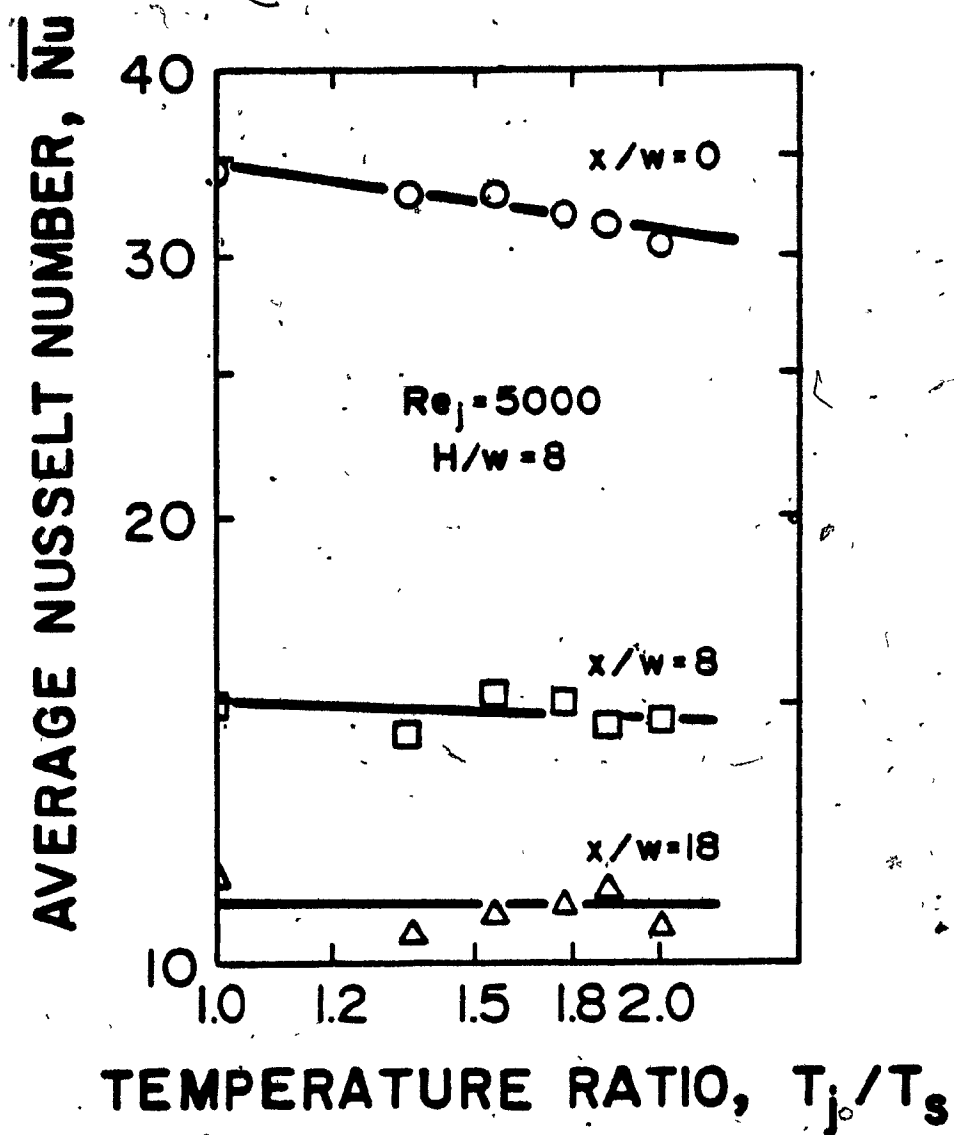
FIGURE 4.15c   Effect of T_j/T_s on $\overline{Nu}_j$ with x/w as Parameter

TABLE 4.3. List of Coefficient and Exponents of Equation 4.16

Range of Re_j	Range of H/w	Range of T_j/T_s	x/w	Coefficient K	Exponent a, for Re_j	Exponent b, for H/w	Exponent c, for T_j/T_s
5,000-20,000	8-12	1.18-2.06	0	0.791	0.485 (58.3)	-0.134 (5.5)	-0.115 (5.6)
5,000-20,000	8-12	1.18-2.06	2	0.680	0.484 (46.5)	-0.113 (3.7)	-0.132 (5.2)
5,000-20,000	8-12	1.18-2.06	3	0.546	0.493 (44.1)	-0.091 (2.8)	-0.142 (5.2)
5,000-20,000	8-12	1.18-2.06	5	0.386	0.519 (40.3)	-0.091 (1.9)	-0.149 (4.73)
5,000-20,000	8-12	1.18-2.06	6	0.344	0.521 (38.9)	-0.071 (1.8)	-0.151 (4.5)
5,000-20,000	8-12	1.18-2.06	8	0.281	0.532 (37.1)	-0.068 (1.6)	-0.148 (4.1)
5,000-20,000	8-12	1.18-2.06	9	0.258	0.533 (37.8)	-0.018 (0.5)	-0.075 (1.9)
5,000-20,000	8-12	1.18-2.06	10	0.237	0.534 (35.2)	-0.068 (1.5)	-0.167 (4.3)
5,000-20,000	8-12	1.18-2.06	12	0.192	0.538 (35.8)	-0.056 (1.3)	-0.21 (5.8)
5,000-20,000	8-12	1.18-2.06	13	0.205	0.541 (35.2)	-0.011 (0.26)	-0.036 (0.81)
5,000-20,000	8-12	1.18-2.06	15	0.186	0.544 (34.7)	-0.007 (0.17)	-0.041 (0.9)
5,000-20,000	8-12	1.18-2.06	18	0.174	0.544 (33.7)	-0.004 (0.089)	-0.04 (0.9)
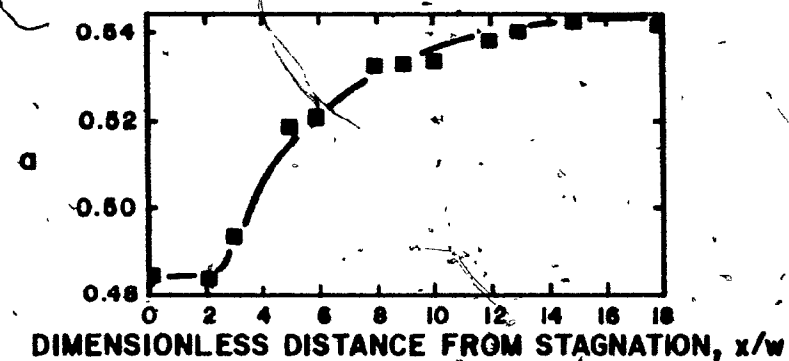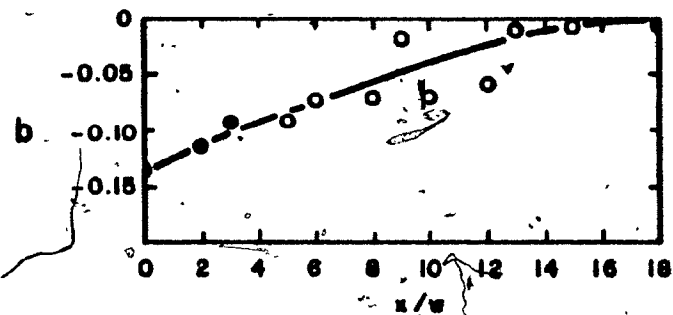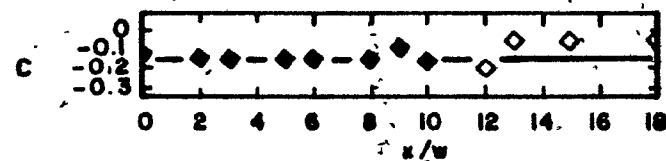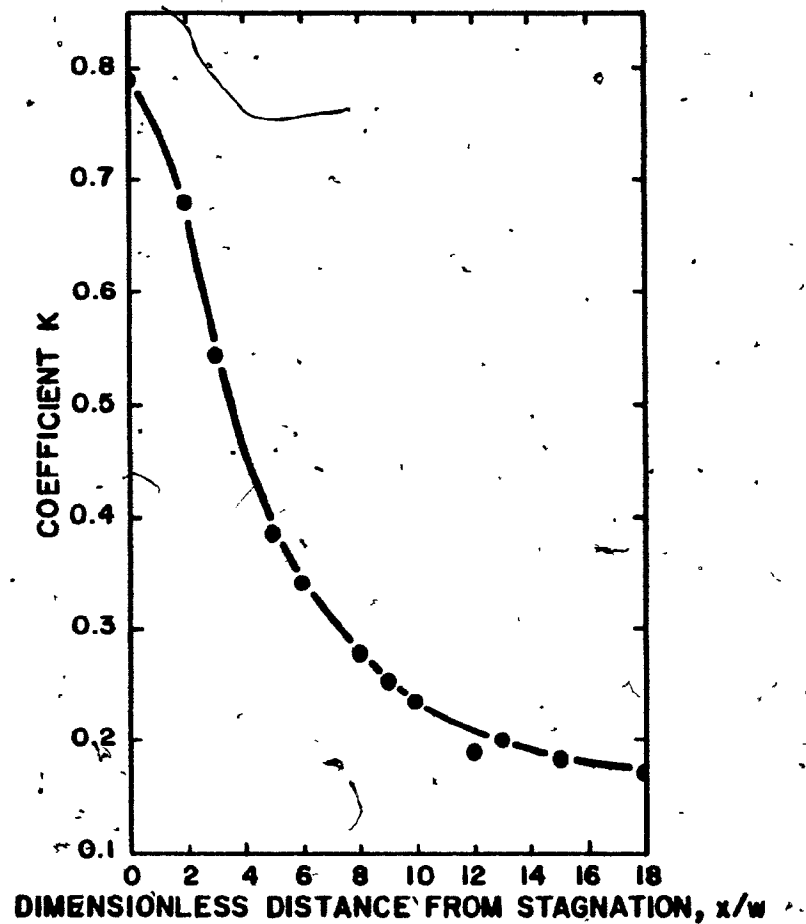
FIGURE 4.16 Coefficient and Exponents of Equation 4.16 as a Function of x/w
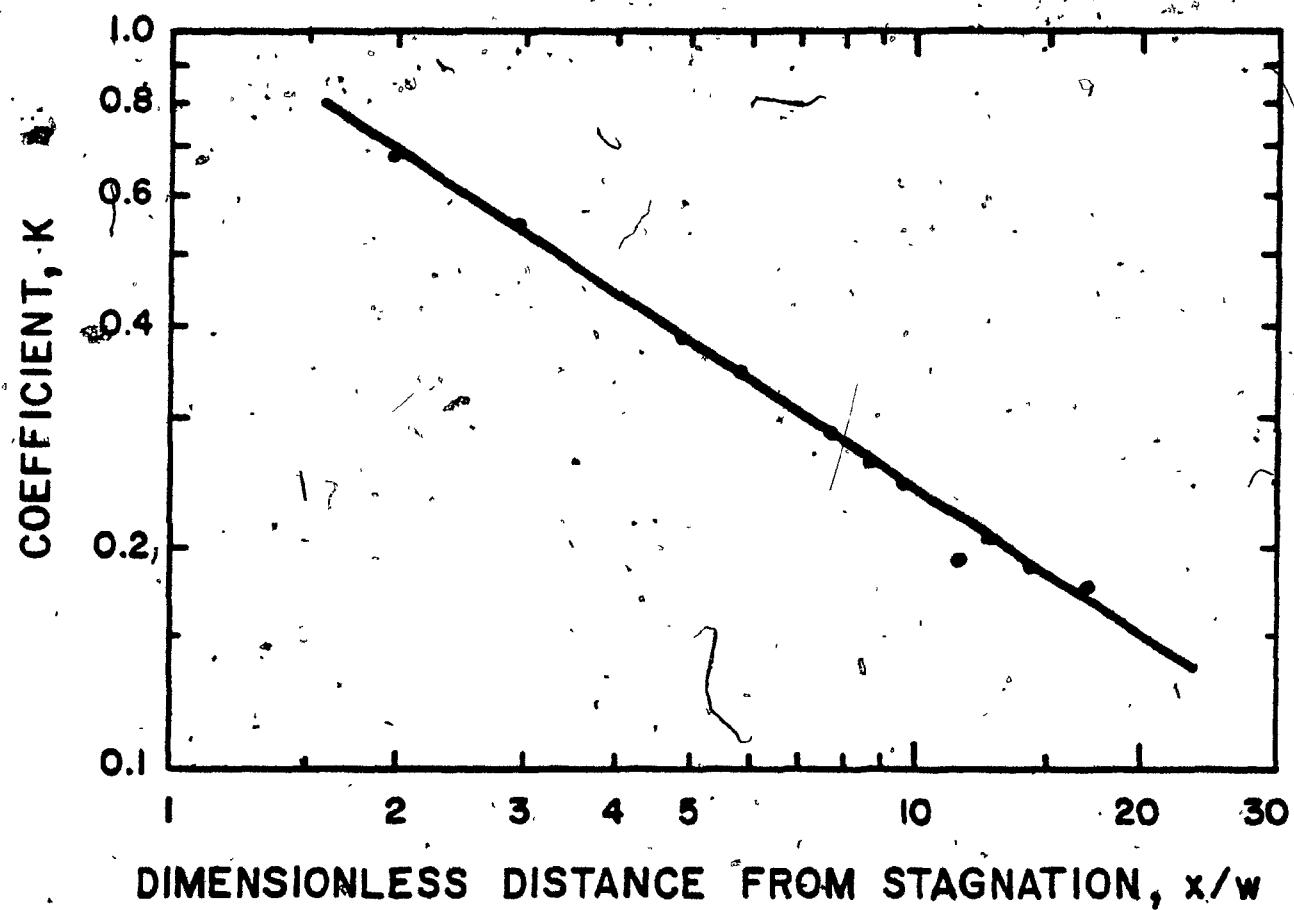
FIGURE 4.17   Effect of x/w on Coefficient K of Equation 4.16

The Reynolds number exponent, a, shows an "S" shaped variation with x/w. The exponent remains unchanged at 0.485 from x/w = 0 to x/w = 2, then increases with x/w, eventually becoming asymptotic to a value of 0.544 at x/w = 18. As the exponent of 0.485 in the near vicinity of the stagnation line is so close to the characteristic value of 0.5, this result provides further confirmation of the occurrence of a laminar boundary layer in the stagnation region. The increase in the Reynolds number exponent with distance from stagnation reflects the transition to a turbulent boundary layer, as discussed in Section 4.3. For the $\overline{Nu}_J$ - Re_j relationship the limiting value for this exponent, about 0.55 for x/w = 18, reflects the averaging of the effects of Re_j from the stagnation region where the dependence is with $Re^{0.5}$, to the wall jet region where the dependence is to $Re^{0.8}$ for the fully turbulent boundary layer.

The individual values of the exponent b, which reflects the sensitivity of $\overline{Nu}_j$ to H/w, are different from zero by a statistically significant amount at the stagnation line, where b = -0.134, and out to 3w from stagnation. For this reason open symbols are used beyond x/w = 3 or Figure 4.16. Although at positions beyond x/w = 3 the individual values of b are not statistically different from zero, from Figure 4.16 it is evident that there is a highly consistent trend of b with x/w over the entire region from stagnation to x/w = 18. It is logical that the magnitude of this exponent should decrease with increasing x/w. Results which are a function of position from stagnation may be interpreted using (H + x)/w as a characteristic distance. From the perspective it follows that H/w is a much less significant variable at high than at

low values of x/w. For example, a variation in H/w between 8 and 12 at x/w = 0 represents a 50% change in (H + x)/w, while at x/w = 18 the same variation in H/w corresponds to only a 15% change in (H + x)/w. Thus the trend for b to approach zero at high values of x/w is as expected.

The exponent c, which is a measure of the effect of T_j/T_s on $\overline{Nu}_j$, does not vary much with x/w. The magnitude of the modest effect of the temperature ratio term may be recalled by reference to Figure 4.3, which corresponds to the value of $c = -0.115$ applied at x/w = 0. Although the individual values of c are different from zero by a statistically significant amount only out to x/w = 10, indicated on Figure 4.16 by the use of closed symbols, it is apparent that the entire set of values of c fluctuate within the same small range over the entire span of x/w from 0 to 18. Thus it appears appropriate to recommend a value of c of -0.12 for the entire range of x/w.

One point must be clarified at this stage that change in temperature difference between the jet and impingement surface from 50° to 300°C corresponding to change in T_j/T_s from 1.18 to 2.06 causes the Nusselt number evaluated at the jet exit temperature to decrease by approximately 6.5%. However the change in heat transfer coefficient, h, with T_j/T_s is much more dramatic. The thermal conductivity, which is the only temperature dependent physical property used in the evaluation of Nusselt number increases by approximately 60% for increase in physical property evaluation temperature, i.e. at jet exit from 60° to 310°C (Appendix H). Consequently the heat transfer coefficient increases, not decreases as the Nusselt number does, by about 50% with increase in temperature difference.

In summary, a regression has been fitted to the experimental data to provide a measure for predicting average heat transfer rates under high temperature single slot confined impinging jet. The equation has the following form:

$$\overline{Nu}_j = K \, Re_j^a (H/w)^b (T_j/T_s)^c \, Pr_j^{1/3} \qquad (4.16)$$

$$5000 \leqslant Re_j \leqslant 20000$$

$$8 \leqslant H/w \leqslant 12$$

$$1.2 \leqslant T_j/T_s \leqslant 2.1$$

$$0 \leqslant x/w \leqslant 18$$

The coefficient K and exponents a, b and c were determined as functions of x/w and are plotted on Figures 4.16 and 4.17 and are listed in Table 4.3. To find average heat transfer up to a particular distance x/w, the user has only to choose the coefficient and exponents of equation 4.16 corresponding to the desired value of x/w.

To test the predictions made with this procedure, ratios of measured to calculated average Nusselt numbers $\overline{Nu}_{exp}/\overline{Nu}_{cal}$ were plotted against each of the parameters Re_j, x/w, H/w and T_j/T_s on Figure 4.18. The uniform scatter around the line $\overline{Nu}_{exp}/\overline{Nu}_{cal} = 1$ indicates that the predicted values do not vary systematically with any of the independent parameters and that these effects have been accounted for properly. Alternately on Figure 4.19, the predicted values are plotted against experimental results. As it is thus demonstrated that the predicted results always lie within $\pm 15\%$ of the experimental results, the proposed correlation for average Nusselt number may be used with confidence.
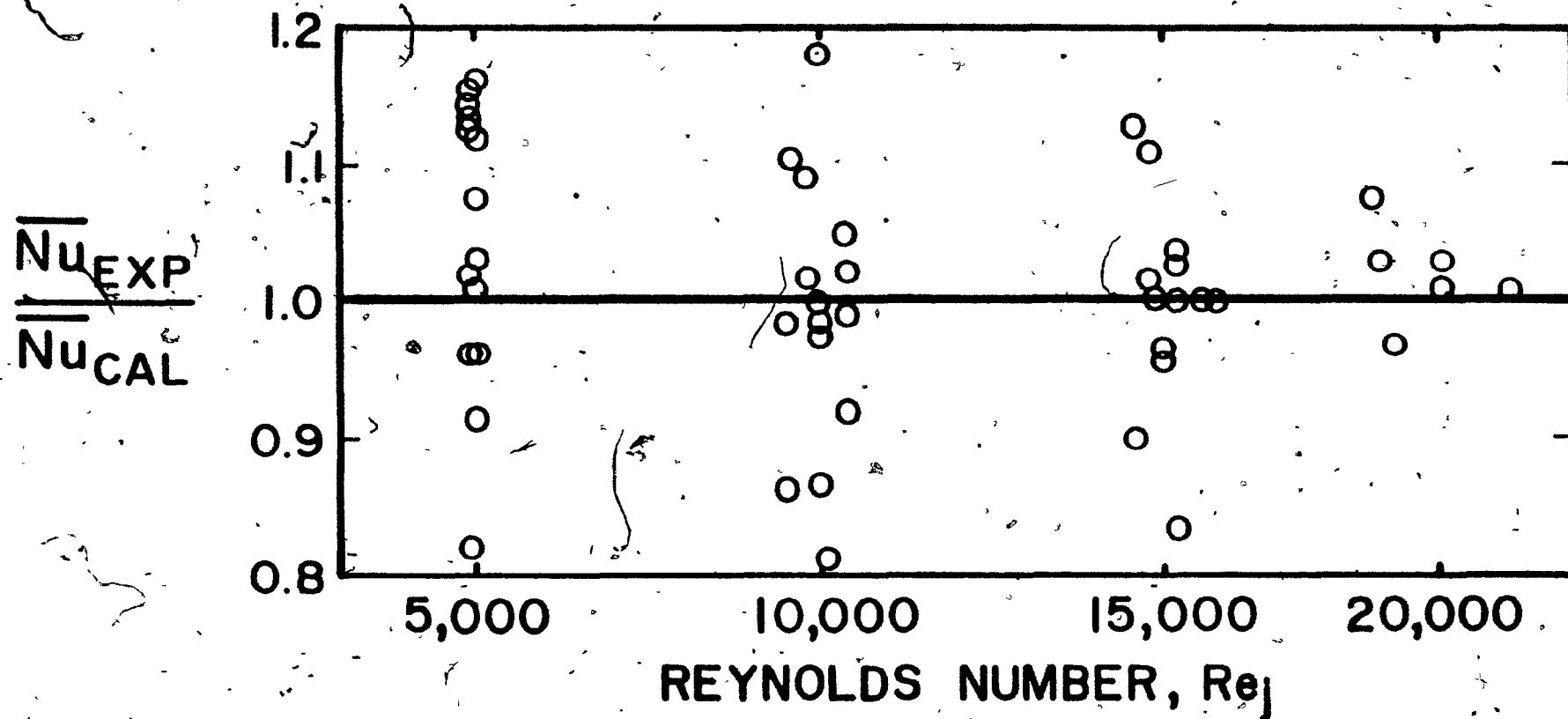
FIGURE 4.18a Illustration of Independence of $\overline{Nu}_{experimental}/Nu_{calculated}$ with Respect to Re_j
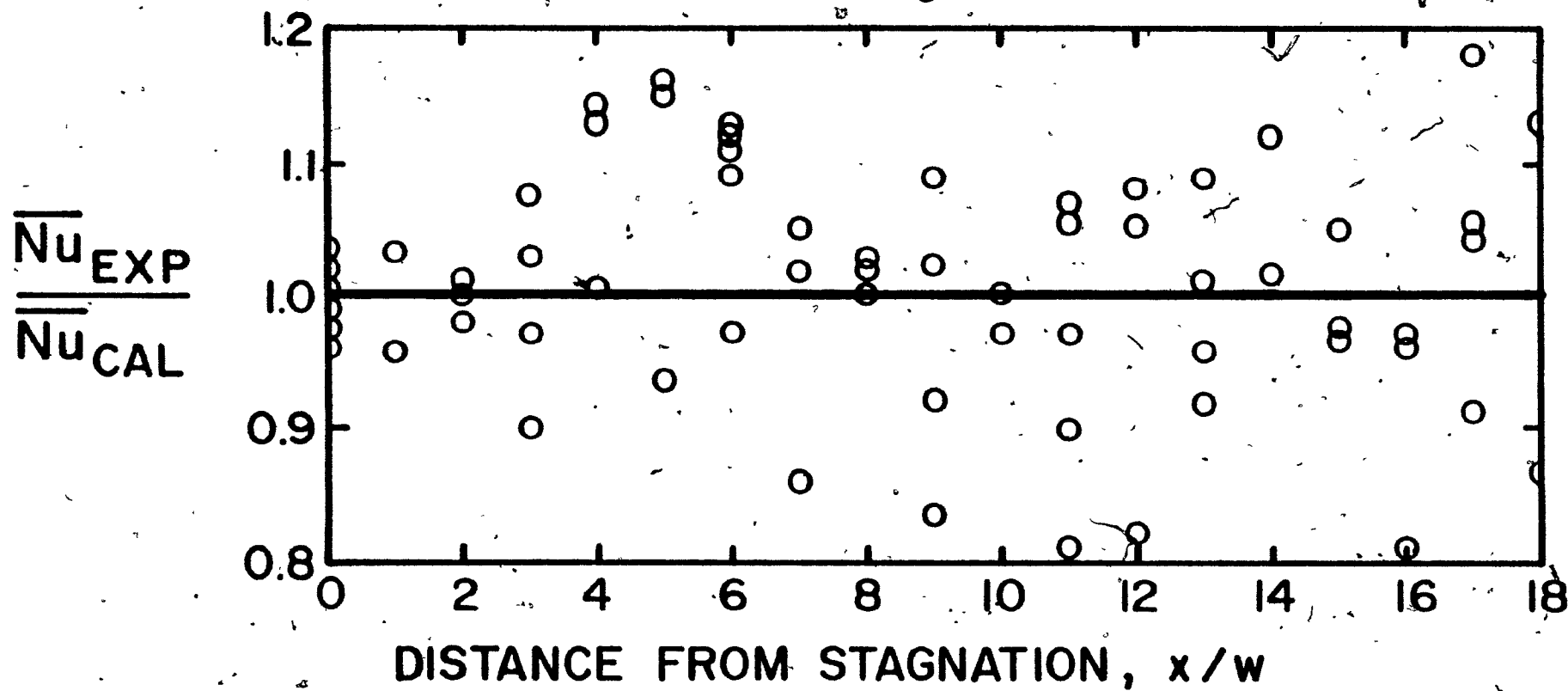
FIGURE 4.18b   Illustration of Independence of $\overline{Nu}_{experimental}/Nu_{calculated}$ with Respect to x/w
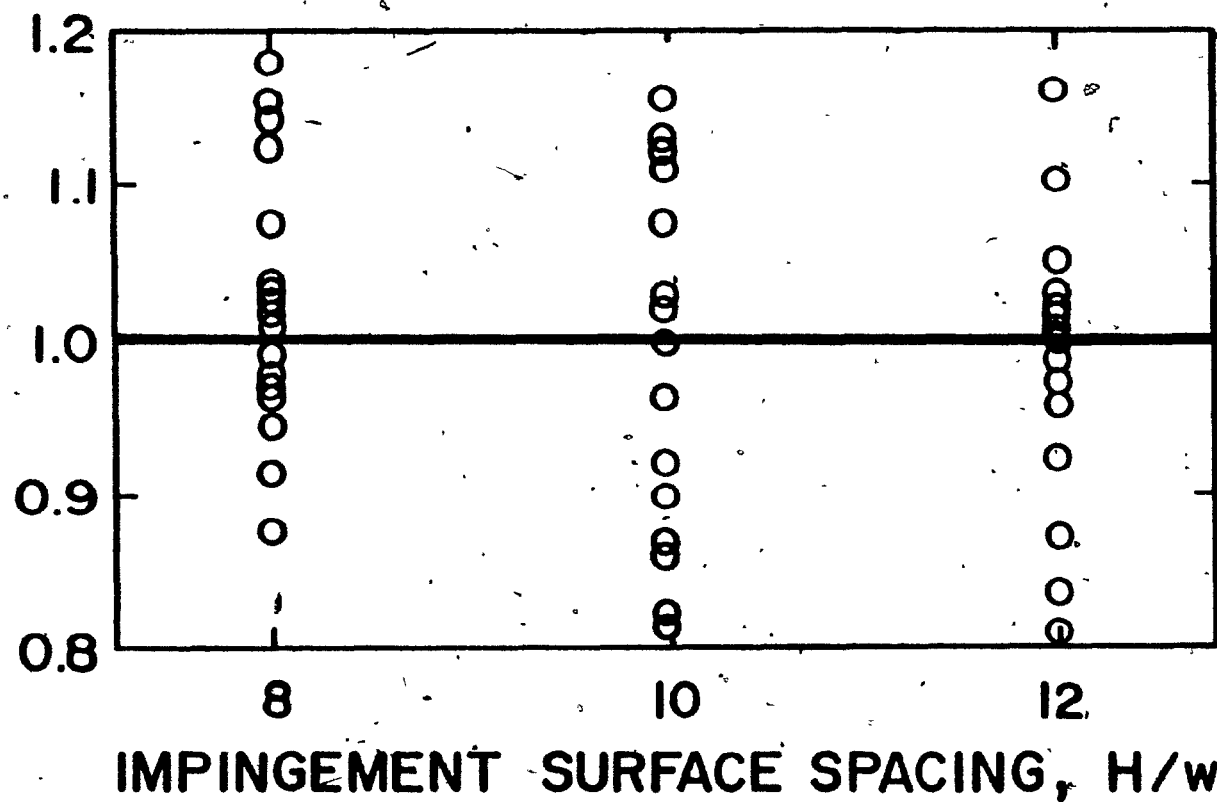
FIGURE 4.18c   Illustration of Independence of $\overline{Nu}_{experimental}/Nu_{calculated}$ with Respect to H/w

$$\frac{\overline{Nu}_{EXP}}{\overline{Nu}_{CAL}}$$

TEMPERATURE RATIO, T_j/T_s
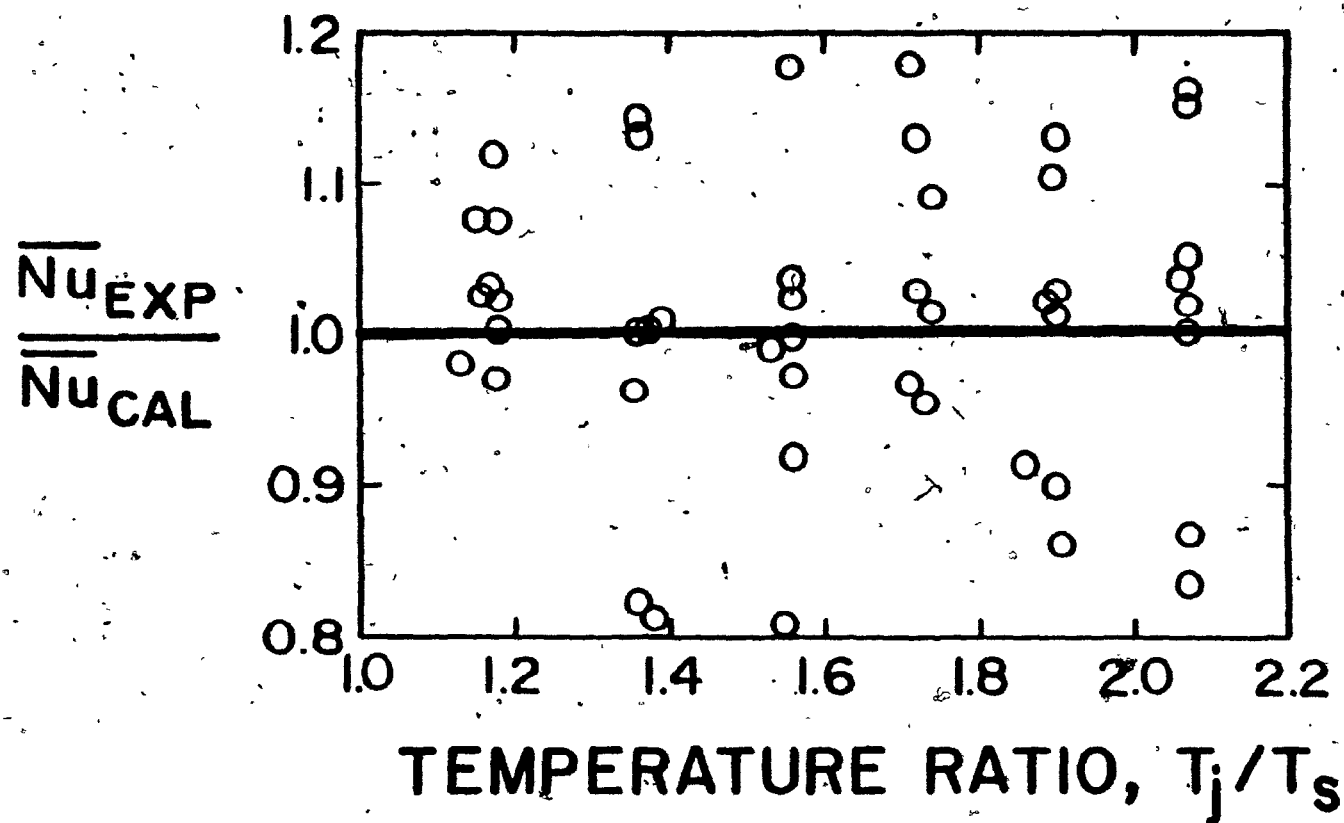
FIGURE 4.18d   Illustration of Independence of $\overline{Nu}_{experimental}/Nu_{calculated}$ with Respect to T_j/T_s
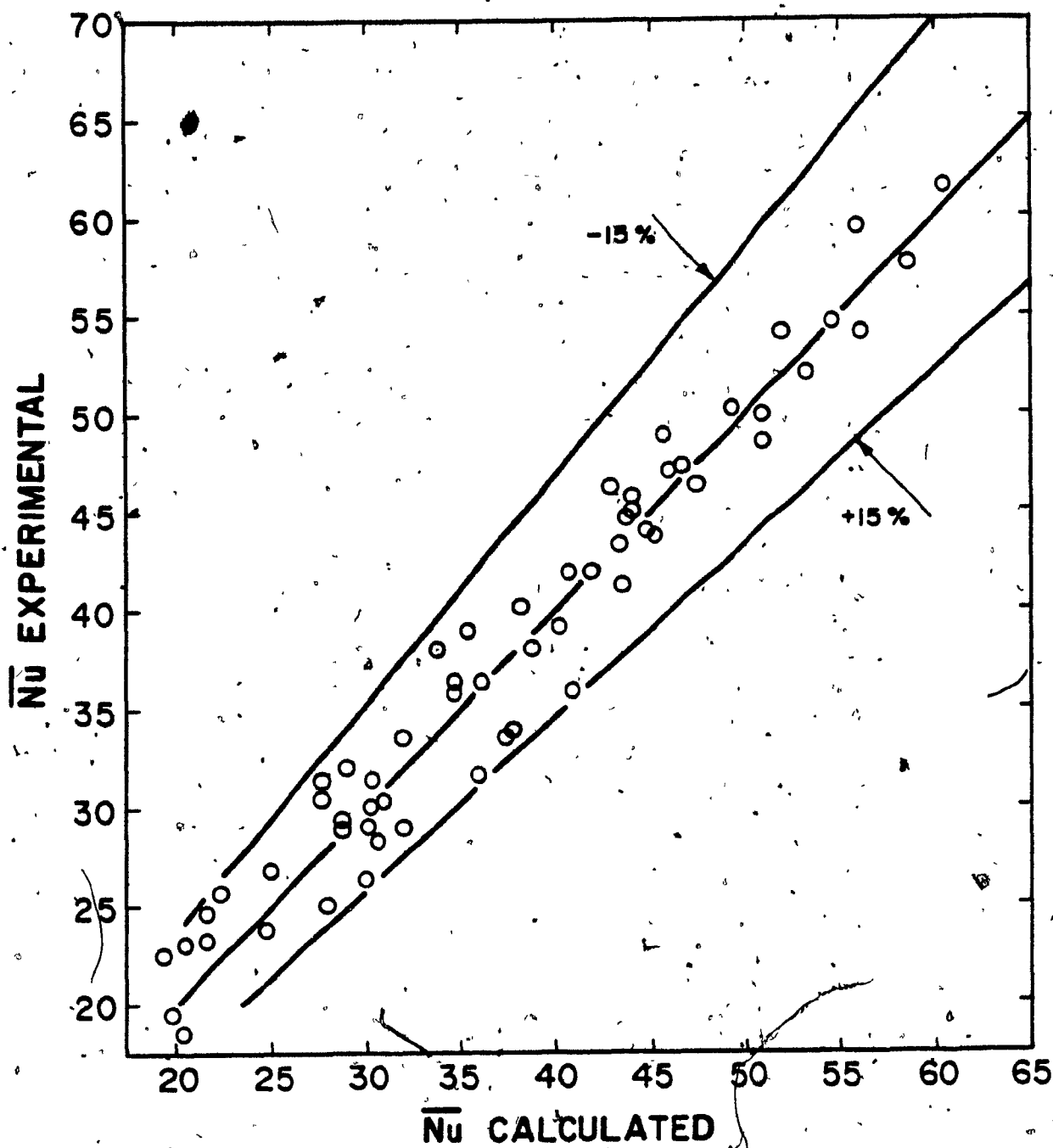
FIGURE 4.19   Comparison of Calculated $\overline{Nu}$ to Experimental $\overline{Nu}$

It is evident from the above analysis using the temperature ratio method, that the effect of temperature on the average Nusselt number changes, though moderately but systematically, with distance from the stagnation line up to about x/w = 6. Consequently it is reasonable to expect that, the reference temperature method would lead to reference temperatures which are dependent on x/w. Since a variable reference temperature would add substantially to the complexity of the practical application of this work no attempt was made to obtain any average Nusselt number correlation using the reference temperature method.

4.5 Analysis as a Confined Flow System

For a confined flow system such as that of the present study the heat transferred from the nozzle exit flow to the impingement surface can be expressed as follows in terms of average heat transfer coefficient.

$$Q_1 = \bar{h}x (T_j - T_s) \tag{4.17}$$

The heat given up by the jet flow can be expressed as

$$Q_2 = \frac{\rho_j v_j w}{2} Cp_j (T_j - T_b) \tag{4.18}$$

where T_b is the average (i.e. mixing-cup) temperature of the air at any location x.

If the heat losses through the confinement surfaces are negligible, the two heat fluxes can be equated to yield

$$\frac{T_j - T_b}{T_j - T_s} = \frac{2\bar{h}x}{\rho_j v_j w Cp_j} = \frac{2 \frac{x}{w} \overline{Nu}_j}{Re_j Pr_j} \tag{4.19}$$

At the exhaust port, where $T_b = T_e$, $x = L$:

$$\frac{T_j - T_e}{T_j - T_s} = \frac{2 \frac{L}{w} \overline{Nu}_j}{Re_j \; Pr_j} \qquad (4.20)$$

In Section 4.4 we saw that the average Nusselt number is proportional approximately to the square root of the Reynolds number. Taking into account, as shown in Section 4.4, that the coefficient K in equation 4.15 varies approximately as $(x/w)^{-2/3}$, this equation can be rewritten as

$$\overline{Nu}_j = K' \; (x/w)^{-2/3} \; Re_j^{0.5} \qquad (4.21)$$

where K', a weak function of x/w, is a variable parameter accounting for the effects of H/w, T_j/T_s and Pr_j.

Hence the temperature difference ratios defined, in equation 4.19 will vary approximately as the inverse square root of Reynolds number, i.e.

$$\frac{T_j - T_b}{T_j - T_s} = K'' \; \frac{x}{w}^{1/3} \Big/ Re_j^{0.5} \qquad (4.22)$$

where $\qquad K'' = \frac{2K'}{Pr_j}$

The above analysis treats the average (mixing-cup) temperature of the confined flow, T_b, but does so in terms of the mean heat transfer coefficient and Nusselt number, $\overline{h}$ and $\overline{Nu}_j$, as conventionally defined for an unconfined flow. It is therefore of interest to consider the definition of heat transfer coefficient for confined and unconfined jet systems, as recently suggested by Saad (1981).

For unconfined flows, convective heat transfer coefficients are obtained by normalizing the convective flux to a ΔT which is the difference between two boundary condition temperatures. In the case

of impinging jets, these temperatures are typically the nozzle exit temperature, T_j, and the heat transfer surface temperature, T_s. As most impingement experimental studies have been carried out with un-confined jets, $T_j - T_s$, has been the ΔT used for normalizing heat fluxes to obtain transfer coefficients. However, as the importance of industrial applications involving confined impingement systems lead to the recent series of investigations with confined jets in this laboratory, including the present study, the general question of the definition of convective heat transfer coefficient in confined impingement flow systems is now examined.

For confined flow systems, convective heat transfer coefficients are based on normalizing heat flux to a ΔT which is the difference between the mixing-cup temperature of the confined flow, T_b, and the heat transfer surface temperature, T_s. Thus for confined flows a local convective heat transfer coefficient is the local heat flux, q, normalized to the local ΔT. A heat balance on the confined flow yields the local value of the bulk temperature of the confined flow, T_b, needed to determine $T_b - T_s$, the local ΔT. This approach is now applied to the confined impingement flow system of the present investigation.

The local heat transfer coefficient determined using the local temperature driving force, $T_b - T_s$, is designated as h_b in order to distinguish it from h, the conventional transfer coefficient which is the local heat flux, q, normalised with respect to $T_j - T_s$, the temperature driving force at the nozzle centerline boundary. Thus for h_b, both q and ΔT are local values which are a function of x, while for h,

the normalization of local heat flux is with respect to the boundary value of ΔT at $x = 0$. The heat transfer coefficient

$$h_b = \frac{q}{T_b - T_s} \tag{4.23}$$

is related to the coefficient based on $T_j - T_s$ as follows:

$$h_b = h \frac{(T_j - T_s)}{(T_b - T_s)} \tag{4.24}$$

or

$$h_b = \frac{h}{1 - K''(x/w)^{1/3}/Re_j^{0.5}} \tag{4.25}$$

The values of h and h_b (and correspondingly of Nu_j and Nu_b, and of $\overline{Nu_j}$ and $\overline{Nu_b}$) coincide at the nozzle centerline, $x = 0$, while away from stagnation h_b is always greater than h, with the difference, $h_b - h$, increasing continuously to the exit port as the local value of ΔT_b decays from its maximum value, $T_j - T_s$, at $x = 0$ to the minimum value of $\Delta T_b = T_e - T_s$, at $x = L$. As is evident that conditions which reduce the relative decrease in ΔT_b from $x = 0$ to $x = L$ would reduce the difference between h and h_b, i.e. the higher the nozzle exit flow rate or $T_j - T_s$, the lower the difference between h and h_b.

To illustrate the magnitude of the difference between local heat transfer coefficients defined in these two alternate ways, values of local Nusselt number (Nu_j and Nu_b) at $x/w = 18$ are listed in Table 4.4 for three cases from the present study. The expected reductions in the relative difference between Nu_j and Nu_b with increasing Re_j and with increasing T_j (i.e. increasing $T_j - T_s$) are shown by comparison of cases 1 and 2 and of cases 1 and 3 respectively.

TABLE 4.4

Comparison of Nu_j and Nu_b

Case	Re_j	H/w	T_j	T_e	$\dfrac{T_e - T_s}{T_j - T_s}$	Nu_j	Nu_b
1	1000	8	309°C	240°C	0.79	3.3	4.25
2	4900	8	307°C	270°C	0,88	11.0	12.7
3	1000	8	54°C	37.5°C	0.68	2.1	3.1

Lateral profiles of Nu_b, not shown, are of course similar in appearance to those for Nu_j shown in Section 4.3, except that away from $x = 0$ the profiles of Nu_j and Nu_b diverge. Profiles of Nu_j reflect the local flow conditions which control convective heat transfer while profiles of Nu_b reflect local flow conditions and, as well, the local ΔT driving force for convective heat transfer. Thus it is important when interpreting profiles of Nusselt number to recall that local convective heat transfer is not determined uniquely by the flow-field but includes also the ΔT or thermal effect. This fact seems not to have been widely understood.

It is conceivable that much of the effect of large ΔT on the heat transfer coefficient could be accounted for if the experimental data were analyzed in terms of h_b rather than h. However, this approach was not followed because it would complicate the use of the results of the present study for the design of impinging jet systems by making it necessary for the user to employ an iterative procedure.

An important general consequence of this analysis as a confined jet system is the additional and valuable insight into the heat transfer results provided by equation (4.22). The temeprature ratio defined in that equation is a measure of the fraction of the sensible heat available in the nozzle exit jet which has been transferred to the impingement surface. Clearly as the lateral distance between the nozzle centerline and the exhaust port is increased, more of the available sensible heat is withdrawn from the inlet jet. Also, while the overall rate of heat transfer increases proportional to $Re_j^{0.5}$ (equation 4.15) it is important to observe from equation 4.22 that the fraction of the available heat which is withdrawn from the inlet jet decreases proportional to $1/Re_j^{0.5}$.

CHAPTER V

SUMMARY AND CONCLUSION

1.   The effect of high temperature difference on local and average heat transfer rates under a confined single slot jet impinging on a cool surface has been documented for 104 combinations of the following ranges of conditions:

Jet Reynolds number, Re_j, 1000 to 20000

Impingement surface spacing from nozzle, 5w to 12w

Temperature difference, ΔT, 50°C to 300°C

Temperature ratio, jet to surface, T_j/T_s, 1.18 to 2.08

Lateral distance from stagnation, x/w, 0 to 18.

The spent fluid exhausted symmetrically through a pair of exhaust ports located at the end of the confinement surface, 23w from the nozzle centerline.

2.   Several methods to incorporate the large effect of temperature dependent physical properties into the heat transfer correlations were tested. For heat transfer at stagnation, two methods, the temperature ratio method and reference temperature method were found to be suitable.

The recommended correlation for stagnation heat transfer, using the temperature ratio method is

$$Nu_{oj} = \left[0.79 \ Re_j^{0.485} \ (H/w)^{-0.134} \ (T_j/T_s)^{-0.115} \ Pr_j^{1/3} \right.$$

The recommended correlation of stagnation heat transfer using the reference temperature method is

$$Nu_{oT_{ref}} = 0.648 \ Re_j^{0.485} \ (H/w)^{-0.138} \ Pr_j^{1/3}$$

where subscript T_{ref} is the reference temperature which was determined to be

$$T_{ref} = T_j - 0.2 \ (T_j - T_s)$$

In both the cases, the subscript j on the dimensionless numbers indicates that their physical properties were evaluated at the jet exit temperature, T_j. The deviation of experimental measurements from either of the correlations was within $\pm 5\%$.

The Reynolds number exponent of approximately 0.5 reflects the laminar character of the boundary layer in the stagnation region, even for highly turbulent jets. This conclusion is consistent with the recent findings of van Heiningen (1982).

The exponents for H/w in the above correlations are smaller than those previously reported for investigations extending to much higher values of H/w. This lower exponent is a natural consequence of the maximum in Nu_o for H/w = 8, at which point the exponent would be zero.

The above two correlations are valid only for Reynolds numbers of $Re_j \geqslant 5000$ and for impingement surface spacings H/w $\geqslant$ 8. For turbulent jets, Nu_o passes through a maximum at H/w = 8, for the laminar jet at Re_j = 1000, Nu_o is independent of H/w over the tested range of spacings, 5w to 12w. In these ranges of conditions, i.e. for $1000 < Re_j < 5000$ and $5 < H/w < 8$, Nu_o may be obtained from the data in the Appendix B.

3. Lateral profiles of local Nusselt number were obtained for the ranges of conditions noted above. These profiles were well defined by local heat flux measurements at 19 positions over both halves of the entire 18w length of the impingement surface. At the closest spacing, H/w = 5, characteristic feature of an off-stagnation minimum and maximum was observed at sufficiently high Re_j. The profiles confirmed features reported by earlier investigators and extended documentation of local profiles to much higher levels of ΔT than those which existed previously.

The local Nusselt number distribution for the entire range of parameters, i.e. $1000 \leqslant Re_j \leqslant 20000$, $5 \leqslant H/w \leqslant 12$ and $1.18 \leqslant T_j/T_s \leqslant 2.08$ is listed in Appendix B.

4.   Following general correlation for average Nusselt number, for $Re_j \geqslant 5000$, and $8 \leqslant H/w \leqslant 12$ was developed, incorporating the temperature ratio method

$$\overline{Nu}_j = K\, Re_j^a\, (H/w)^b\, (T_j/T_s)^c\, Pr_j^{1/3}$$

where subscript j indicates evaluation of physical properties at the nozzle exit temperature, T_j. The coefficient K and exponents a, b and c are functions of x/w as given in Figure 4.16 and listed in Table 4.3. The deviation of experimental data from this correlation was within $+15\%$.

.   As the heat transfer averaging distance is extended toward the maximum value of x/w = 18, the exponent, a, for Re_j increases from approximately 0.5 to about 0.55. This increase is attributed to the turbulent character of the wall jet. For a fully developed turbulent boundary layer the Reynolds number exponent for local Nu would be in the order of 0.8.

Likewise, the exponent, b, for H/w, which has the value of -0.134 for Nu_o, approaches zero for heat transfer averaged over the entire lateral distance from the stagnation line to x/w = 18. This diminishing effect of H/w on $\overline{Nu}_j$ with increasing x/w was interpreted in terms of the diminishing effect of H/w on the total distance covered by the impingement flow, H/w + x/w.

In the ranges of conditions, $1000 < Re_j < 5000$ and $5 < H/w < 8$, for which the logarithmic linear correlation form does not apply for reasons noted earlier, $\overline{Nu}_j$ may be obtained from the data in Appendix C.

No correlation was developed between average Nusselt number and geometric and flow parameters using the reference temperature method. From the analysis using the temperature ratio method it became apparent that the reference temperature would be a function of x/w. The added complexity of a variable reference temperature is undesirable and, with the temperature ratio method available, is also unnecessary.

5. The analysis of confined jet impingement heat transfer in terms of a channel flow approach was explored. At each location along the impingement surface, the temperature driving force was defined as the difference between the local mixing-cup temperature and the impingement surface temperature, rather than the difference between the latter temperature and the nozzle exit temperature. The more realistic values of local heat transfer coefficient obtained in this way, which must be higher than local values obtained with the conventional use of $T_j - T_s$ as the ΔT for convective heat transfer, provide a more realistic representation of local heat transfer coefficient but would entail significantly more effort to calculate, correlate and to use in design. However, this analysis revealed that the fraction of total available heat which is transferred to the impingement heat transfer surface is proportional to $(x/w)^{1/3}$ and to $1/Re_j^{0.5}$, whereas the overall heat transfer rate is proportional to $Re_j^{0.5}$.

REFERENCES

Beltaos, S. and N. Rajaratnam (1973): Plane turbulent impinging jets, J. of Hydraulic Research, Vol. 11, No. 1, pp 30-59.

Beltaos, S. and N. Rajaratnam (1974): Impinging circular turbulent jets, Prov. of ASCE, Vol. 100, No. HY10, p. 1313.

Burgess, B.W., S.M. Chapman and W. Seto (1972): The Papridryer Process, Part I: The basic concepts and laboratory results, Pulp and Paper Mag. Can., Vol. 73, No. 11, pp 314-322.

Burgess, B.W., W. Seto, E. Koller and J.T. Pye (1972): The Papridryer Process, Part II: Mill trial, Pulp and Paper Mag. Can., Vol. 73, No. 11, pp 323-331.

Cadek, F.F. (1968): A Fundamental investigation of jet impingement heat transfer, Ph.D. Thesis, University of Cincinnati.

Cadek, F.F. and R.D. Zerkle (1974): Local heat transfer characteristics of two dimensional impinging air jets - theory and experiments, Proc. Fifth Int. Heat transfer Conf., Tokyo, FC 1.4 pp 15-19.

Daane, R.A. and S.T. Han (1961): An analysis of air-impingement drying, TAPPI, Vol. 44, No. 1, pp 73-80.

Folayan, C.O. and J.H. Whitelaw (1977): Impingement cooling and its application to combustor design, Joint Gas Turbine Congress, Tokyo, JSME, GTSJ, ASME, pp 69-76.

Gardon, R. and J.C. Akfirat (1965): The role of turbulence in determining the heat transfer characteristics of impinging jets, Int. J. of Heat and Mass transfer, Vol. 8, pp 1261-1272.

Gardon, R. and J.C. Akfirat (1966): Heat transfer characteristics of impinging two dimensional air jets, Trans. ASME, J. of Heat Transfer, Vol. 88, pp 101-108.

Gardon, R. and J. Cobonpue (1962): Heat transfer between a flat plate and jets of air impinging on it, Proc. 2nd Int. developments in Heat transfer pp 454-460.

Gauntner, J.W., J.N.B. Livingwood and P. Hrycak (1970): Survey of literature on flow characteristics of a single turbulent jet impinging on a flat plate, NASA TN D-5652.

Huang, G.C. (1963): Investigations of Heat transfer coefficients for air flow through round jets impinging normal to a heat transfer surface, Trans ASME, J. of Heat transfer Vol. 85, pp 237-245.

Kays, W.M. (1966): Convective heat and mass transfer, McGraw-Hill Book Company.

Kays, W.M. and W.B. Nicoll (1963): Laminar flow Heat transfer to a Gas with large temperature differences.
Trans ASME, J. of Heat transfer Vol. 84, pp 329-338.

Livingwood, J.N.B. and P. Hrycak (1973): Impingement heat transfer from turbulent air jets to flat plates - A literature survey, NASA TM X-2778.

Martin, H. (1977): Heat and Mass transfer between impinging jets and solid surfaces. Advances in Heat Transfer, Vol. 13, Academic Press, New York.

Metzger, D.E. (1962): Spot cooling and heating of surfaces with high velocity impinging air jets. Part-I slot jets on plane surfaces, Technical Report No. 52, Dept. of Mech. Engineering, Stanford University.

Mujumdar, A.S. and W.J.M. Douglas (1972): Impingement heat transfer: A literature survey, TAPPI Engg. Conf., New Orleans.

Obot, N.T. (1980): Flow and Heat transfer for round turbulent jets impinging on permeable and impermeable surfaces, Ph.D. Thesis, Chem. Engg. Dept., McGill University.

Perry, K.P. (1954): Heat transfer by convection from a hot gas jet to a plane surface, Proc. Inst. of Mech. Engineers, Vol. 168, pp 775-780.

Petukhov, B.S. (1970): Heat transfer and friction in turbulent pipe flow with variable physical properties, Advances in Heat Transfer, Vol. 6, Academic Press, New York.

Poreh, M. and J.E. Cermak (1959): Flow characteristics of a circular submerged jet impinging normally on a smooth boundary, 6th Mid-Western Conf. on Fluid Mechanics, University of Texas, p.198.

Saad, N.R. (1981): Flow and heat transfer for multiple turbulent impinging slot jets, Ph.D. Thesis, Chem. Engg. Dept., McGill University.

Schauer, J.J. and R.H. Eustis (1963): The flow development and heat transfer characteristics of plane turbulent impinging jets, Technical Report No. 3, Mech. Engg. Dept., Stanford University.

Shah, R.K. and A.L. London (1978): Laminar flow forced convection in ducts; a source book for compact heat exchanger analytical data, Academic Press, New York.

Sparrow, E.M. and T.C. Wong (1975): Impingement transfer coefficients due to initially laminar slot jets, Int. J. of Heat and Mass transfer, Vol. 18, pp 597-605.

Thurlow (1954): Communication to Perry, Proc. Inst. of Mech. Engineers, Vol. 168, pp 781-784.

Van Heiningen, A.R.P., A.S. Mujumdar and W.J.M. Douglas (1976): Numerical prediction of the flow field and impingement heat transfer caused by a laminar slot jet, Trans. ASME, J. of Heat Transfer, Vol. 98, No. 4, pp 654-658.

Van Heiningen, A.R.P., A.S. Mujumdar and W.J.M. Douglas (1977): Flow and heat transfer characteristics of turbulent slot jet impinging on a moving wall, Turbulent Shear Flow Symposium, Penn. State University.

Van Heiningen (1982): Heat transfer under an impinging slot jet, Ph.D. Thesis, Chem. Engg. Dept., McGill University.

APPENDICES

APPENDIX A

List of Experimental Conditions

t_j (°C)	t_s (°C)	H/w	Re_j	t_j (°C)	t_s (°C)	H/w	Re_j
50.0	3.2	5	1000	101.8	3.8	5	1000
51.9	3.5	5	5000	103.5	4.3	5	4900
49.1	6.2	5	9700	97.8	4.5	5	10500
51.1	10.6	5	13800	102.2	4.1	5	15900
52.3	10.2	5	18800	102.4	3.9	5	21600
53.5	2.9	8	1000	98.9	4.0	8	1000
53.6	3.2	8	5000	105.3	4.4	8	4900
52.8	7.5	8	10400	110.8	5.5	8	10200
55.2	8.3	8	14500	111.5	7.6	8	15600
55.6	7.7	8	18400	104.1	8.6	8	20100
54.2	3.3	10	1000	104.2	3.3	10	1000
52.3	3.7	10	5000	102.3	3.7	10	4900
49.5	11.8	10	10000	112.5	6.0	10	10100
50.9	10.5	10	13600	106.2	5.6	10	15800
52.0	8.8	10	18100	101.4	4.3	10	21800
55.2	3.3	12	1000	105.1	3.3	12	1000
52.1	3.9	12	5000	102.0	3.9	12	4900
55.0	8.6	12	10100	104.0	6.4	12	10300
55.8	8.1	12	14500	113.4	7.6	12	15600
57.6	8.9	12	19100	105.2	5.1	12	21100
155.2	3.1	5	1000	207.8	4.6	5	1000
150.0	4.6	5	5000	202.6	6.1	5	5000
156.4	5.4	5	9900	203.6	3.8	5	9800
159.3	6.1	5	14700	208.3	5.5	5	14600

t_j (°C)	t_s (°C)	H/w	Re_j	t_j (°C)	t_s (°C)	H/w	Re_j
159.3	3.4	8	1000	212.3	5.1	8	1000
158.5	4.4	8	5000	207.6	6.4	8	4900
160.8	5.5	8	10000	210.9	5.6	8	9700
161.5	7.6	8	14800	205.2	3.9	8	15000
169.6	3.4	10	1000	222.0	4.8	10	1000
154.9	3.1	10	4900	204.9	4.7	10	5000
162.5	6.6	10	10400	212.5	6.0	10	9800
156.2	5.6	10	15200	206.2	5.6	10	15000
150.7	3.8	12	1000	214.0	5.6	12	1000
155.9	5.2	12	4900	204.5	4.6	12	5000
154.0	6.4	12	10000	206.0	7.6	12	10000
163.4	7.6	12	15000	208.4	4.6	12	14600
259.7	3.8	5	1010	304.2	4.0	5	1000
260.0	4.7	5	4800	301.1	5.3	5	5000
258.1	4.9	5	9600	305.7	6.2	5	10000
261.0	5.6	5	14600	306.0	6.5	5	15000
257.2	3.7	8	1000	309.3	4.8	8	1000
254.3	5.8	8	4900	306.6	7.2	8	4900
258.1	7.2	8	9800	302.0	5.6	8	9900
259.2	8.3	8	14600	303.0	6.2	8	15200
260.0	4.2	10	1000	310.0	4.2	10	1000
255.6	5.4	10	4900	300.8	5.0	10	5000
264.6	7.3	10	9500	306.0	6.1	10	10000
260.8	7.8	10	14600	303.4	5.5	10	15300
257.4	3.2	12	1000	307.4	3.2	12	1000
255.2	5.8	12	4900	303.6	5.1	12	5000
258.6	7.1	12	9600	303.5	5.5	12	10000
258.2	7.0	12	14800	305.6	6.4	12	15200

APPENDIX B

Local Nusselt Numbers

T_j/T_s	NN	Rej	0	1	2	3	4	5	6	7	8	9	10	11	12	13	14	15	16	17	18
1.169	5	1000	14.65	11.07	8.13	6.81	6.05	5.50	5.05	4.69	4.23	3.78	3.42	3.16	3.01	2.93	2.76	2.64	2.44	2.23	2.01
1.175	5	5000	29.17	23.02	17.71	15.30	14.34	13.78	13.22	12.56	12.06	11.36	10.97	10.61	10.24	9.66	9.21	8.78	8.53	7.89	7.61
1.153	5	9700	41.19	30.40	24.05	22.98	22.95	21.53	19.79	18.59	18.70	18.21	18.03	17.65	17.20	16.95	16.51	16.62	16.42	16.11	15.82
1.142	5	13800	45.12	34.37	28.96	25.22	27.83	29.03	29.37	29.19	28.47	26.30	25.71	25.74	25.31	24.96	24.52	24.12	23.87	23.56	23.15
1.149	5	18800	55.16	41.25	34.13	32.94	34.35	31.14	35.81	35.97	35.24	33.63	32.11	32.18	31.74	31.32	31.00	30.68	30.24	30.01	29.88
1.184	8	1000	13.87	10.98	7.54	7.11	6.35	5.94	5.55	5.11	4.85	4.39	3.99	3.77	3.07	2.90	2.84	2.71	2.50	2.19	1.96
1.150	8	5000	34.22	29.23	23.87	20.23	17.82	16.80	16.10	15.32	14.78	14.28	13.76	13.21	13.15	12.73	12.43	12.14	11.64	11.43	11.22
1.162	8	10400	47.33	45.57	39.93	34.01	31.43	29.95	28.60	27.20	26.06	23.55	21.85	22.49	21.96	21.63	21.00	20.99	20.45	20.11	19.86
1.167	8	14500	54.77	53.63	45.39	40.37	37.76	36.69	34.44	33.12	31.43	28.80	26.88	26.85	26.43	26.02	25.52	25.43	24.73	24.11	23.82
1.171	8	18400	61.05	58.25	51.37	47.70	44.05	41.80	39.72	38.16	36.58	33.78	31.57	31.40	30.86	30.27	29.91	29.46	29.00	28.68	28.11
1.184	10	1000	15.00	12.30	9.94	8.65	7.44	6.81	6.25	5.93	5.13	4.27	3.63	3.53	3.36	3.25	2.77	2.33	2.11	2.06	1.95
1.175	10	5000	32.73	28.42	23.90	19.50	17.76	16.29	15.55	14.98	14.25	13.92	13.77	13.04	13.43	12.90	12.53	12.35	12.04	11.49	11.07
1.132	10	10000	43.81	37.05	31.65	28.19	26.02	25.30	24.70	24.07	23.66	23.23	21.21	21.41	21.00	20.73	20.35	19.99	19.49	19.13	18.63
1.142	10	13600	51.95	43.32	37.90	34.82	33.07	32.36	31.69	31.17	30.63	29.32	28.02	28.06	27.64	27.42	27.14	26.52	26.11	25.87	25.67
1.153	10	19100	63.24	58.54	48.06	43.46	40.82	39.06	37.88	37.23	36.58	35.30	34.00	34.18	33.86	33.51	33.00	32.67	31.14	30.87	30.44
1.188	12	1000	15.46	12.62	10.30	9.02	7.78	6.97	6.27	5.82	5.38	4.90	4.56	4.08	4.07	3.98	3.91	3.40	2.98	2.77	2.76
1.174	12	5000	30.18	27.13	23.21	19.91	17.45	15.93	15.25	14.49	13.96	13.74	13.35	12.88	12.72	12.21	11.87	11.59	11.59	11.14	10.62
1.153	12	10100	44.10	41.25	36.77	32.71	29.99	28.38	27.45	26.71	26.48	25.88	24.90	24.81	24.43	24.00	23.62	23.24	22.86	22.41	22.00
1.169	12	14500	50.32	47.80	41.75	37.99	35.28	33.96	33.16	32.47	17.09	32.19	31.32	30.75	30.36	29.98	29.31	29.00	28.66	28.41	28.12
1.172	12	19100	59.56	56.50	49.15	45.01	42.11	40.12	38.82	38.57	38.50	37.75	34.07	34.02	33.87	33.62	33.11	32.87	32.61	32.51	32.02
1.354	5	1000	14.33	12.07	9.05	7.51	6.94	6.59	6.15	5.79	5.44	5.09	4.86	4.50	3.95	3.60	3.25	3.07	2.89	2.78	2.63
1.358	5	4900	28.19	22.56	17.97	15.36	14.24	14.16	13.61	13.03	12.41	12.05	11.24	10.80	10.37	10.01	9.50	9.07	8.57	8.08	7.56
1.336	5	10500	41.37	38.39	26.16	21.06	20.53	21.66	23.18	23.14	22.39	20.71	20.97	19.51	19.05	18.65	17.99	17.68	17.38	17.03	16.75
1.354	5	15900	49.61	47.65	31.78	24.42	23.40	26.42	27.67	28.38	27.96	27.16	26.51	25.18	24.22	24.20	23.53	22.90	22.39	21.84	21.41
1.356	5	21630	56.92	53.16	33.96	32.64	31.38	28.97	33.21	34.55	33.86	33.29	33.04	32.30	31.90	31.16	30.34	30.04	29.96	29.75	28.56
1.343	8	1000	13.70	12.07	9.81	7.98	7.05	6.40	5.94	5.70	5.31	5.10	4.92	4.64	4.48	4.36	4.13	4.00	3.90	3.73	3.52
1.360	8	4900	32.99	29.49	25.56	21.25	18.71	17.60	15.78	15.22	14.29	13.87	13.10	12.88	12.22	12.05	11.46	11.22	10.73	10.49	9.98
1.380	8	10200	44.99	39.12	32.34	28.13	27.92	26.37	25.78	24.77	23.49	23.38	22.94	22.22	21.57	20.85	20.09	19.82	18.95	18.33	17.97
1.370	8	15600	54.05	45.71	39.37	34.03	31.87	30.16	29.10	28.20	27.37	26.18	27.52	26.77	26.67	25.53	25.32	24.95	24.37	23.86	23.53
1.339	8	20100	62.28	60.37	55.17	49.45	45.51	42.99	40.87	39.46	38.05	35.63	33.98	33.86	32.00	31.26	30.46	29.82	29.24	28.74	28.21
1.365	10	1000	14.74	11.86	9.42	8.07	7.00	6.53	5.82	5.41	4.76	4.01	3.45	3.39	3.15	3.02	2.62	2.23	2.04	2.02	1.99
1.356	10	4900	31.69	28.53	23.88	19.62	17.18	15.61	15.14	14.78	14.20	13.98	13.96	13.33	13.67	13.29	13.03	12.95	12.75	12.26	11.86
1.382	10	10100	45.34	38.96	32.28	26.96	23.84	21.95	22.07	19.98	20.55	19.34	19.29	18.29	18.63	16.87	17.43	17.48	17.10	16.43	15.76
1.361	10	15800	54.66	46.87	40.02	35.25	32.76	30.76	29.19	27.82	27.05	25.98	25.34	24.77	24.41	24.10	23.95	23.59	23.40	23.47	23.10
1.350	10	21800	64.72	61.78	47.23	38.23	34.78	33.48	33.55	32.32	31.34	30.90	30.34	29.68	29.73	28.99	28.66	29.04	27.55	27.40	26.83
1.369	12	1000	15.16	12.45	10.18	8.96	7.79	7.01	6.33	5.89	5.47	4.99	4.66	4.18	4.17	4.09	4.03	3.52	3.09	2.88	2.68
1.355	12	4900	29.04	26.06	22.28	19.06	16.68	15.22	14.55	13.83	13.32	13.10	12.73	12.30	12.14	11.66	11.33	11.05	11.05	10.63	10.12
1.350	12	10300	43.42	39.47	34.21	30.18	29.33	27.46	25.79	24.38	23.85	23.09	22.43	21.99	21.34	20.89	20.74	20.46	19.37	19.19	18.86
1.377	12	15600	53.14	46.65	41.28	37.08	34.41	34.20	30.86	30.22	30.20	29.63	28.56	28.21	27.36	26.91	26.46	25.87	25.80	25.20	24.90
1.360	12	21100	64.91	58.42	52.76	45.43	40.65	36.86	34.82	33.44	32.94	34.06	32.57	31.63	30.60	33.31	31.90	31.61	27.71	27.29	26.79

Tj/Tc	H/W	kr	0	1	2	3	4	5	6	7	8	9	10	11	12	13	14	15	16	17	18
1.551	5	1000	14.16	11.??	9.02	7.28	6.68	6.26	5.94	5.44	5.06	4.48	4.13	3.57	3.18	2.99	2.85	2.63	2.50	2.29	2.02
1.524	5	5000	25.19	22.49	17.72	16.27	15.96	15.19	14.86	12.95	12.53	12.10	11.66	11.41	11.13	10.94	10.73	10.57	10.37	10.11	9.86
1.542	5	9900	40.89	31.13	26.56	23.01	21.92	21.88	22.63	22.62	22.32	21.27	20.74	20.32	19.72	19.06	18.68	17.75	17.54	16.58	16.11
1.549	5	14700	46.96	36.95	30.73	27.01	26.11	26.18	27.74	27.61	27.13	26.54	26.01	25.30	24.55	23.87	23.61	23.29	22.35	21.94	21.56
1.564	8	1000	13.52	10.15	8.54	6.99	6.19	5.66	5.23	4.92	4.63	4.40	4.04	3.62	3.20	2.96	2.75	2.63	2.54	2.23	2.04
1.560	8	5000	33.36	29.32	25.64	22.01	19.12	18.01	17.16	16.32	15.67	15.24	14.73	14.21	14.20	13.55	13.36	13.54	13.26	12.48	12.51
1.556	8	10000	43.92	38.18	31.53	27.40	27.18	25.64	25.05	24.06	23.28	22.70	22.26	21.57	20.84	20.14	19.39	19.14	18.53	17.69	17.11
1.549	8	14900	52.22	44.24	37.20	33.04	30.93	29.32	28.29	27.43	26.51	27.44	26.71	26.15	26.07	24.98	24.79	24.40	23.88	23.27	22.92
1.631	10	1000	14.34	12.89	10.77	8.83	7.57	7.13	6.27	6.04	5.30	5.32	5.13	4.78	4.76	4.48	3.64	3.15	3.44	2.97	2.71
1.550	10	4900	31.13	27.60	22.49	18.78	16.70	15.47	14.77	13.89	14.25	13.69	13.32	12.93	12.87	12.44	12.22	12.43	11.46	11.17	10.87
1.557	10	10400	44.90	39.26	33.01	28.13	25.21	23.51	23.73	21.68	21.97	20.81	20.80	20.02	20.02	18.39	18.53	18.61	18.14	17.31	16.95
1.540	10	15200	57.93	49.74	42.28	36.97	34.02	32.22	32.30	30.52	30.82	30.09	29.35	28.58	28.24	28.02	27.51	26.87	26.34	26.10	25.85
1.531	12	1000	15.09	12.98	11.48	9.66	8.75	6.77	6.68	5.69	5.40	5.28	5.01	4.90	4.51	4.09	3.63	3.28	2.70	2.46	2.10
1.542	12	4900	23.66	24.13	22.57	19.24	17.34	15.64	14.63	13.87	13.61	13.13	12.66	12.86	12.56	12.19	11.92	11.84	11.61	11.43	11.19
1.529	12	10000	41.97	38.03	32.98	29.07	28.23	26.45	24.87	23.85	23.10	22.41	21.81	21.43	20.55	20.15	20.07	19.85	18.82	18.69	18.32
1.555	12	14900	50.91	44.92	39.67	35.57	32.99	32.67	29.42	28.75	28.19	27.07	26.48	25.79	25.11	24.64	24.17	23.63	23.48	22.92	22.18
1.732	5	1000	13.78	11.67	8.77	7.08	6.50	6.09	5.78	5.29	4.92	4.36	4.02	3.47	3.12	2.93	2.79	2.57	2.44	2.24	2.19
1.704	5	5000	27.45	20.68	17.24	15.78	15.52	14.82	14.51	12.67	12.24	11.81	11.39	11.17	10.89	10.71	10.52	10.33	10.19	9.96	9.73
1.722	5	9800	38.79	30.51	25.95	22.42	21.30	21.22	21.97	22.01	21.71	20.69	20.19	19.79	19.50	18.89	18.51	17.58	17.39	16.44	15.94
1.728	5	14600	46.50	37.63	30.50	26.83	25.96	26.06	26.34	25.88	25.21	24.56	24.00	25.33	23.74	22.01	20.92	20.01	19.70	19.04	18.82
1.745	8	1000	13.14	10.07	8.30	6.77	6.01	5.50	5.08	4.78	4.50	4.28	3.93	3.52	3.24	2.99	2.78	2.66	2.57	2.25	2.00
1.720	8	4900	31.88	27.95	24.37	20.86	18.09	17.02	16.19	15.42	14.80	14.41	13.87	13.40	13.33	12.74	12.57	12.74	12.49	11.76	11.21
1.737	8	9700	43.00	37.38	30.83	26.78	26.74	25.05	24.45	23.48	22.71	22.14	21.71	21.05	20.78	20.07	19.32	19.07	18.20	17.61	17.12
1.727	8	15000	52.58	44.57	37.50	33.32	31.18	29.59	28.55	27.69	26.77	27.71	26.99	26.46	26.39	25.29	25.10	24.70	24.20	23.82	23.46
1.782	10	1000	14.03	12.81	10.39	8.58	7.30	6.86	6.01	5.79	5.14	5.15	4.98	4.62	4.39	4.12	3.42	2.94	3.21	2.76	2.51
1.721	10	5000	30.87	27.40	22.35	18.90	16.63	15.42	14.74	13.87	14.24	13.69	13.33	12.94	12.75	12.33	12.12	12.34	11.38	11.09	10.73
1.740	10	9800	42.88	37.95	32.15	27.70	25.01	23.49	23.75	21.82	21.93	20.84	20.85	19.95	19.82	18.19	18.18	18.27	17.76	16.89	16.34
1.720	10	15000	51.44	44.31	37.53	32.70	29.93	28.30	28.12	26.45	26.50	25.89	25.29	24.68	24.21	24.70	24.91	24.39	23.99	23.50	23.11
1.748	12	1000	14.56	12.44	11.00	9.26	8.38	6.48	6.40	5.45	5.18	5.05	4.80	4.69	4.37	3.96	3.52	3.18	2.62	2.39	2.00
1.720	12	5000	28.04	23.64	22.16	18.92	17.09	15.42	14.39	13.64	13.39	12.92	12.45	12.44	11.95	11.60	11.34	11.27	11.05	10.88	10.34
1.707	12	10000	41.34	37.40	32.43	28.57	27.73	25.29	24.45	23.47	22.76	22.11	21.54	21.17	20.54	20.16	20.10	19.90	18.88	18.78	18.42
1.734	12	14600	50.34	44.53	39.27	35.18	32.48	32.23	28.99	28.30	29.30	28.71	28.21	27.68	27.62	27.05	26.49	25.89	25.66	25.05	24.42

APPENDIX B (cont'd)

T_j/T_s	M/..	Ref	)	1	2	3	4	5	6	7	8	9	10	11	12	13	14	15	16	17	18
1.924	5	1000	13.73	11.93	8.81	7.23	6.62	6.02	5.86	5.39	4.94	4.60	3.82	3.54	3.55	2.73	2.53	2.48	2.10	2.16	2.02
1.919	5	4800	27.70	21.92	16.56	13.82	13.06	12.63	13.09	12.74	12.37	11.82	11.67	11.29	10.99	10.64	10.39	10.10	9.88	9.76	9.54
1.911	5	9600	38.54	30.39	23.52	20.24	19.50	19.64	20.01	19.63	19.15	18.67	18.16	19.39	17.52	16.85	16.30	16.23	15.77	15.62	15.49
1.917	5	14600	46.49	37.08	30.07	26.48	25.57	25.36	25.32	27.51	27.28	27.04	26.31	25.70	25.26	24.46	24.22	23.82	23.16	22.33	22.11
1.916	8	1000	13.08	11.98	9.72	7.78	6.76	5.95	5.59	5.19	4.91	4.71	4.48	4.31	4.22	4.05	3.86	3.71	3.46	3.39	3.10
1.880	8	4900	31.43	27.11	21.97	18.40	17.41	16.33	15.41	14.78	14.43	13.89	13.61	13.19	12.91	12.70	12.31	12.02	11.69	11.73	11.41
1.895	8	9800	43.85	37.70	31.37	27.51	25.19	24.18	23.45	22.69	22.16	21.31	20.63	20.30	20.21	19.74	19.37	18.79	18.04	17.68	17.51
1.892	8	14600	50.93	43.56	36.97	32.87	30.57	29.03	28.25	27.20	26.69	25.77	25.34	24.53	24.69	23.74	23.07	22.78	22.40	21.62	21.01
1.923	10	1000	14.20	12.02	9.91	7.84	6.88	6.19	5.75	5.27	4.95	4.64	4.50	4.26	3.99	3.82	3.57	3.48	3.32	3.18	3.08
1.900	10	4900	30.20	26.72	23.09	20.13	18.24	17.07	16.40	16.01	15.66	12.66	15.04	14.76	14.51	14.25	13.86	13.07	12.54	12.13	11.98
1.918	10	9500	41.92	36.59	31.43	28.45	27.16	26.72	24.80	24.05	23.45	22.87	22.37	21.78	20.82	20.34	19.88	19.64	19.71	18.72	18.24
1.930	10	14600	51.48	45.40	39.74	35.93	33.22	31.51	30.48	29.75	28.99	28.62	23.77	27.43	26.81	26.16	25.70	25.13	19.19	24.36	23.86
1.920	12	1000	14.56	10.46	9.84	8.20	6.99	5.62	5.28	4.81	4.55	4.37	4.17	3.92	3.27	3.18	3.04	2.83	2.75	2.55	2.18
1.995	12	4900	28.26	25.04	21.90	18.52	17.27	15.75	14.91	14.35	13.82	13.44	12.99	12.66	12.62	12.28	12.33	12.00	11.50	11.36	11.12
1.898	12	9600	44.33	39.30	32.99	28.94	26.67	24.84	23.73	22.74	22.34	21.77	21.43	20.68	19.35	18.78	18.39	17.67	17.37	16.87	16.51
1.897	12	14800	50.13	44.17	39.11	35.93	33.58	32.03	26.96	30.23	29.86	29.41	28.83	28.38	28.16	27.29	20.99	26.56	26.25	25.70	24.67
2.384	5	1000	13.59	11.13	7.98	6.57	5.85	5.32	4.90	4.40	3.97	3.53	3.14	2.89	2.63	2.55	2.45	2.24	2.03	1.90	1.87
2.063	5	5000	27.65	22.08	17.09	14.15	13.18	12.90	12.69	12.38	11.89	11.52	11.15	10.70	10.44	10.02	9.56	9.41	9.10	8.86	8.40
2.073	5	10000	39.88	31.58	24.58	21.39	20.68	20.16	20.93	20.47	19.98	19.30	18.76	18.29	17.76	17.31	16.95	16.80	16.71	16.29	15.93
2.372	5	15000	46.64	36.36	28.91	25.19	24.16	25.00	26.33	26.13	25.51	25.22	24.48	23.78	22.91	22.03	20.52	21.10	20.72	20.30	20.17
2.096	8	1000	13.52	12.39	10.05	8.04	6.99	6.15	5.78	5.37	5.08	4.87	4.62	4.46	4.40	4.22	4.02	3.86	3.61	3.53	3.31
2.069	8	4900	32.46	28.18	22.61	18.92	16.92	15.84	15.06	14.31	13.85	13.42	12.97	13.35	12.59	12.30	11.96	11.64	11.44	11.18	10.88
2.064	8	9900	43.26	37.16	30.31	26.56	24.53	24.40	22.52	21.89	21.34	20.69	20.05	19.62	18.09	18.49	18.02	17.82	17.48	17.06	16.58
2.362	8	15200	52.04	45.41	37.24	32.54	29.38	28.27	27.42	27.67	25.58	24.48	24.54	23.69	23.02	22.81	22.16	21.82	21.52	20.74	20.11
2.103	10	1000	14.30	12.10	9.87	7.85	6.92	6.22	5.78	5.30	4.98	4.67	4.53	4.28	4.06	3.89	3.64	3.55	3.38	3.23	3.11
2.064	10	5000	31.20	27.85	23.53	19.72	17.69	16.74	16.51	15.40	14.57	13.78	13.26	12.97	13.04	12.62	12.39	11.79	11.77	11.13	11.03
2.074	10	10000	42.79	37.26	31.68	27.20	24.89	23.65	22.94	21.71	21.26	19.84	19.65	19.58	18.47	16.60	16.15	15.71	15.43	15.12	
2.369	10	15300	52.26	46.78	39.38	34.51	31.02	28.99	27.67	26.72	25.74	25.50	25.79	24.76	24.46	23.32	22.66	22.58	23.25	21.28	21.01
2.101	12	1000	14.65	10.52	8.89	8.25	7.03	5.65	5.31	4.84	4.57	4.39	4.19	3.94	3.57	3.47	3.31	3.09	2.99	2.78	2.65
2.098	12	5000	29.76	28.99	22.70	19.41	17.31	17.28	16.22	14.93	14.39	14.07	13.81	13.39	13.08	12.73	12.62	12.23	11.84	11.54	11.21
2.070	12	10000	41.19	37.06	34.99	31.99	31.15	30.31	30.03	29.31	28.51	28.13	27.93	27.25	25.29	24.52	23.08	22.42	21.81	21.42	21.16
2.371	12	15200	51.11	44.15	42.98	38.61	38.40	35.08	35.46	34.73	32.94	32.83	32.59	31.79	30.64	29.64	29.43	28.26	27.94	27.32	27.02

APPENDIX C

Average Nusselt Numbers

T_i/T_2	H/n	Pe_j	0	1	2	3	4	5	6	7	8	9	10	11	12	13	14	15	16	17	18
1.169	5	1000	11.65	12.86	11.28	10.16	9.34	8.70	8.18	7.74	7.35	7.00	6.67	6.38	6.12	5.89	5.68	5.49	5.31	5.14	4.92
1.175	5	5000	29.17	26.10	23.30	21.30	19.91	18.89	18.08	17.39	16.79	16.25	15.77	15.34	14.95	14.57	14.21	13.87	13.56	13.24	13.02
1.153	5	9700	41.19	35.80	32.08	29.81	28.43	27.28	26.85	26.04	25.12	24.36	23.72	23.17	22.67	22.23	21.82	21.56	21.22	20.94	20.83
1.142	5	13800	48.12	41.24	37.15	34.16	32.90	32.25	31.84	31.51	31.17	30.68	30.23	29.86	29.51	29.18	28.87	28.59	28.32	28.05	27.86
1.149	5	19800	55.16	48.20	43.51	40.87	39.57	38.16	37.82	37.59	37.33	36.95	36.51	36.15	35.81	35.49	35.19	34.91	34.63	34.38	34.14
1.184	8	1000	13.87	12.43	10.80	9.88	9.17	8.63	8.19	7.81	7.48	7.17	6.88	6.62	6.35	6.10	5.88	5.69	5.50	5.31	5.21
1.180	8	5000	34.22	31.73	29.11	26.89	25.07	23.70	22.61	21.70	20.93	20.26	19.67	19.13	18.68	18.25	17.86	17.51	17.16	16.84	16.19
1.162	8	10000	47.33	46.45	44.28	41.71	39.65	38.04	36.69	35.50	34.45	33.36	32.32	31.49	30.76	30.11	29.01	28.97	28.47	28.00	27.72
1.157	8	14500	54.77	54.20	51.26	48.54	46.38	44.77	43.29	42.02	40.84	39.64	38.48	37.51	36.64	35.88	35.20	34.58	34.00	33.46	33.27
1.171	8	18400	61.05	59.65	56.89	54.59	52.48	50.71	49.13	47.76	46.52	45.24	44.00	42.95	42.02	41.18	40.43	39.74	39.11	38.55	38.42
1.184	10	1000	15.00	13.65	12.41	11.47	10.67	10.02	9.48	9.04	8.61	8.17	7.76	7.41	7.10	6.82	6.55	6.29	6.04	5.82	5.46
1.175	10	5000	32.73	30.57	28.35	26.25	24.55	23.18	22.09	21.20	20.43	19.77	19.23	18.71	18.31	17.92	17.56	17.24	16.93	16.63	16.32
1.132	10	10000	43.81	40.43	37.50	35.18	33.34	32.00	30.96	30.09	29.38	28.76	28.07	27.52	27.02	26.57	26.15	25.77	25.40	25.05	24.67
1.142	10	13600	51.95	47.64	44.39	42.00	40.21	38.90	37.87	37.03	36.32	35.62	34.93	34.36	33.84	33.38	32.97	32.57	32.18	31.84	31.51
1.153	10	18100	63.24	60.89	56.61	53.32	50.82	48.86	47.29	46.04	44.98	44.02	43.11	42.36	41.70	41.12	40.58	40.08	39.56	39.07	38.88
1.138	12	1000	15.46	14.04	12.79	11.85	11.03	10.36	9.77	9.28	8.85	8.45	8.10	7.76	7.48	7.23	7.01	6.78	6.56	6.35	6.11
1.174	12	5000	30.18	28.64	26.83	25.10	23.57	22.30	21.29	20.44	19.72	19.12	18.60	18.12	17.71	17.31	16.95	16.62	16.32	16.03	15.83
1.165	12	10100	44.10	42.68	40.71	38.71	36.96	35.53	34.38	33.42	32.65	31.97	31.33	30.79	30.30	29.85	29.43	29.05	28.66	28.34	28.00
1.169	12	14500	50.32	49.06	46.62	44.44	42.61	41.17	40.02	39.06	36.63	36.19	35.75	35.33	34.95	34.60	34.24	33.91	33.61	33.21	33.02
1.172	12	19100	59.56	58.03	55.07	52.55	50.40	48.74	47.32	46.23	45.37	44.61	43.65	42.85	42.16	41.55	40.99	40.48	40.01	39.96	39.72
1.354	5	1000	14.38	13.20	11.82	10.74	9.98	9.42	8.95	8.55	8.21	7.90	7.62	7.36	7.10	6.85	6.61	6.39	6.18	5.99	5.53
1.358	5	4900	28.19	25.37	22.90	21.02	19.66	18.75	18.01	17.39	16.84	16.34	15.88	15.45	15.06	14.70	14.35	14.02	13.70	13.39	12.92
1.336	5	10500	41.37	39.88	35.30	31.88	29.61	28.29	27.55	27.00	26.49	25.91	25.40	24.76	24.35	23.97	23.60	23.26	22.94	22.63	22.33
1.354	5	15900	49.61	48.63	43.01	38.36	35.37	33.88	32.99	32.15	31.73	31.31	30.91	30.47	30.03	29.64	29.26	28.88	28.52	28.17	27.83
1.336	5	21600	56.92	55.04	48.01	44.17	41.61	39.51	38.61	38.10	37.63	37.20	36.82	36.44	36.09	35.74	35.38	35.05	34.75	34.47	34.16
1.343	8	1000	13.70	12.88	11.86	10.89	10.12	9.50	8.99	8.58	8.22	7.91	7.64	7.39	7.16	6.96	6.77	6.60	6.44	6.29	6.12
1.360	8	4900	32.94	31.24	29.35	27.32	25.60	24.27	23.06	22.08	21.21	20.48	19.81	19.23	18.69	18.22	17.78	17.36	16.97	16.61	16.01
1.380	8	10200	44.99	42.05	38.82	36.14	34.50	33.14	32.09	31.18	30.38	29.68	29.07	28.49	27.96	27.46	26.96	26.52	26.07	25.64	25.11
1.370	8	15600	54.05	49.88	46.04	43.04	40.81	39.03	37.61	36.44	35.43	34.71	34.05	33.45	32.92	32.40	31.92	31.49	31.07	30.74	30.21
1.339	8	20100	62.28	60.91	58.99	56.61	54.39	52.49	50.83	49.41	48.15	46.89	45.72	44.65	43.68	42.79	41.97	41.21	40.50	39.85	39.42
1.365	10	1000	14.74	13.30	12.01	11.02	10.22	9.60	9.06	8.61	8.18	7.76	7.37	7.04	6.74	6.47	6.22	5.97	5.74	5.53	5.24
1.356	10	4900	31.69	30.11	28.03	25.93	24.18	22.75	21.67	20.80	20.07	19.46	18.96	18.49	18.12	17.78	17.46	17.18	16.92	16.66	16.32
1.382	10	10100	45.34	42.15	38.86	35.89	33.48	31.55	30.20	28.92	27.99	27.13	26.42	25.78	25.23	24.63	24.15	23.74	23.35	22.96	22.01
1.361	10	15800	54.66	50.77	47.18	44.20	41.91	40.05	38.50	37.16	36.04	35.04	34.15	33.37	32.68	32.07	31.53	31.03	30.58	30.19	29.88
1.353	10	21800	64.72	63.25	57.91	52.99	49.35	46.70	44.82	43.26	41.94	40.83	39.74	38.96	38.30	37.68	37.12	36.64	36.14	35.68	35.24
1.369	12	1000	15.16	13.81	12.60	11.69	10.91	10.26	9.70	9.22	8.81	8.42	8.08	7.76	7.48	7.24	7.02	6.81	6.59	6.38	6.00
1.355	12	4900	29.04	27.55	25.79	24.11	22.63	21.39	20.41	19.59	18.89	18.32	17.81	17.35	16.95	16.57	16.22	15.90	15.61	15.34	15.01
1.350	12	10300	43.42	41.45	39.03	36.82	35.32	34.01	32.84	31.78	30.90	30.12	29.42	28.80	28.23	27.70	27.24	26.81	26.38	25.98	25.42
1.377	12	15600	51.14	49.90	47.08	44.54	42.51	41.13	39.66	38.38	37.56	36.77	36.02	35.37	34.75	34.19	33.68	33.19	32.76	32.34	32.10
1.360	12	21100	64.91	61.67	58.70	55.38	52.43	49.84	47.66	45.89	44.44	43.41	42.42	41.52	40.68	40.16	39.25	38.80	38.18	37.61	37.07

T/E	H/W	Rej	0	1	2	3	4	5	6	7	8	9	10	11	12	13	14	15	16	17	18
1.551	5	1000	14.16	13.07	11.72	10.61	9.82	9.23	8.76	8.35	7.98	7.63	7.31	7.00	6.71	6.44	6.20	5.98	5.77	5.58	5.24
1.524	5	5000	28.19	25.34	22.80	21.17	20.13	19.30	18.67	17.95	17.35	16.82	16.35	15.94	15.57	15.24	14.94	14.67	14.41	14.02	13.88
1.542	5	9900	40.99	35.67	32.58	30.04	28.41	27.32	26.65	26.15	25.72	25.28	24.87	24.49	24.12	23.76	23.42	23.07	22.74	22.40	22.07
1.549	5	14700	46.96	42.45	38.54	35.66	33.75	32.49	31.62	31.15	30.70	30.28	29.89	29.51	29.13	28.74	28.40	78.08	27.74	27.41	27.12
1.564	8	1000	13.52	11.83	10.73	9.80	9.08	8.51	8.04	7.65	7.31	7.02	6.75	6.49	6.24	6.00	5.79	5.59	5.41	5.23	5.02
1.560	8	5000	33.36	31.34	29.44	27.58	25.89	24.57	23.51	22.62	21.85	21.18	20.60	20.07	19.61	19.18	18.79	18.46	18.16	17.84	17.02
1.556	8	10000	43.92	41.05	37.87	35.26	33.64	32.31	31.27	30.37	29.58	28.89	28.29	27.73	27.20	26.70	26.21	25.77	25.34	24.91	24.55
1.549	8	14900	52.22	48.23	44.55	41.67	39.52	37.82	36.46	35.33	34.35	33.66	33.03	32.46	31.96	31.47	31.02	30.61	30.21	29.93	29.46
1.601	10	1000	14.34	13.61	12.66	14.71	10.88	10.25	9.68	9.23	8.79	8.45	8.14	7.86	7.63	7.40	7.15	6.90	6.70	6.49	6.39
1.550	10	5000	31.13	29.37	27.08	25.00	23.34	22.03	20.99	20.11	19.46	18.88	18.37	17.92	17.53	17.17	16.84	16.56	16.26	15.98	15.50
1.557	10	10400	44.80	42.03	39.02	36.30	34.08	32.32	31.09	29.91	29.03	28.21	27.54	26.91	26.38	25.81	25.32	24.90	24.51	24.11	23.87
1.540	10	15200	57.93	53.84	49.99	46.73	44.19	42.21	40.79	39.51	38.54	37.70	36.94	36.24	35.63	35.08	34.58	34.10	33.64	33.22	32.73
1.531	12	1000	15.09	14.04	13.19	12.30	11.59	10.79	10.20	9.64	9.17	8.78	8.44	8.14	7.86	7.59	7.33	7.07	6.82	6.58	6.28
1.542	12	4900	25.66	26.40	25.12	23.65	22.39	21.26	20.32	19.51	18.85	18.28	17.77	17.36	16.99	16.65	16.34	16.05	15.79	15.55	15.24
1.529	12	10000	41.97	40.00	37.66	35.51	34.06	32.79	31.66	30.68	29.84	29.10	28.43	27.85	27.29	26.78	26.33	25.93	25.51	25.13	24.96
1.555	12	14900	50.91	47.92	45.17	42.77	40.79	39.44	38.01	36.85	35.89	35.01	34.23	33.53	32.88	32.29	31.75	31.24	30.79	30.35	29.96
1.732	5	1000	13.78	12.72	11.40	10.32	9.56	8.98	8.52	8.12	7.76	7.42	7.11	6.81	6.53	6.27	6.04	5.82	5.62	5.44	5.12
1.704	5	5000	27.45	24.06	21.79	20.29	19.33	18.58	18.00	17.33	16.77	16.27	15.83	15.44	15.09	14.78	14.49	14.23	13.99	13.19	12.88
1.722	5	9800	38.79	34.65	31.75	29.42	27.79	26.70	26.02	25.52	25.10	24.65	24.25	23.88	23.54	23.21	22.90	22.56	22.26	21.93	21.63
1.728	5	14600	46.50	42.06	38.21	35.36	33.48	32.25	31.40	30.71	30.10	29.55	29.04	28.73	28.35	27.90	27.43	26.97	26.54	26.12	25.80
1.745	8	1000	13.14	11.61	10.50	9.57	8.86	8.30	7.84	7.46	7.13	6.84	6.58	6.32	6.09	5.87	5.66	5.47	5.30	5.13	4.98
1.720	8	4900	31.88	29.92	28.07	26.27	24.63	23.36	22.34	21.47	20.73	20.10	19.53	19.02	18.58	18.17	17.79	17.48	17.18	16.88	16.52
1.737	8	9700	43.00	40.19	37.07	34.50	32.95	31.63	30.60	29.71	28.93	28.26	27.66	27.11	26.66	26.15	25.70	25.28	24.87	24.46	24.00
1.727	8	15000	52.58	48.57	44.98	41.99	39.83	38.12	36.76	35.62	34.64	33.95	33.31	32.74	32.25	31.76	31.31	30.90	30.51	30.22	29.84
1.782	10	1000	14.03	13.42	12.41	11.45	10.62	9.99	9.42	8.97	8.54	8.20	7.91	7.64	7.39	7.15	6.90	6.66	6.45	6.25	5.90
1.721	10	5000	30.87	29.13	26.87	24.88	23.23	21.93	20.90	20.02	19.38	18.81	18.31	17.87	17.47	17.10	16.77	16.49	16.19	15.91	15.68
1.740	10	9800	42.88	40.41	37.66	35.17	33.14	31.53	30.42	29.35	28.52	27.75	27.13	26.53	26.01	25.45	24.97	24.55	24.15	23.75	23.21
1.720	10	15000	51.44	47.87	44.43	41.49	39.18	37.37	36.05	34.85	33.92	33.12	32.40	31.76	31.18	30.72	30.33	29.96	29.61	29.27	28.82
1.748	12	1000	14.46	13.45	12.63	11.79	11.11	10.34	9.77	9.23	8.78	8.41	8.08	7.80	7.53	7.28	7.03	6.79	6.54	6.31	6.11
1.720	12	5000	28.04	25.84	24.61	23.19	21.97	20.86	19.95	19.16	18.52	17.96	17.46	17.04	16.65	16.29	15.96	15.66	15.39	15.14	14.98
1.737	12	10000	41.34	39.37	37.06	34.93	33.49	32.24	31.13	30.17	29.35	28.62	27.98	27.41	26.88	26.40	25.98	25.60	25.21	24.85	24.44
1.734	12	14600	50.34	47.43	44.71	42.33	40.36	39.01	37.57	36.41	35.62	34.93	34.32	33.77	33.29	32.85	32.43	32.02	31.64	31.28	30.84

T_j/T_c	H/w	Rej.	0	1	2	3	4	5	6	7	8	9	10	11	12	13	14	15	16	17	18
1.924	5	1000	13.73	12.83	11.49	10.42	9.66	9.05	8.60	8.20	7.84	7.51	7.18	6.87	6.62	6.34	6.09	5.86	5.64	5.45	5.24
1.919	5	4800	27.70	22.42	22.01	19.93	18.51	17.50	16.82	16.31	15.87	15.47	15.12	14.80	14.51	14.23	13.98	13.73	13.51	13.30	13.11
1.911	5	9600	39.54	34.46	30.82	28.17	26.44	25.30	24.55	23.93	23.40	22.93	22.50	22.24	21.87	21.51	21.17	20.86	20.56	20.29	19.99
1.917	5	14600	46.69	41.88	37.95	35.08	33.18	31.88	30.94	30.51	30.14	29.83	29.51	29.20	28.89	28.57	28.28	28.00	27.71	27.41	27.13
1.916	8	1000	13.08	12.53	11.59	10.64	9.86	9.21	8.69	8.26	7.89	7.57	7.29	7.04	6.82	6.62	6.44	6.27	6.10	5.95	5.57
1.860	8	4900	31.43	29.27	26.84	24.73	23.26	22.11	21.15	20.36	19.70	19.12	18.62	18.16	17.76	17.40	17.06	16.74	16.45	16.18	15.58
1.895	8	9800	43.85	40.78	37.64	35.11	33.13	31.63	30.46	29.49	28.68	27.94	27.28	26.70	26.20	25.74	25.31	24.90	24.50	24.12	23.83
1.892	8	14600	50.93	47.25	43.82	41.08	38.98	37.32	36.03	34.92	34.01	33.18	32.47	31.81	31.26	30.72	30.21	29.75	29.32	28.89	28.74
1.923	10	1000	14.20	13.11	12.01	10.96	10.15	9.49	8.95	8.49	8.10	7.75	7.46	7.19	6.94	6.72	6.51	6.32	6.15	5.98	5.46
1.909	10	4900	30.20	28.46	26.67	25.04	23.68	22.57	21.69	20.98	20.39	19.62	19.20	18.83	18.50	18.20	17.91	17.60	17.31	17.02	16.85
1.918	10	9800	41.92	39.25	36.65	34.60	33.11	32.04	31.01	30.14	29.40	28.74	28.16	27.63	27.11	26.63	26.18	25.77	25.41	25.04	24.86
1.900	10	14600	51.48	48.44	45.54	43.14	41.16	39.55	38.25	37.19	36.28	35.51	34.45	33.86	33.32	32.81	32.33	31.88	31.14	30.76	30.29
1.920	12	1000	14.56	12.51	11.29	10.52	9.81	9.11	8.57	8.10	7.70	7.37	7.08	6.81	6.54	6.30	6.09	5.88	5.70	5.52	5.42
1.895	12	4900	28.26	26.65	25.07	23.43	22.20	21.12	20.24	19.50	18.87	18.33	17.84	17.41	17.04	16.70	16.41	16.13	15.86	15.61	15.01
1.898	12	9600	44.33	42.11	39.07	36.54	34.56	32.94	31.63	30.52	29.61	28.82	28.15	27.53	26.90	26.32	25.79	25.29	24.82	24.38	23.99
1.897	12	14800	50.13	47.15	44.47	42.33	40.58	39.16	37.41	36.52	35.78	35.14	34.57	34.05	33.60	33.15	32.34	31.98	31.64	31.31	30.92
2.094	5	1000	13.49	12.51	11.00	9.89	9.09	8.46	7.95	7.51	7.11	6.76	6.43	6.13	5.86	5.63	5.41	5.22	5.03	4.85	4.62
2.363	5	5000	27.65	24.86	22.27	20.24	18.83	17.84	17.10	16.51	16.00	15.55	15.15	14.78	14.45	14.13	13.83	13.55	13.29	13.04	12.87
2.273	5	10000	39.88	35.73	32.01	29.36	27.62	26.38	25.60	24.96	24.41	23.90	23.43	23.00	22.60	22.22	21.87	21.55	21.27	20.99	20.72
2.072	5	15000	46.64	41.50	37.30	34.27	32.25	31.04	30.36	29.82	29.34	28.93	28.52	28.13	27.73	27.32	26.93	26.56	26.22	22.89	25.59
2.096	8	1000	13.52	12.96	11.99	11.00	10.20	9.52	8.99	8.54	8.15	7.82	7.53	7.28	7.06	6.85	6.66	6.49	6.32	6.16	5.20
2.369	8	4900	32.46	30.32	27.75	25.54	23.82	22.49	21.43	20.54	19.79	19.16	18.59	18.16	17.73	17.34	16.98	16.65	16.34	16.05	15.76
2.064	8	9900	43.26	40.21	36.91	34.32	32.36	31.04	29.82	28.83	28.00	27.27	26.61	26.03	25.42	24.92	24.46	24.05	23.66	23.29	23.00
2.062	8	15200	52.04	48.72	44.90	41.81	39.32	37.48	36.04	35.00	33.95	33.00	32.24	31.52	30.87	30.29	29.75	29.26	28.77	28.35	27.91
2.103	10	1000	14.30	13.19	12.09	11.04	10.21	9.55	9.01	8.55	8.15	7.80	7.50	7.23	6.99	6.77	6.56	6.37	6.20	6.03	5.85
2.364	10	5000	31.20	29.52	27.53	25.58	24.00	22.79	21.89	21.08	20.36	19.70	19.12	18.60	18.18	17.78	17.42	17.07	16.76	16.44	16.21
2.374	10	10000	42.79	40.03	37.25	34.74	32.76	31.25	30.06	29.01	28.15	27.32	26.62	26.04	25.54	25.03	24.47	23.95	23.47	23.02	22.95
2.069	10	15300	52.26	49.52	46.14	43.23	40.79	38.82	37.24	35.93	34.79	33.87	33.13	32.43	31.82	31.21	30.64	30.14	29.73	29.26	29.28
2.101	12	1000	14.65	12.59	11.36	10.58	9.87	9.17	8.61	8.14	7.75	7.41	7.12	6.85	6.60	6.38	6.17	5.98	5.80	5.64	5.58
2.088	12	5000	29.76	27.88	26.15	24.46	23.03	22.07	21.24	20.45	19.78	19.21	18.71	18.27	17.87	17.51	17.18	16.87	16.57	16.29	16.00
2.070	12	10000	41.19	39.12	37.74	36.30	35.27	34.45	33.82	33.25	32.73	32.26	31.87	31.49	31.01	30.55	30.05	29.57	29.12	28.69	28.11
2.071	12	15200	51.01	47.58	46.04	44.24	43.07	41.74	40.85	40.08	39.28	38.65	38.09	37.57	37.02	36.53	36.04	35.54	35.11	34.67	34.28

APPENDIX D

Specifications of Marinite I

Density : 737 Kg/m^3

Thermal expansion : 6.91 x 10^{-6}/°C up to 150°C

(shrinkage thereafter)

Shrinkage length : 0.2% at 300°C

Thermal conductivity

at 300°C : 0.114 W/m-°K

APPENDIX E

Working Principle and Specification of Microfoil

Heat Flux Sensor

The Microfoil heat flux sensor (Model 20450-1), manufactured by RDF Corp., may be represented electrically as multijunction thermopiles. Basically, the RDF microfoil sensors differ from conventional thermopile sensors in that they eliminate the use of plated junctions and are fabricated with homogeneous thermoelectric alloys in each leg between junctions. The legs are manufactured from 0.005 mm foils which greatly reduce the thermal losses due to lead conduction. Furthermore, the thermal junctions are formed in the shape of accurately controlled platelets functioning as controlled heat sinks for each junction. Thus, the accuracy and repeatability of their calibration become independent of mounting conditions.

The microfoil sensors are fabricated from three laminated sections. The upper and lower sections are manufactured from silicone-impregnated glass cloth. The critical layer is the one in the centre and serves as a thermal barrier.

As shown in Figure E.1, the thermoelectric junctions are formed from two materials designated as A and B, on the upper surface of the barrier. In series with these are corresponding junctions on the lower surface. The two output leads, therefore, are of the same material as the one coming from the first junction on the upper surface and the other from the last junction on the lower surface. Although only one pair of junctions is required for a complete sensor, multiple pairs of junctions are installed to insure maximum signal. Any time

thermal energy is transferred through the barrier, a temperature gradient, ΔT, is generated across the barrier, which is directly proportional to the heat transfer rate. Hence, each pair of thermoelectric junctions forms a completed thermocouple circuit whose voltage output is proportional to the temperature gradient.

The sensors are equipped with reference Copper-Constantan thermocouples. The dimensions and further specifications of the sensor and thermocouple are tabulated in Table E.1. As shown, the sensors exhibit a very small response time, 0.02 s, as defined by the time required for the junctions to reach 62% of an instantaneous step change in the temperature. The heat flow sensors are individually calibrated by the supplier for the heat transfer rate.

TABLE E.1

Specification of Micro-foil Heat Flux Sensor (Model 20450-1)

Nominal dimension   11 mm x 7 mm

Heat sensing area   4.78 mm x 1.9 mm

Thermal resistance 5.28×10^{-4} °K/W-m^{-2}

Response time   0.020 (62% response to step change)

Maximum operating temp.   260°C
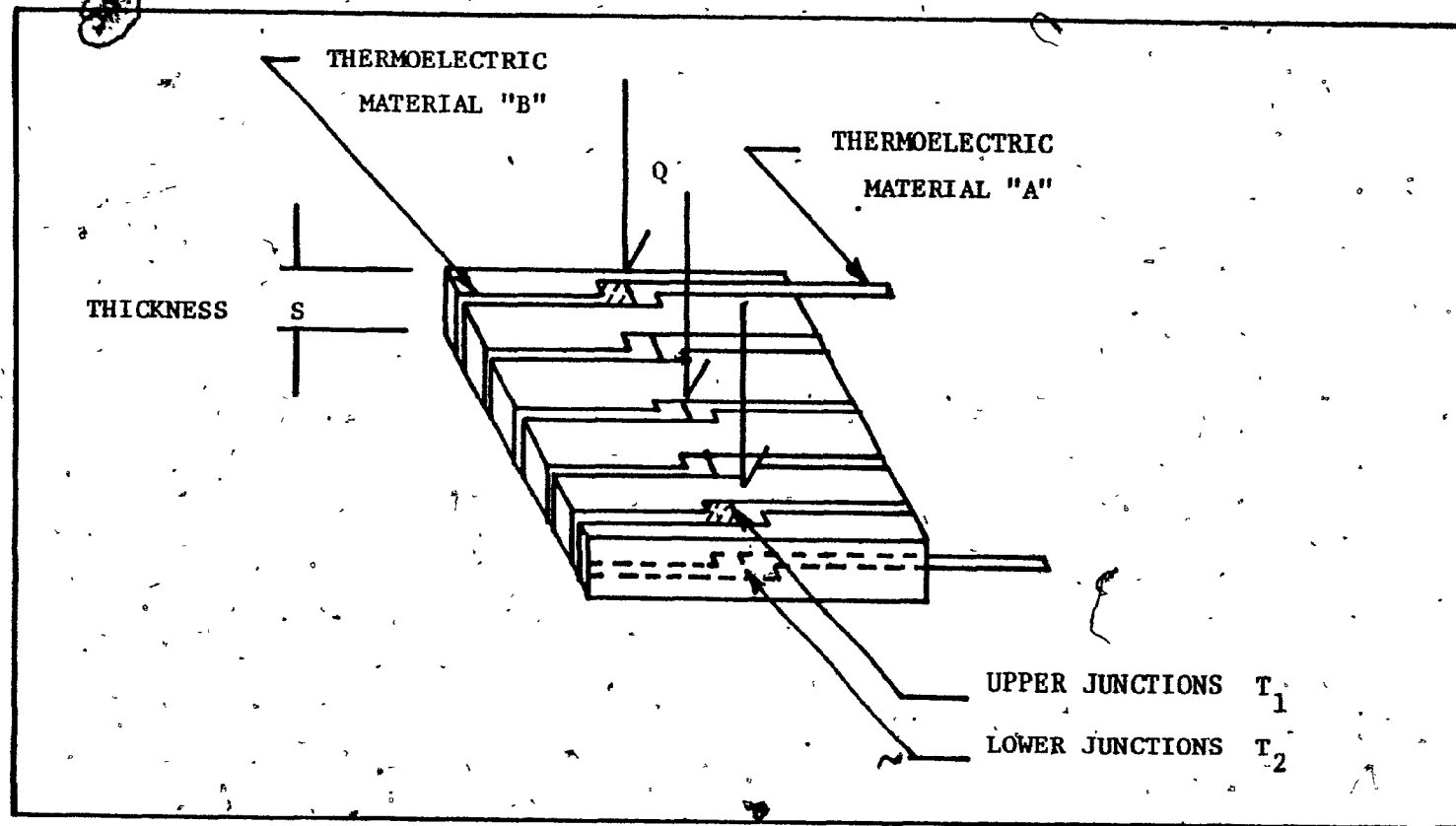
THERMOELECTRIC MATERIAL "B"

THERMOELECTRIC MATERIAL "A"

Q

THICKNESS   S

UPPER JUNCTIONS T_1

LOWER JUNCTIONS T_2

FIGURE E.1   The Microfoil Heat Flow Sensor

APPENDIX F

Correction for Difference in Conductivity between
Impingement Surface and Sensor Material

A schematic diagram of the heat flux sensor mounted on the impingement surface is shown on Figure F.1(a). Assuming heat conduction in y-direction only, the system may be expressed by the composite wall network shown on F.1(b). Thus

$$q_m = \frac{T_s^* - T_a}{R_1 + R_2 + R_3} \qquad (F.1)$$

where q_m is the measured heat flux through the sensor

T_s^* is the temperature of the sensor surface

T_a is the temperature at the bottom of the impingement plate

R_1 is the thermal resistance of the sensor

R_2 is the thermal resistance of the adhesive

R_3 is the thermal resistance of the plate below the sensor

and

$$q = \frac{T_s - T_a}{R_4} \qquad (F.2)$$

where q is the true impingement heat flux

T_s is the temperature of the impingement surface

R_4 is the thermal resistance of the plate.
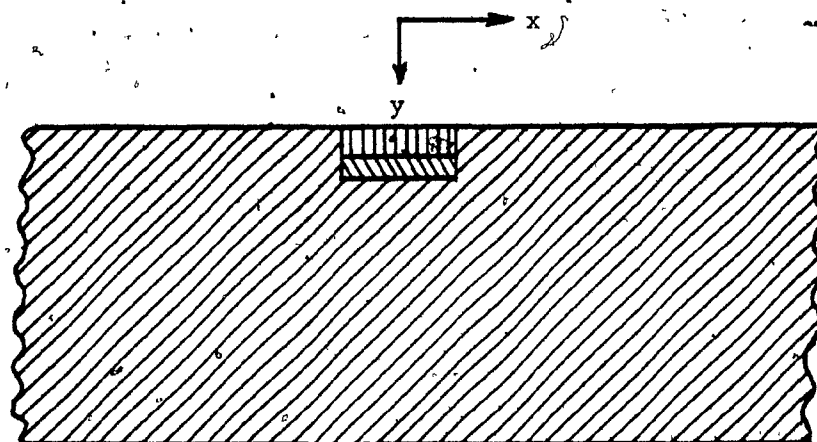
Here $R_1 = 5.28 \times 10^{-4}$ °K/W-m^{-2}

$R_2 = 5.78 \times 10^{-6}$ °K/W-m^{-2}

$R_3 = 1.58 \times 10^{-5}$ °K/W-m^{-2}

$R_4 = 1.57 \times 10^{-5}$ °K/W-m^{-2}

Three unknown variables q, T_s^* and T_a are solved from equations F.1 and F.2 by an iterative approach. The q obtained thus is the true heat flux to the impingement surface and is used to calculate the heat transfer coefficient.
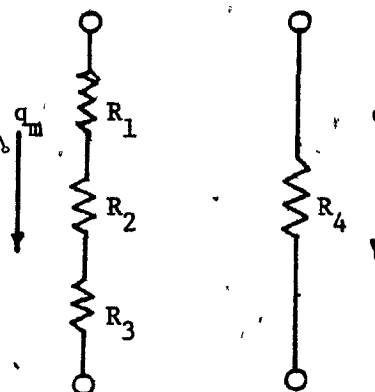
copper   sensor   adhesive

FIGURE F-1 (a)

FIGURE F-1 (b)

APPENDIX G

Radiant Heat Transfer

At steady state condition, the total heat transfer to the impingement surface may be expressed by the following equation
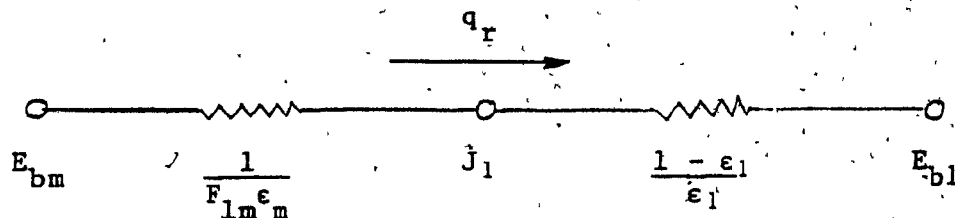
$$q = q_c + q_r \qquad (G.1)$$

where q = total heat flux to the impingement surface

q_c = convective heat flux

q_r = radiant heat flux

The radiant heat transfer from a medium to a surface may be represented by the following network

Thus the radiant heat transfer

$$q_r = (E_{bm} - E_{b1}) \quad \frac{1}{F_{1m}\epsilon_m} + \frac{1-\epsilon_1}{\epsilon_1}$$

$$= \frac{\sigma\{(T_1)^4 - (T_s)^4\}}{\frac{1}{F_{1m}\epsilon_m} + \frac{1-\epsilon_1}{\epsilon_1}}$$

where σ = Stephan-Boltzman constant = 5.67×10^{-8} W/m²-K⁴

F_{1m} = shape factor = 1

ϵ_m = emissivity of air = 0.1

ϵ_1 = emissivity of copper surface = 0.023

Thus from Equation G.1, the convective heat transfer is obtained as

$$q_c = q - 1.08 \times 10^{-9} \{(T_j)^4 - (T_s)^4\} \qquad (G.2)$$

APPENDIX H

Physical Properties of Air

Temperature °C	μ centipoise	K W/m°k	C_p J/Kg °K	ρ Kg/m³
50	0.0193	0.028	1006	1.092
100	0.0216	0.032	1011	0.946
150	0.0237	0.035	1016	0.835
200	0.0257	0.039	1025	0.746
250	0.0274	0.042	1036	0.674
300	0.0292	0.045	1045	0.616

Reference:

Holman, J.P., Heat Transfer, 3rd Edition, McGraw-Hill Book Co., New York.